

---


Electronic Theses and Dissertations, 2004-2019

---

2004

## New Organic/inorganic Hybrid Sol-gel Nanocomposite Materials For Raman Gain In Fiber Optics

Stephen James Andrasik  
*University of Central Florida*

 Part of the [Chemistry Commons](#)

Find similar works at: <https://stars.library.ucf.edu/etd>

University of Central Florida Libraries <http://library.ucf.edu>

This Masters Thesis (Open Access) is brought to you for free and open access by STARS. It has been accepted for inclusion in Electronic Theses and Dissertations, 2004-2019 by an authorized administrator of STARS. For more information, please contact [STARS@ucf.edu](mailto:STARS@ucf.edu).

---

### STARS Citation

Andrasik, Stephen James, "New Organic/inorganic Hybrid Sol-gel Nanocomposite Materials For Raman Gain In Fiber Optics" (2004). *Electronic Theses and Dissertations, 2004-2019*. 3.

<https://stars.library.ucf.edu/etd/3>

NEW ORGANIC/INORGANIC HYBRID SOL-GEL NANOCOMPOSITE  
MATERIALS FOR RAMAN GAIN IN FIBER OPTICS

by

STEPHEN J. ANDRASIK  
B.S. University of Central Florida, 2001

A thesis submitted in partial fulfillment of the requirements  
for the degree of Master of Science  
in the Department of Chemistry  
in the College of Arts and Sciences  
at the University of Central Florida  
Orlando, Florida

Spring Term  
2004

© 2004 Stephen Andrasik

## ABSTRACT

The recent increased availability of additional wavelengths in the telecommunications window of about 1300-1600 nm has generated an interest in new optical materials and devices that can operate outside the normally used regions of 840 nm, 1310 nm, and 1550 nm. Specifically, methods to amplify fiber optical data transmission in the regions where there is limited or no existing methods to achieve amplification is of interest in the chemistry and photonic communities. Raman gain is one method that has been proposed to passively amplify optical data transmission through a distributed process. Amplification is obtained through a nonlinear light scattering process where an optical wave is amplified at the expense of a higher frequency pump wave. Multiple wavelengths can be evenly amplified simultaneously in a desired region by specific selection of one or more pump wavelengths.

Herein, the synthesis and characterization of new hybrid inorganic/organic sol-gels and monomers capable of producing broad wavelength Raman scattering over a spectral range of 1200-1670 nm are presented. The synthetic methodology developed facilitates the systematic approach to produce sol-gel derivatives with functional groups known to be strongly Raman scattering. Additionally, a method to synthesize and characterize a large number of different compounds using a combinatorial approach was demonstrated. Thio based derivatives of sulfonyldiphenol, isopropylidenediphenol, and triallyloxy triazine were synthesized in addition

to thio derivatives of poly(hydroxystyrene). Micro-Raman spectra of the hybrid sol-gels, thio-based derivatives, and IR spectra of select sol-gel monomers were obtained.

This is dedicated to my family.

I would like to thank my parents for their constant encouragement,

my wife, Hong, for her patients,

and my daughter, Heather, for instilling my desire.

## TABLE OF CONTENTS

LIST OF FIGURES .....	vii
LIST OF TABLES .....	xi
LIST OF SCHEMES.....	xii
LIST OF ABBREVIATIONS.....	xiii
INTRODUCTION .....	1
RESEARCH OBJECTIVE .....	14
EXPERIMENTAL: SYNTHESIS AND CHARACTERIZATION OF ORGANIC HYBRID SOL-GELS AND MONOMERS.....	16
RESULTS AND DISCUSSION OF SOL-GELS AND MONOMERS .....	29
RESULTS AND DISCUSSION OF RAMAN SCATTERING FOR SELECT SOL-GELS AND MONOMERS .....	49
CONCLUSIONS AND FUTURE WORK.....	57
APPENDIX A <sup>1</sup> H NMR SPECTRA.....	59
APPENDIX B SELECT IR SPECTRA.....	77
APPENDIX C RAMAN GAIN .....	80
APPENDIX D RAMAN SPECTRA .....	82
LIST OF REFERENCES.....	101

## LIST OF FIGURES

1. Attenuation in standard silica optical fiber.....	2
2. Attenuation in Lucent Technologies AllWave™ optical fiber.....	2
3. Electrooptic configuration for generic fiber optic network.....	4
4. Generic optical fiber design.....	5
5. Absorption loss in standard glass fiber and Lucent's Allwave™ fiber.....	11
6. Synthetic approach for multiple sol-gel samples.....	30
7. 300 MHz <sup>1</sup> H NMR of allyl bromide in CDCl <sub>3</sub> .....	60
8. 300 MHz <sup>1</sup> H NMR of sulfonylbisphenol in CD <sub>3</sub> COCD <sub>3</sub> .....	61
9. 300 MHz <sup>1</sup> H NMR of <b>31</b> in CD <sub>3</sub> COCD <sub>3</sub> .....	62
10. 300 MHz <sup>1</sup> H NMR of <b>32</b> in CDCl <sub>3</sub> .....	63
11. 300 MHz <sup>1</sup> H NMR of <b>33</b> in CDCl <sub>3</sub> .....	64
12. 300 MHz <sup>1</sup> H NMR of isopropylidenediphenol in CD <sub>3</sub> COCD <sub>3</sub> .....	65
13. 300 MHz <sup>1</sup> H NMR of <b>34</b> in CD <sub>3</sub> COCD <sub>3</sub> .....	66
14. 300 MHz <sup>1</sup> H NMR of <b>35</b> in CD <sub>3</sub> COCD <sub>3</sub> .....	67
15. 300 MHz <sup>1</sup> H NMR of <b>36</b> in CDCl <sub>3</sub> .....	68
16. 300 MHz <sup>1</sup> H NMR of cyanuric acid in CD <sub>3</sub> COCD <sub>3</sub> .....	69
17. 300 MHz <sup>1</sup> H NMR of triallyloxy-1,3,5-triazine in CDCl <sub>3</sub> .....	70
18. 300 MHz <sup>1</sup> H NMR of <b>37</b> in CDCl <sub>3</sub> .....	71



19. 300 MHz $^1\text{H}$ NMR of <b>38</b> in $\text{CDCl}_3$ .....	72
20. 300 MHz $^1\text{H}$ NMR of poly(4-hydroxystyrene) in $\text{CD}_3\text{COCD}_3$ .....	73
21. 300 MHz $^1\text{H}$ NMR of <b>39</b> in $\text{CD}_3\text{COCD}_3$ .....	74
22. 300 MHz $^1\text{H}$ NMR of brominated poly(4-hydroxystyrene) in $\text{CD}_3\text{COCD}_3$ .....	75
23. 300 MHz $^1\text{H}$ NMR of <b>41</b> in $\text{CD}_3\text{COCD}_3$ .....	76
24. IR spectrum 3-(trimethoxysilyl)propyl isocyanate .....	78
25. IR spectrum of 2(ethylanylino)ethanol reaction mixture.....	78
26. IR spectrum of sol-gel <b>6</b> in diffuse reflectance mode. ....	79
27. IR spectrum of sol-gel <b>13</b> in diffuse reflectance mode. ....	79
28. Raman gain model sol-gel <b>28</b> .....	81
29. Raman spectrum sol-gel <b>1</b> .....	83
30. Raman spectrum sol-gel <b>3</b> .....	83
31. Raman spectrum sol-gel <b>5</b> .....	84
32. Raman spectrum sol-gel <b>6</b> .....	84
33. Raman spectrum sol-gel <b>7</b> .....	85
34. Raman spectrum sol-gel <b>8</b> .....	85
35. Raman spectrum sol-gel <b>9</b> .....	86
36. Raman spectrum sol-gel <b>10</b> .....	86
37. Raman spectrum sol-gel <b>11</b> .....	87
38. Raman spectrum sol-gel <b>12</b> .....	87
39. Raman spectrum sol-gel <b>13</b> .....	88
40. Raman spectrum sol-gel <b>14</b> .....	88

41. Raman spectrum sol-gel <b>15</b> .....	89
42. Raman spectrum sol-gel <b>16</b> .....	89
43. Raman spectrum sol-gel <b>17</b> .....	90
44. Raman spectrum sol-gel <b>18</b> .....	90
45. Raman spectrum sol-gel <b>19</b> .....	91
46. Raman spectrum sol-gel <b>20</b> .....	91
47. Raman spectrum sol-gel <b>21</b> .....	92
48. Raman spectrum sol-gel <b>22</b> .....	92
49. Raman spectrum sol-gel <b>23</b> .....	93
50. Raman spectrum sol-gel <b>24</b> .....	93
51. Raman spectrum sol-gel <b>25</b> .....	94
52. Raman spectrum sol-gel <b>26</b> .....	94
53. Raman spectrum sol-gel <b>27</b> .....	95
54. Raman spectrum model sol-gel <b>28</b> .....	95
55. Raman spectrum model sol-gel <b>29</b> .....	96
56. Raman spectrum model sol-gel <b>30</b> .....	96
57. Raman spectrum compound <b>31</b> .....	97
58. Raman spectrum compound <b>32</b> .....	97
59. Raman spectrum compound <b>33</b> .....	98
60. Raman spectrum compound <b>35</b> .....	98
61. Raman spectrum compound <b>37</b> .....	99
62. Raman spectrum compound <b>39</b> .....	99

63. Raman spectrum compound <b>41</b> .....	100
---	-----

## LIST OF TABLES

1. Dispersed organic monomers used in sol-gel synthesis.....	17
2. Grafted organic monomers used in sol-gel synthesis. ....	18
3. Raman scattering frequencies for common functional groups. ....	31

## LIST OF SCHEMES

1. Synthesis of model sol-gel <b>28</b> .....	33
2. Synthesis of model sol-gels <b>29, 30</b> .....	33
3. Synthesis of dispersed monomer sol-gels <b>1-9</b> .....	34
4. Synthesis of grafted monomer sol-gels <b>10-27</b> .....	35
5. Synthesis of compound <b>31</b> .....	36
6. Synthesis of compound <b>32</b> .....	38
7. Synthesis of compound <b>33</b> .....	39
8. Synthesis of compound <b>34</b> .....	40
9. Synthesis of compound <b>35</b> .....	41
10. Synthesis of compound <b>36</b> .....	42
11. Synthesis of compound <b>37</b> .....	44
12. Synthesis of compound <b>38</b> .....	45
13. Synthesis of polymer <b>39</b> .....	46
14. Attempted synthesis of polymer <b>40</b> .....	47
15. Synthesis of polymer <b>41</b> .....	48

## LIST OF ABBREVIATIONS

$\theta_c$	critical angle
$\mu\text{m}$	micrometer
$\delta$	ppm
$\lambda$	wavelength
>	greater than
$^{\circ}\text{C}$	degrees Celsius
AIBN	azobisisobutylnitrile
aq	aqueous
B-O	boron oxygen bond
$\text{B}_2\text{O}_3$	boron oxide
$\text{CDCl}_3$	deuterated chloroform
$\text{CD}_3\text{COCD}_3$	deuterated acetone
$\text{CH}_2\text{Cl}_2$	methylene chloride
CVD	chemical vapor deposition
$\text{cm}^{-1}$	wavenumber
d	doublet
dB/Km	decibels per kilometer
DMSO	dimethylsulfoxide

EDFA	erbium doped fiber amplifier
EtOH	ethanol
FT-IR	fourier transformed infrared
g/mm	gratings per millimeter
g	gram
GaAlAs	gallium aluminum arsenide
GaAs	gallium arsenide
Gbit/s	gigabit per second
Ge-O	germanium oxygen bond
GeO <sub>2</sub>	germanium oxide
GW/cm <sup>2</sup>	gigawatt per cubic centimeter
h	hour
HCl	hydrochloric acid
HeNe	helium neon
<sup>1</sup> H NMR	proton nuclear magnetic resonance
H <sub>2</sub> O	water
Hz	hertz
in	inch
InGaAsP	indium gallium arsenide phosphide
IR	infrared
<i>J</i>	coupling constant
Km	kilometer

KOH	potassium hydroxide
LiAlH <sub>4</sub>	lithium aluminum hydride
lit.	literature
m	multiplet
M	molar or moles per liter
MCVD	modified chemical vapor deposition
MeOH	methanol
MgSO <sub>4</sub>	magnesium sulfate
MHz	megahertz
min	minute
mm	millimeter
mmHg	millimeters of mercury
mmol	millimole
mL	milliliter
mol%	mole percent
mp	melting point
mW	milliwatt
N <sub>2</sub>	nitrogen
NaHCO <sub>3</sub>	sodium bicarbonate
NaOH	sodium hydroxide
n <sub>0</sub>	refractive index of fiber core
n <sub>1</sub>	refractive index of fiber cladding layer



nm	nanometer
$\text{OH}^-$	hydroxide
OVD	outside vapor deposition
PCVD	plasma assisted chemical vapor deposition
P-O	phosphorus oxygen bond
$\text{P}_2\text{O}_5$	diphosphorus pentoxide
$\text{P}(\text{Ph})_4\text{Br}$	tetraphenylphosphonium bromide
ppm	parts per million
ps	picoseconds
quart	quartet
quint	quintet
RF	radio frequency
RT	room temperature
s	singlet
$\text{SiF}_4$	tetrafluoro silane
$\sin^{-1}$	arcsin
Si-gel	silica gel
Si-O	silicon oxygen bond
$\text{SiO}_2$	silicon dioxide
t	triplet
TEOS	tetraethoxysilane
THF	tetrahydrofuran

THz	terahertz
TLC	thin layer chromatography
TMS	trimethyl silane
UV	ultraviolet
v/v	volume per volume
VAD	vapor axial deposition
WDM	wavelength division multiplexing

## INTRODUCTION

The quest to improve fiber optic communications and the need to meet the recent increased demand for bandwidth has generated numerous advances in fiber optic technology. One recent advancement was the development of Lucent Technologies AllWave™ Fiber, enabling more data to be sent at wavelengths that were not previously accessible for telecommunications.<sup>1-3</sup> Lucent's new fiber provides a 50% larger spectrum than conventional fiber by significantly lowering attenuation in the 1300 nm to 1550 nm telecommunication window (Figure 1, 2). The development of the AllWave™ Fiber came as a major breakthrough in the fiber optic industry, because the newly patented fabrication process for the fiber nearly eliminates water molecules in glass fibers that arise during fabrication. The presence of water, or the  $\text{OH}^-$  ion, severely limits the telecommunication window to three major regions (840 nm, 1310 nm, 1550 nm) due to several absorption bands associated with OH. Consequently this has generated a need for new materials and devices that can operate in this region.

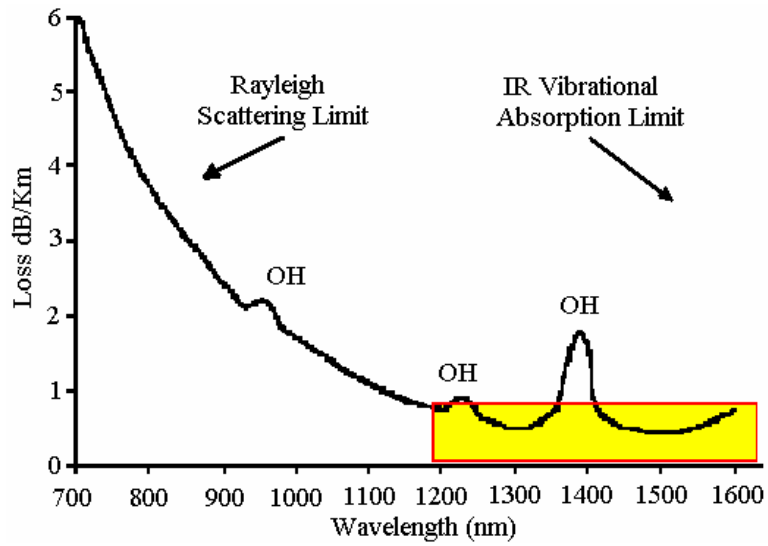


**Figure 1.** Attenuation in standard silica optical fiber.<sup>1</sup>

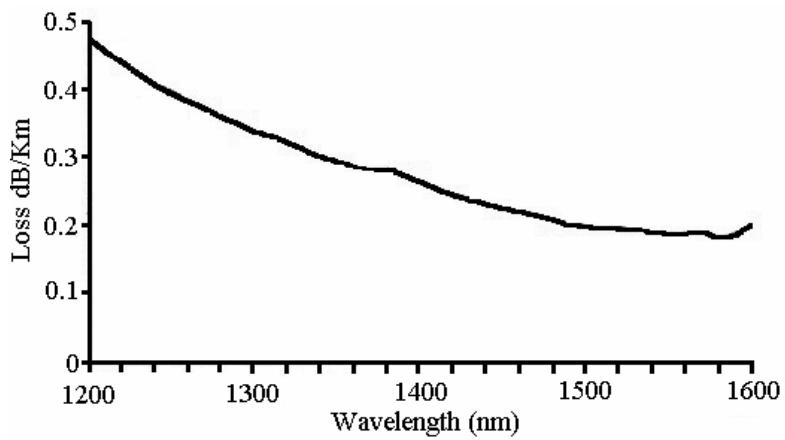


**Figure 2.** Attenuation in Lucent Technologies AllWave™ optical fiber.<sup>1</sup>

Region of graph is represented by yellow box, Figure 1.

Methods to compensate for inherent losses during data transmission through a fiber is one example where new materials and devices are being investigated.<sup>4,5</sup> Raman gain is one method that has been proposed to compensate for these losses.<sup>6-10</sup> Raman gain is a method to amplify optical signals and can be achieved when a pump laser of higher frequency is sent through the fiber superimposed with the data transmission. Under certain conditions the pump laser can transfer some of its energy to the data transmission resulting in amplification of the signal. What makes Raman gain so attractive is that gain can be achieved over a broad and selective wavelength region, existing fibers can be utilized, and the use of fiber optic amplifiers can significantly reduce the cost of the fiber optic network when compared to semiconductor and electrooptic amplifiers that are frequently used in fiber optic networks.

The basic construction of a fiber optic network can quickly become very complicated depending on the application and transmission requirements of the network (Figure 3). The basic configuration of a fiber optic network consists of an electrooptic device where conversion of data transmission from the drive current to optical power takes place. Generation of the optical signal is accomplished with the use of a laser diode, which is coupled into the fiber. The basic design consists of a fiber with a cylindrical axis of symmetry. The fiber is constructed of a core with a high refractive index surrounded by a cladding layer of low refractive index. The difference in refractive index between the two layers guides the light through the fiber when light from inside the fiber is incident at an angle greater than the critical angle, resulting in total internal reflectance at the fiber interface (Figure 4). As the optical data transmission travels down the fiber it is attenuated. Depending on the degree of attenuation and the configuration of the optical network, the signal may be amplified prior to or after detection of the optical signal and

conversion to photocurrent. At the end of the fiber the optical data transmission exits the fiber and is coupled into a photodetector where the light energy is converted to a photocurrent. The photocurrent is then amplified and converted to the proper signal format.

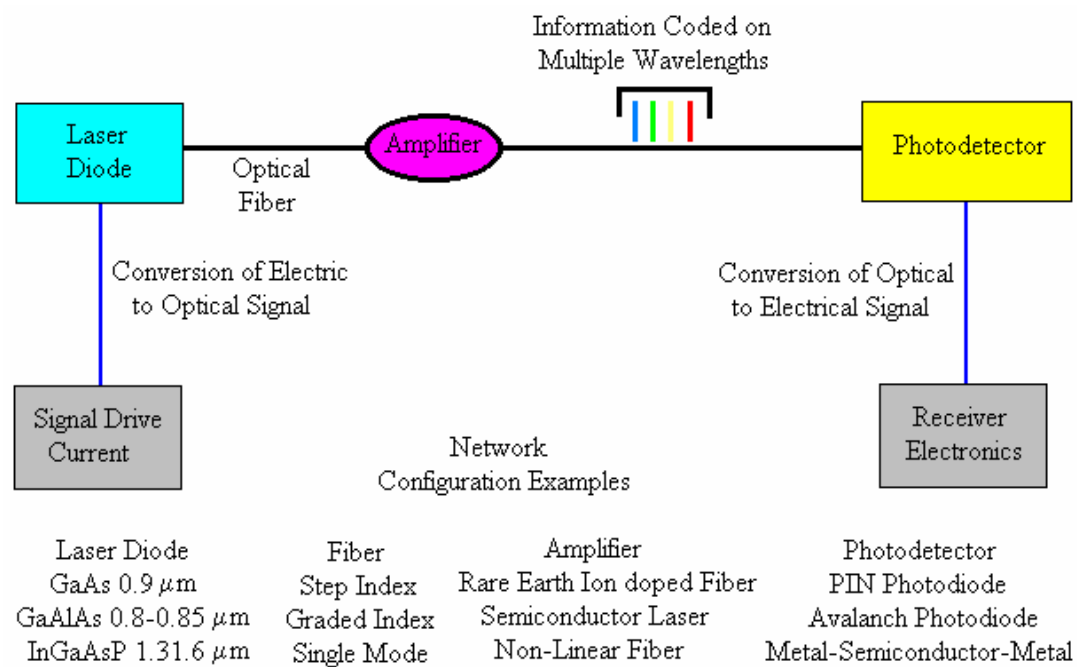


**Figure 3.** Electrooptic configuration for generic fiber optic network.<sup>22</sup>

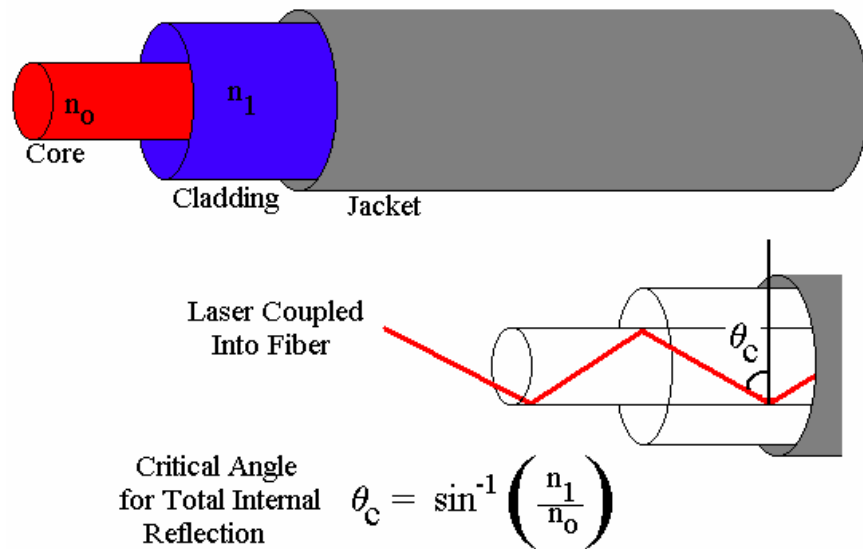


**Figure 4.** Generic optical fiber design.<sup>22</sup>

Fabrication of high quality optical fibers for telecommunications requires precise control of the glass composition in order to fabricate fibers with low impurities and accurate refractive index profiles. High purity silica is the most common material used for fiber optic cables.<sup>2, 11</sup> The use of silica fiber is limited by two main absorption bands in the UV and mid-IR regions (0.8-1.6  $\mu\text{m}$ ) as previously described. The refractive index profile in silica can be adjusted by adding dopants such as  $\text{GeO}_2$  or  $\text{P}_2\text{O}_5$  resulting in an increase of index, or dopants such as  $\text{B}_2\text{O}_3$  or  $\text{SiF}_4$  can be added to lower the refractive index of the silica fiber. There are many different types of fibers fabricated to meet a wide range of applications, including single mode and multi-mode fibers, graded index fibers, and optical amplification fibers to mention a few.

Conventional low-loss silica fiber begins with a large glass preform made of high purity materials with the desired refractive index profile. The glass preform is typically several centimeters in diameter and about one meter in length. The dimensions and dopant distribution in the core and cladding layer are maintained once the fiber is fabricated from the preform. First, the preform is uniformly heated in an electric resistance furnace. Once the melting point of the glass is obtained, thin glass fibers are drawn upwards from the preform in a drawing tower. The diameter of the fiber is controlled by the rate at which the fiber is pulled from the preform and is monitored for thickness by a laser interferometer. Water contamination of the fiber is controlled by passing the fiber through a vat containing a polymer to give it a protective coating. The coated fiber is then spooled evenly onto a 20-centimeter diameter mandrel.

The manufacturing of high quality glass preforms is accomplished primarily by a process called chemical vapor deposition (CVD). Submicron silica particles are deposited in the form of high purity soot onto a silica substrate at 1800 to 2000 °C. The soot is then sintered to form optical quality glass. There are two basic manufacturing techniques commonly used to deposit the soot, called the Inside process and Outside process. There are two variations of the inside process known as the Modified Chemical Vapor Deposition process (MCVD) and the Plasma assisted Chemical Vapor Deposition process (PCVD). In each method the composition is carefully controlled to accomplish the desired refractive index by applying the soot in thin layers. In MCVD depositing and sintering of the deposited  $\text{SiO}_2$  is accomplished at the same time by application of a heat source over a small area on the outside of the silica tube. PCVD provides for very precise control of the preform index profile by depositing the soot by direct RF excitation of a microwave-generated plasma. The microwave field can move very quickly



resulting in multiple thin layers of material. In each of the methods (MCVD, PCVD) a final heating to around 2150 °C is required to collapse the preform into a state from which the glass is ready to be drawn. Two variations of the outside process are known as Outside Vapor Deposition (OVD) and Vapor Axial Deposition (VAD). These two processes are very similar and involve a torch consisting of discrete holes in a pattern of concentric rings, which provide a different constituent element for the chemical reactions.

An alternative method for fabricating glass preforms and optical quality fibers has been demonstrated using sol-gel chemistry.<sup>4, 12</sup> Currently there are two main routes to SiO<sub>2</sub> glass fibers. One method involves the hydrolysis and condensation of silicon alkoxides in the presence of H<sub>2</sub>O, EtOH, and HCl. However, there are several difficulties associated with this process that limits the optical quality of the fibers. Fibers can be directly spun from the viscous sol at or near room temperature. Unfortunately, this method leads to fibers with an abnormal cross-section from an ideal circular shaped fiber to ellipsoidal, dumbbell, and more complex morphologies. The abnormal cross section results from shrinkage of the fibers during the drying process. Another consideration is the tensile strength of sol-gel fibers. The tensile strength of the sol-gel derived fibers have been demonstrated to be lower than commercially available fibers but are still high enough for practical use.<sup>4</sup>

Water content in the sol-gel derived fibers is a major drawback to the potential use in optical applications. The presence of residual OH absorption peaks limits the signal transmission in optical fiber to three transmission windows at approximately 0.85 μm, 1.3 μm, and 1.5 μm. A major advantage to processing sol-gels at room temperature is the ability to dope organic

compounds into the sol-gel matrix.<sup>13, 14</sup> The introduction of organic compounds provides the ability to selectively tailor the optical properties of the glass fiber such as refractive index, absorption, and nonlinear optical properties.<sup>15</sup> Due to some of the physical and chemical problems associated with the low temperature sol-gel process it is not used commercially and is not a feasible alternative to the standard high temperature (2000 °C) fabrication process.

Another technique used to produce optical quality fibers from sol-gel chemistry involves melt-drawing of SiO<sub>2</sub> preforms, used commercially by Bell Labs. This fabrication process of sol-gel preforms leads to fibers with high purity and efficient conversion from raw material to glass fibers. In 1999, Bell Labs scientist, John MacChesney, received the John Tyndall award at the international Optical Fiber Communications conference.<sup>16</sup> He was cited for the invention and development of the MCVD process and for co-inventing high purity sol-gel overcladding for optical fiber with Bell Labs scientist Dave Johnson. A variety of different methods have been used to produce glass preforms for melt-drawing of optical fiber through sol-gel chemistry. One example prepared by Shibata et al. produced a high quality GeO<sub>2</sub> doped silica core fiber from the sol-gel process. A homogeneous sol of Si(OC<sub>2</sub>H<sub>5</sub>)<sub>4</sub> and Ge(OC<sub>4</sub>H<sub>9</sub>)<sub>4</sub> was prepared under basic conditions and cast into a rod shaped mold. The rod was then consolidated into a bubble free transparent glass rod under helium atmosphere at 1250-1350 °C. A silica cladding layer was then applied by CVD and the preform was drawn into optical fiber at 2000 °C. Although this method produces high purity glass preforms, CVD is often needed to apply cladding layers and high temperatures (2000 °C) are still required for sintering and drawing of fiber making it impossible to introduce organic compounds into optical fiber through this method.

Monolithic glass materials are typically prepared by one of three general methods. Under acidic or basic conditions a sol-gel can be prepared from the gelation of colloidal powders. Another method involves the hydrolysis and polycondensation of alkoxide precursors followed by hypercritical drying. Hypercritical drying is a method to remove the pore liquid once the gel point of the sol has been achieved. The pore liquid is removed as a gas phase under hypercritical conditions resulting in an extremely low density areogel. Alternatively, the pore liquid can be removed by thermal evaporation. Removal of the pore liquid by this method results in significant shrinkage of the sol-gel to produce a hard dense xerogel. The term xerogel is applied to dense sol-gels that have been produced using either the first or last general method to produce a sol-gel. The low-density sol-gels produced by hypercritical drying are referred to as areogels. Thermal removal of the pore liquid requires aging and drying of the polymerized gel under ambient atmospheres and results in much longer aging and drying times than hypercritical drying.

Perhaps one of the most attractive features of sol-gel chemistry is the ability to produce an amorphous three dimensional glass network at low temperatures. Unlike high temperature ceramic and glass chemistry, the sol-gel process is frequently done at temperatures below 100 °C. The most common method used involves acid catalyzed hydrolysis and polymerization of metal-organic precursors to form a glass from a liquid medium. The hydrolysis and polymerization processes occur simultaneously. In the early stages of hydrolysis and polymerization the mixture is referred to as a sol. The sol is not a single-phase system, but consists of a suspension of small particles of one phase suspended in a liquid phase. As polymerization continues the small particles begin to form a three-dimensional network referred to as the gel phase. The gel becomes a soft solid capable of maintaining its shape.

The performance of fiber optic data transmission can be degraded by many different mechanisms such as attenuation, source-coupling loss, detector-coupling loss, splice loss, and connector loss. Adjusting core diameter and numerical aperture of the fiber can minimize much of the loss associated with coupling of the optical signal. However, attenuation poses a more significant problem that requires the fabrication of a high quality fiber with a consistent refractive index in both the core and cladding layers and has minimal amounts of impurities. There are several mechanisms that contribute to attenuation alone such as scattering, reflection, and absorption. Rayleigh scattering, for example, is a function of wavelength ( $1/\lambda^4$ ) and results from inconsistencies in the refractive index of the fiber. Absorption due to impurities introduced during fiber fabrication is another source of attenuation. Ultraviolet resonance results from the crystal structure of the atoms. Whereas, the infrared resonance tail is associated with the dopant oxide bonds that are typically found in optical fiber such as Ge-O (11  $\mu\text{m}$ ), P-O (8  $\mu\text{m}$ ), B-O (7.3  $\mu\text{m}$ ), and Si-O (9  $\mu\text{m}$ ). The OH absorption overtone peaks due to the fundamental OH vibration at 2730 nm results in absorption bands at 725, 825, 875, 950, 1130, 1240, and 1390 nm. The need to develop methods to compensate for signal loss in optical fiber results from the many different types of mechanisms that are involved in this process.

There are numerous types of optical amplifiers available to counteract attenuation and increase the transmission distance of an optical link. One common method is to use the optical fiber as an amplifier. Fiber optic amplifiers are fabricated by selectively doping the fibers with rare earth elements that have transition bands in the near infrared spectrum. When these rare earth elements are doped into the fiber they can absorb light from a pumping wavelength which

can subsequently be used to amplify the incident signal. The rare earth elements are specific to the region to which amplification can occur. One of the most common elements doped in silica glass today is erbium, which can amplify signals in the 1550 nm band for communications (Figure 5). Neodymium is efficient around 1360 nm to 1400 nm in silica, and praseodymium is efficient in this same region when it is doped in fluorozirconate glasses and at 1300 nm in chalcogenide glasses. Doping fibers with rare earth elements has been a very effective method to produce fiber optic amplifiers. However, new methods of amplification need to be developed due to the newly expanded telecommunications window spanning the full region of around 1300-1600 nm.

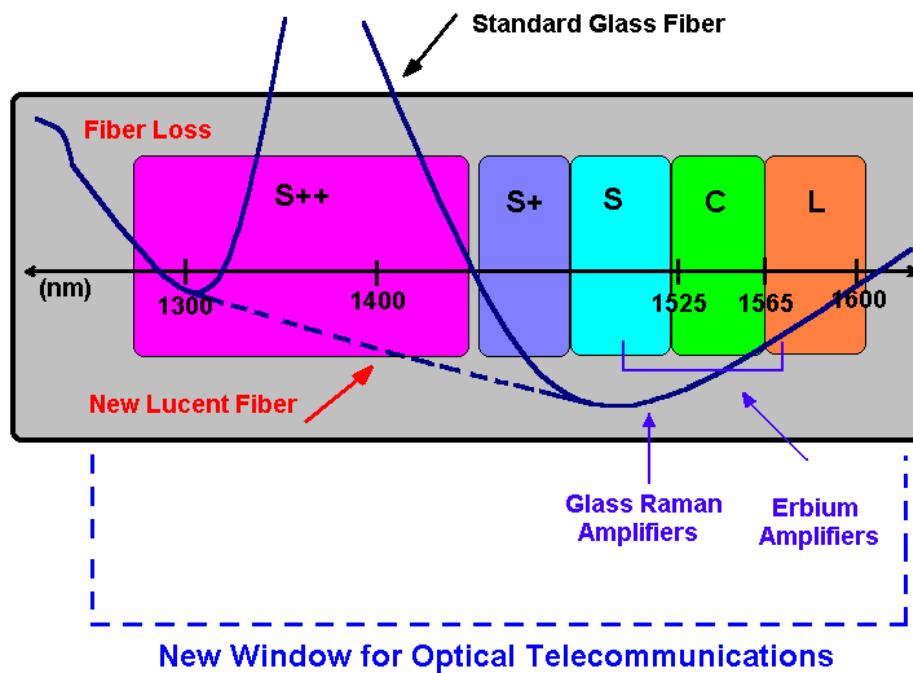


**Figure 5.** Absorption loss in standard glass fiber and Lucent’s Allwave™ fiber.

Raman gain has recently achieved recognition as an alternative method of amplification in fiber optics. Despite its recent gain in popularity, Raman scattering, the process that results in Raman gain, was first discovered in 1928 by Chandrasekhara Venkata Raman. In 1930, he later received the Nobel prize in physics for his work on the scattering of light.<sup>17</sup> Amplification by Raman gain is attractive because existing fibers can be used avoiding costly fabrication of new fibers or devices. It has been demonstrated that Raman gain can be achieved over a broad wavelength region (100 nm) by using multiple pump lasers. In addition to broadband amplification, the wavelength region in which amplification is achieved can be adjusted to the desired region based on the pump lasers. Consequently, the cost and availability of lasers for a particular region may limit its use.

Amplification of fiber optic data transmission by Raman gain results from a process called Raman scattering. The scattering occurs when photons interact with the nuclei of atoms resulting in an excited vibrational level of the nucleus. This process can occur if a sufficiently powerful optical wave can interact with the nuclei such as that of a laser as it passes through an optical fiber. With Raman scattering the electromagnetic radiation is scattered inelastically. The incident electromagnetic field produces a dipole by polarizing the electron cloud of each atom. The radiation that is scattered inelastically results in a new optical wave known as a Stoke's wave and will propagate in the forward direction with the original optical wave. The scattering process results in multiple Stoke's waves rather than a single new wave. Anti-Stoke's wave are also possible resulting in a optical wave of higher frequency, but the statistical possibility of this occurring is much less than that of a Stoke's wave and can be neglected. Consequently, the Raman scattering process produces a broadband frequency shift with respect to the original

optical wave. This broadband Stokes wave is typically frequency downshifted from the original wave by about 12 THz or 100 nm.

Raman gain can be obtained in any conventional optical fiber resulting in amplification of broadband data transmission. Emori and Kado have demonstrated the ability to produce gain-flattened amplification using multi-wavelength pumping in conventional fibers.<sup>6,9</sup> Additionally, Morita, *et al.* demonstrated the use of a hybrid Raman/EDFA for ultra-long-distance 40 Gbit/s based wavelength division multiplexing (WDM) transmission demonstrating the versatility of Raman gain.<sup>8,18</sup> Raman gain is particularly attractive for long-haul transmission in locations such as deep sea transcontinental and remote terrestrial regions that are difficult to access. An important feature of Raman gain is that amplification is distributed over long lengths of fiber from a couple to tens of kilometers. The need for costly electrooptic devices can be reduced or eliminated lowering the cost of the network and the possibility of system failure.

Consequently, Raman gain is an attractive alternative for providing amplification in fiber optic data transmission. The ability to obtain amplification in existing fibers means that it can be implemented immediately with only minor modification to the network such as the addition of pump lasers. Additionally, the flexibility of obtaining broadband amplification over the entire telecommunication window allows for extreme flexibility especially in WDM systems. The use of Raman gain in areas of the network that may be difficult to access can reduce costly repairs and improve the reliability of the network. Despite its limited use currently, Raman gain may become very commonly used as new materials capable of efficient gain become available.

## RESEARCH OBJECTIVE

Relatively little work has been conducted on materials for Raman gain. What has been investigated is based essentially on existing inorganic materials such as GeO<sub>2</sub> doped optical fibers. Consequently, the investigation of organic hybrid materials is of particular interest. High optical quality organic hybrid sol-gels will be prepared from organic compounds possessing functional groups capable of producing strong Raman scattering. Various derivatives of thio-based monomers will be synthesized and evaluated for Raman scattering.

Synthesis of hybrid organic sol-gels will be prepared using a combinatorial approach by preparing multiple samples in small volume, so compounds can be screened for their Raman scattering efficiency and to decrease the processing time needed to obtain a fully polymerized and hardened sol-gel. Organic derivatives will be chosen based on the presence of functional groups known to be strong Raman scattering. Evaluation of dispersed and grafted organic derivatives will be investigated. A general procedure will be prepared to produce hybrid sol-gels of high optical quality free of defects such as bubbles, cracks, inclusions, and phase separation of the organic component within the sol-gel. Raman scattering characterization of thio-based monomers for grafting and dispersion into the sol-gel matrix will be undertaken in addition to the hybrid sol-gels due to the strong Raman scattering of the S-H group. Derivatives of the thio-



based monomers will be prepared from sulfonylbisphenol, isopropylidenediphenol, and triallyloxy triazine. Thiolated derivatives of poly(hydroxystyrene) and brominated poly(hydroxystyrene) will also be investigated.

## EXPERIMENTAL: SYNTHESIS AND CHARACTERIZATION OF ORGANIC HYBRID SOL-GELS AND MONOMERS

Reactions were conducted under N<sub>2</sub> or ambient atmospheres as indicated. THF was distilled over LiAlH<sub>4</sub> before use. All other reagents were used as received from commercial suppliers. FT-IR spectroscopy measurements were obtained on a Perkin-Elmer Model PE-1300 F0241. IR measurements of sol-gels were performed in diffuse reflectance mode or neat in transmittance mode. <sup>1</sup>H NMR was recorded in CDCl<sub>3</sub> or CD<sub>3</sub>COCD<sub>3</sub> on a Varian 300 NMR spectrometer at 300 MHz (referenced to TMS at δ = 0.0 ppm). Chemical shifts of <sup>1</sup>H NMR were interpreted with the assistance of a computer modeling program in CS ChemDraw Ultra version 5.0 by CambridgeSoft Corporation. Raman spectroscopy measurements were obtained on a JY Horiba LabRam Analytical Raman Microscope equipped with a HeNe laser (20 mW, 632.8 nm). All measurements were obtained using a holographic grating (600 g/mm).

*Synthesis of dispersed organically modified sol-gels.* TEOS (0.336 mL, 1.50 mmol), acetone (1.091 mL, 14.9 mmol), and 1 M HCl (0.058 mL, 3.22 mmol H<sub>2</sub>O) were added to nine different (1.7 mL) centrifuge tubes, sealed, and sonicated for 15 min at 40 °C to partially hydrolyze the TEOS. A different monomer was then added to each tube (Table 1) followed by the addition of 1M HCl (0.150 mL, 8.33 mmol H<sub>2</sub>O). The final molar ratio of TEOS/H<sub>2</sub>O/acetone was (1:7:9). The centrifuge tubes were then sealed and sonicated at 50 °C for an additional hour. The tubes containing an organically doped sol-gel were then placed into

individual heating wells in an aluminum heating block and maintained at a constant 50 °C to complete the polymerization process. After 48 h the lid of each tube was loosened to help promote solvent evaporation. After 3 d all solvent and water had evaporated to give fully polymerized dense sol-gels.

**Table 1.** Dispersed organic monomers used in sol-gel synthesis.

Monomer	Amount (g)	Weight %
<b>1</b> 2-Methyl-3-butyn-2-ol	0.013	1
<b>2</b> Octadecane thiol	0.043	3
<b>3</b> Disperse red-19	0.005	0.4
<b>4</b> 2,2',4,4',4''-Pentamethoxy-triphenylmethanol	0.062	4
<b>5</b> 1,5-Pentanediol	0.016	1
<b>6</b> 2-(N-ethylanilino)ethanol	0.029	2
<b>7</b> Pentaerythritol triallyl ether	0.038	3
<b>8</b> Hydroxypropyl acrylate	0.020	1
<b>9</b> Mercaptophenol	0.019	1

---

All monomers were 0.15 mmol  
DR-19 was 0.015 mmol

*Synthesis of grafted organically modified sol-gels.* Modified organic monomers were prepared by reacting the monomer directly to the precursor of the sol-gel through a urethane forming reaction. Monomers (Table 2) were placed in glass vials (5.0 mL) and dry THF (1.0 mL) was added. 3-(Trimethoxysilyl)propylisocyanate was added in the same molar amount as each monomer. The reaction vials were sealed and sonicated for 3 h at 50 °C. Completion of the urethane reaction was confirmed using IR spectroscopy with the disappearance of the characteristic peak of the hydroxyl group of the monomer around 3500 cm<sup>-1</sup>.

**Table 2.** Grafted organic monomers used in sol-gel synthesis.

Monomer	Amount (g)	Weight %
<b>10, 11</b> 2-Methyl-3-butyn-2-ol	0.013 0.051	1 1
<b>12, 13</b> Octadecane thiol	0.043 0.172	3 5
<b>14, 15</b> Disperse red-19	0.005 0.005	0.4 0.4
<b>16, 17</b> 2,2',4,4',4''-Pentamethoxy-triphenylmethanol	0.062 0.248	5 7
<b>18, 19</b> 1,5-Pentanediol	0.016 0.064	1 2
<b>20, 21</b> 2-(N-ethylanilino)ethanol	0.025 0.100	2 3
<b>22, 23</b> Pentaerythritol triallyl ether	0.038 0.154	3 4
<b>24, 25</b> Hydroxypropyl acrylate	0.020 0.079	2 2
<b>26, 27</b> Mercaptophenol	0.019 0.076	1 2

---

All monomers were 0.15 mmol and 0.60mmol. DR-19 was 0.015 mmol

The copolymerization of the grafted monomers with TEOS was accomplished by transferring the grafted monomers in THF into centrifuge tubes (2.0 ml) and adding TEOS (0.336 mL, 1.5 mmol). HCl (1M) was added to all tubes, keeping the molar ratio of TEOS/H<sub>2</sub>O/THF (1:7:7) constant. Addition of 1M HCl to tubes containing 0.15 mmol of monomer received 0.208 mL 1M HCl (11.6 mmol H<sub>2</sub>O), and tubes containing 0.60 mmol monomer received 0.265 mL 1M HCl (14.7 mmol H<sub>2</sub>O). The two tubes containing 0.015 mmol of monomer received 0.191 mL 1M HCl (10.6 mmol H<sub>2</sub>O). The centrifuge tubes were sealed and sonicated for 90 min at 50 °C, then placed in individual heating wells in an aluminum heating block maintained at a constant 50 °C for 3 d. After which the lid of each tube was loosened to help promote solvent evaporation. After a total of 10 d all solvent and water had evaporated to give fully polymerized dense sol-gels.

*Synthesis of reference sol-gel (28).* TEOS (4.0 mL, 18 mmol), EtOH (9.0 mL, 161 mmol), and 1 M HCl (2.3 mL, 128 mmol H<sub>2</sub>O) (1:9:7 TEOS, H<sub>2</sub>O, EtOH) were added to a three-necked round bottom flask equipped with a condenser and brought to reflux temperature for 15 min. The sol was then transferred to a disposable test tube, sealed, and placed in an oil bath at 45-50 °C. After 24 h the tube was unsealed and left in the oil bath at 45 °C to complete the polymerization process. Fourteen days later the fully polymerized sol-gel was removed from the oil bath resulting in a clear fully hardened sol-gel. The final sample shrunk 74% from its original volume.

*Synthesis of reference sol-gel (29).* The reference sol-gel was prepared by doping it with 5 mol% 3-(trimethoxysilyl)propylisocyanate. TEOS (2.0 mL, 8.9 mmol), 3-(trimethoxysilyl)propylisocyanate (0.10 mL, 0.45 mmol), EtOH (3.2 mL, 56 mmol), and 1 M HCl (1.7 mL, 94 mmol H<sub>2</sub>O) (1:10:6 monomer, H<sub>2</sub>O, EtOH) were added to a 15 mL vial equipped with a magnetic stir bar. The vial was sealed and stirred for 1 h at room temperature. The sol was then transferred to a disposable test tube, sealed, and left at room temperature to complete the polymerization process. Seventeen days later the fully polymerized sol-gel was removed to give a clear, fully hardened sol-gel.

*Synthesis of reference sol-gel (30).* The reference sol-gel was prepared by doping it with 10 mol% 3-(trimethoxysilyl)propylisocyanate. TEOS (2.0 mL, 8.9 mmol), 3-(trimethoxysilyl)propylisocyanate (0.22 mL, 0.89 mmol), EtOH (3.3 mL, 59 mmol), and 1 M HCl (1.8 mL, 98 mmol H<sub>2</sub>O) (1:10:6 monomer, H<sub>2</sub>O, EtOH) were added to a 15 mL sealed vial equipped with a magnetic stir bar and stirred for 1 h at room temperature. The sol was then transferred to a sealed disposable test tube and left at room temperature to complete the polymerization process. Fifteen days later the fully polymerized sol-gel was removed to give a clear fully hardened sol-gel.

*Synthesis of 1,1'-Sulfonylbis[4-(2-propenyloxy)benzene] (31).* 4,4'-Sulfonyldiphenol (10.0 g, 0.040 mol) and tetraphenylphosphonium bromide (0.90g, 0.002 mol) were added to a 500 mL 3-necked flask fitted with N<sub>2</sub> inlet, stir bar and stopper. Aqueous KOH (75 mL, 1.3M) was added to the flask followed by allyl bromide (8.5 ml, 0.096 mol) in CH<sub>2</sub>Cl<sub>2</sub> (80 mL). The reaction mixture was stirred at room temperature for 24 h. TLC analysis (3:2 hexanes/THF) indicated the reaction was complete by the disappearance of the starting material and formation

of a single new spot. The aqueous layer was then extracted thrice with CH<sub>2</sub>Cl<sub>2</sub> (75 mL). The combined organic layer was washed once with deionized water (150 mL). The organic solvent was then removed using a rotovap to give a white solid. The phosphonium bromide catalyst was removed by gravity filtration after dissolving the product in THF. The solution was dried with anhydrous MgSO<sub>4</sub>, filtered, and then the THF was removed under reduced pressure. The crude white product was recrystallized twice in absolute ethanol, resulting in 11.4 g (86 % yield) of shiny white flakes (mp = 139-141 °C, lit. 141-142 °C).<sup>20</sup> <sup>1</sup>H NMR (300 MHz, CD<sub>3</sub>COCD<sub>3</sub>) (Figure 9) δ 4.6 (d, *J* = 5.2 Hz, 2 H), 5.2 (d, *J* = 10.6 Hz, 2 H), 5.4 (d, *J* = 17.8 Hz, 2 H), 6.1 (m, 1 H), 7.1 (d, *J* = 8.7 Hz, 2 H), 7.8 (d, *J* = 8.9 Hz, 2 H).

*Synthesis of 1,1'-Sulfonylbis[4-(3-acetylsulfanyl-propoxy)benzene] (32).* 1,1'-Sulfonylbis[4-(2-propenyloxy)benzene] (**31**) (34.8 g, 0.11 mol) was added to 150 mL dichlorobenzene and dissolved at 80 °C in a 500 mL 3-necked flask equipped with a condenser, N<sub>2</sub> inlet, stir bar, and stopper. Thiolacetic acid (36 mL, 0.51 mol) was added to the flask drop wise over 2-3 min from an addition funnel. AIBN (1.26 g, 7.7 mmol) was divided into 4 equal portions and added at 20 min intervals. Two additional portions of AIBN (0.316 g, 1.9 mmol) were added at 24 and 36 h into the reaction. After 2 d another portion of thiolacetic acid (10.5 ml, 0.15 mol) and AIBN (0.70 g, 4.3 mmol) were added to the mixture. Completion of the reaction was monitored by TLC (3:2 hexanes/THF) and was determined to be complete after 4 d. Dichlorobenzene and unreacted thiolacetic acid were removed by short-pass distillation at reduced pressure (0.7 mmHg) to give a viscous clear red oil. The final product crystallized after several days in a stoppered flask resulting in 29.1 g (57% yield) of dark orange crystals. <sup>1</sup>H NMR

(300 MHz, CDCl<sub>3</sub>) (Figure 10)  $\delta$  2.1 (quint,  $J = 6.8$  Hz, 2 H), 2.3 (s, 3 H), 3.0 (t,  $J = 7.0$  Hz, 2 H), 4.0 (t,  $J = 6.1$  Hz, 2 H), 6.9 (d,  $J = 9.0$  Hz, 2 H), 7.8 (d,  $J = 8.9$  Hz, 2 H).

*Synthesis of 1,1'-Sulfonylbis[4-(3-thiol-propoxy)benzene] (33).* 1,1'-Sulfonylbis[4-(3-acetylsulfanyl-propoxy)benzene] (**32**) (27.48 g, 0.057 mol) was dissolved in toluene (50 mL). The mixture was then added to a 3-necked flask equipped with a 9 in fractional distillation column, condenser, stir bar, and stopper. EtOH (50 mL) and an HCl/methanol solution (100 mL, 10% v/v) were added to the flask. The temperature of the mixture was brought to reflux temperature. After 20 h the reaction was checked by NMR and was determined to be complete. Toluene and any excess EtOH and acidic methanol were removed by rotavap to give a brownish-red semi-solid material. The compound was then dissolved in THF (250 mL) and extracted twice with saturated NaHCO<sub>3</sub> (100 mL). The aqueous layer was then extracted thrice with THF (50 mL). The combined organic layer was then washed 3 times with brine (50 mL). The organic layer was dried with MgSO<sub>4</sub>, and solvent was removed. The crude product (32.47 g) was a yellow semi-solid material. The impure compound was passed through a Si-gel column using chloroform as the mobile phase. Removal of chloroform by rotovap resulted in a white semi-transparent oil (17.2 g/ 76% yield). <sup>1</sup>H NMR (300 MHz, CDCl<sub>3</sub>) (Figure 11)  $\delta$  2.0 (quint,  $J = 6.4$  Hz, 2 H), 2.7 (quart,  $J = 6.9$  Hz, 2 H), 2.8 (t,  $J = 6.9$  Hz, 1 H), 4.1 (t,  $J = 6.0$  Hz, 2 H), 6.9 (d,  $J = 8.6$  Hz, 2 H), 7.8 (d,  $J = 8.8$  Hz, 2 H).

*Synthesis of 1,1'-isopropylbis[4-(2-propenyloxy)benzene] (34).* 4,4'-isopropylidenediphenol (36.5 g, 0.16 mol) and tetraphenylphosphonium bromide (0.3.4 g, 0.008 mol) were added to a 500 mL 3-necked flask fitted with N<sub>2</sub> inlet, stir bar, and stopper. Aqueous



NaOH (300 mL, 1.3M) was added to the flask followed by allyl bromide (33 ml, 0.38 mol) in CH<sub>2</sub>Cl<sub>2</sub> (300 mL). The reaction mixture was stirred at room temperature for 24 h. TLC analysis (3:2 hexanes/THF) indicated the reaction was complete by the disappearance of the starting material and formation of a single new spot. The aqueous layer was then extracted thrice with CH<sub>2</sub>Cl<sub>2</sub> (75 mL). The combined organic layer was washed once with deionized water (150 mL). The organic solvent was then removed using a rotovap to give a cloudy viscous oil. The phosphonium bromide catalyst was precipitated and removed by gravity filtration after dissolving the product in THF. The solution was dried with anhydrous magnesium sulfate, filtered, and then the THF was removed under reduced pressure. The crude oily product was passed through a short plug (300 mL, 8M) of basic alumina (3:2 hexanes/THF). The compound was passed a second time through a new plug of basic alumina using chloroform. Compound **34** was determined by TLC (3:2 hexanes/THF) and NMR to be pure, resulting in a clear transparent liquid (48.6 g, 97% yield). <sup>1</sup>H NMR (300 MHz, CD<sub>3</sub>COCD<sub>3</sub>) (Figure 13) δ 1.6 (s, 3 H), 4.5 (d, *J* = 5.2 Hz, 2 H), 5.1 (d, *J* = 10.5 Hz, 1 H), 5.4 (d, *J* = 17.2 Hz, 1 H), 6.0 (m, 1 H), 6.8 (d, *J* = 8.8 Hz, 2 H), 7.1 (d, *J* = 8.9 Hz, 2 H).

*Synthesis of 1,1'-isopropylbis[4-(3-acetylsulfanyl-propoxy)benzene] (35).* 1,1'-Isopropylbis[4-(2-propenyloxy)benzene] (**34**) (22.5 g, 0.073 mol) was placed neat in a 100 mL 3-necked flask equipped with a condenser, N<sub>2</sub> inlet, stir bar, and stopper. Thiolacetic acid (25 mL, 0.35 mol) was added to the flask drop-wise over 2-3 min from an addition funnel and temperature was brought up to 80 °C. AIBN (0.84 g, 5.0 mmol) was divided into 4 equal portions and added at 30 min intervals. The reaction was determined by TLC (3:2 hexanes/THF)

to be complete after 24 h. Excess thiolacetic acid was removed by short pass distillation. The final product (33.4 g, 99% yield) was a dark red-orange oil. <sup>1</sup>H NMR (300 MHz, CD<sub>3</sub>COCD<sub>3</sub>) (Figure 14) δ 1.6 (s, 3 H), 2.0 (quint, *J* = 6.9 Hz, 2 H), 2.3 (s, 3 H), 3.0 (t, *J* = 7.1 Hz, 2 H), 4.0 (t, *J* = 6.1 Hz, 2 H), 6.8 (d, *J* = 8.8 Hz, 2 H), 7.1 (d, *J* = 8.9 Hz, 2 H).

*Synthesis of 1,1'-isopropylbis[4-(3-thiol-propoxy)benzene] (36).* 1,1'-Isopropylbis[4-(3-acetylsulfanyl-propoxy)benzene] (**35**) (33.4 g, 0.072 mol) was dissolved in toluene (50 mL). The mixture was then added to a 3-necked flask equipped with a 9 in fractional distillation column, condenser, stir bar, and stopper. EtOH (50 mL) and an HCl/methanol solution (100 mL, 10% v/v) were added to the flask. The temperature of the mixture was brought to reflux temperature. After 5 d, the reaction was checked by NMR and was determined to be complete. Toluene and any excess ethanol and acidic methanol were removed by short pass distillation to give a sticky orange solid material (25.6 g, 95% yield). <sup>1</sup>H NMR (300 MHz, CDCl<sub>3</sub>) (Figure 15) δ 1.4 (t, *J* = 8.1 Hz, 1 H), 1.6 (s, 3 H), 2.1 (quint, *J* = 6.2 Hz, 2 H), 2.7 (quart, *J* = 7.3 Hz, 2 H), 4.1 (t, *J* = 5.8 Hz, 2 H), 6.8 (d, *J* = 8.6 Hz, 2 H), 7.1 (d, *J* = 8.5 Hz, 2 H).

*Attempted synthesis of 2,4,6-(3-acetylsulfanyl-propoxy)-1,3,5-triazine (37).* 2,4,6-Triallyloxy-1,3,5-triazine (32.4 g, 0.13 mol) was dissolved in benzene (120 mL) and placed in a 500 mL 3-necked flask equipped with a condenser, N<sub>2</sub> inlet, stir bar, and stopper. Thiolacetic acid (67 mL, 0.94 mol) was added to the flask drop-wise over several min from an addition funnel and the temperature was brought up to 80 °C. AIBN (2.3 g, 0.014 mol) was divided into 4 equal portions and added at 20-30 min intervals. After 5 h another portion of AIBN (0.529 g, 0.003 mol) was added. The reaction mixture was clear, light yellow, and viscous. The progress of

the reaction was monitored by TLC (3:2 hexanes, THF) and the use of a strong oxidizing stain (p-anisaldehyde). The reaction was stopped after 21 h once all of the starting material had disappeared. The clear yellow and viscous semi solid material was cooled to room temperature and extracted twice with aqueous NaOH (150 mL, 10% v/v) followed by two extractions with brine (150 mL). Benzene was then removed by short pass distillation to give a highly viscous tan semi-solid material (186 g). The final product was found to be insoluble in most organic solvents with the exception of being only slightly soluble in DMSO.

*Synthesis of 2,4,6-(3-acetylsulfanyl-propoxy)-1,3,5-triazine (37).* AIBN (3.0 g, 0.018 mol) was added to thiolacetic acid (87 ml, 1.22 mol) in benzene (75 mL) to a 500 mL 3-necked flask equipped with a condenser, N<sub>2</sub> inlet, stir bar, and stopper. The temperature of the mixture was increased to 75 °C. Triallyloxy-1,3,5-triazine (42.5 g, 0.17 mol) was dissolved in benzene (75 mL) and was added to the flask containing the AIBN and thiolacetic acid over 24 min through an addition funnel. The reaction was monitored by TLC (3:2 hexanes, THF) and the use of a strong oxidizing stain (p-anisaldehyde). The reaction was stopped after 48 h once all starting material had been consumed. Solvent was removed by rotovap at 50 °C to give a viscous amber colored oil. After several days the product crystallized while in a sealed flask to give needle-like crystals. The crystals were filtered and dried under reduced pressure (81.9 g, 91% yield). <sup>1</sup>H NMR (300 MHz, CDCl<sub>3</sub>) (Figure 18) δ 2.1 (quint, *J* = 6.6 Hz, 2 H), 2.3 (s, 3 H), 3.0 (t, *J* = 7.1 Hz, 2 H), 4.4 (t, *J* = 6.2 Hz, 2 H).

*Synthesis of 2,4,6-(3-thiol-propoxy)-1,3,5-triazine (38).* 2,4,6-(3-Acetylsulfanyl-propoxy)-1,3,5-triazine (**37**) (91.4 g, 0.19 mol) was dissolved in toluene (50 mL) to which EtOH (50 mL) and an HCl/methanol solution (100 mL, 10% v/v) were added. The mixture was placed in a 500 mL 3-necked flask equipped with a 9 in fractional distillation column, condenser, stir bar, and stopper. The temperature of the mixture was brought to reflux temperature. After 24 h the reaction was checked by NMR and was determined to be complete. The solution was cooled to room temperature resulting in a clear yellow solution containing cyanuric acid (mp = 360 °C, lit. > 360 °C) (Figure 16) in the form of a white precipitate.<sup>20</sup> The remaining solvent was removed by short pass distillation at 60 °C to give a yellow semi-solid material. The crude product was dissolved in CH<sub>2</sub>Cl<sub>2</sub>, affording a clear yellow solution with a white precipitate at the bottom of the flask. The mixture was washed twice with saturated NaHCO<sub>3</sub> (150 mL) followed by deionized water (150 mL). The organic layer was dried with MgSO<sub>4</sub> and passed through a gravity filter to remove the white precipitate byproduct and drying agent. CH<sub>2</sub>Cl<sub>2</sub> was removed by rotovap to give a clear yellow oil (54.8 g, 60% yield). <sup>1</sup>H NMR (300 MHz, CDCl<sub>3</sub>) (Figure 19) δ 1.9 (quint, *J* = 6.7 Hz, 2 H), 2.8 (t, *J* = 7.1 Hz, 2 H), 3.7 (t, *J* = 6.1 Hz, 2 H).

*Synthesis of poly(4-vinylphenol) (39).* Poly(4-hydroxyphenol) (10.21 g, 0.084 mol) and tetraphenylphosphonium bromide (1.76 g, 0.42 mmol) were added to a 500 mL 3-necked flask fitted with N<sub>2</sub> inlet, stir bar, and stopper. Aqueous NaOH (200 mL, 1.0M) was added to the flask, followed by allyl bromide (17.4 mL, 0.200 mol) in CH<sub>2</sub>Cl<sub>2</sub> (200 mL). The reaction mixture was stirred at room temperature for 7 d. Completion of the reaction was determined by NMR. The reaction mixture was extracted twice with aqueous HCl (75 mL, 10 % v/v). The organic layer

was then extracted thrice with  $\text{CH}_2\text{Cl}_2$  (50 mL). The combined organic layer was washed once with deionized water (150 mL). The organic solvent was then removed using a rotovap to give a clear yellow viscous oil. The phosphonium bromide catalyst was precipitated and removed by gravity filtration after dissolving the product in THF. The solution was dried with anhydrous magnesium sulfate, filtered, and then the THF was removed under reduced pressure to give a brown crude solid. The crude polymer was dissolved in a small amount of THF (15 mL) and precipitated in cold methanol. The precipitate was gravity filtered and dried to give a tan powder (11.8 g, 87% yield).  $^1\text{H}$  NMR (300 MHz,  $\text{CD}_3\text{COCD}_3$ ) (Figure 21)  $\delta$  2.9 (s, 1 H), 4.5 (s, 2 H), 5.2 (s, 1 H), 5.4 (s, 1 H), 6.1 (s, 1 H), 6.7 (s, 4 H).

*Attempted synthesis of poly[4-(3-acetylsulfanyl-propoxy)-phenol] (40).* Poly(4-vinylphenol) (**39**) was dissolved in benzene (100 mL) and placed in a separatory funnel. Thiolacetic acid (15 mL, 0.202 mol) and benzene (100 mL) were added to a 500 mL 3-necked flask equipped with a condenser,  $\text{N}_2$  inlet, stir bar, and stopper. The temperature of the mixture was increased to 75 °C and was followed by the addition of AIBN (0.49 g, 0.003 mol). Poly(4-vinylphenol) in benzene was added through an addition funnel over 40 min to the flask containing thiolacetic acid and AIBN. The reaction was checked by NMR and stopped after 3 d.  $\text{CH}_2\text{Cl}_2$  (150 mL) was added to the reaction mixture, and the polymer was then washed with 4 portions saturated  $\text{NaHCO}_3$  (150 mL) and twice with deionized water (150 mL). The organic layer was extracted twice with  $\text{CH}_2\text{Cl}_2$  (75 mL) and dried with  $\text{MgSO}_4$ . The drying agent was removed by gravity filtration and the solvent was removed with the rotovap.

*Synthesis of poly(4-vinylphenol) brominated (41).* Poly(4-hydroxyphenol) brominated (35.4 g, 0.18 mol) and tetraphenylphosphonium bromide (3.8 g, 9.0 mmol) were added to a 500 mL 3-necked flask fitted with N<sub>2</sub> inlet, stir bar, and stopper. Aqueous NaOH (200 mL, 1.0 M) was added to the flask followed by allyl bromide (38 mL, 0.43 mol) in CH<sub>2</sub>Cl<sub>2</sub> (200 mL). The reaction mixture was stirred at room temperature for 6 d. Completion of the reaction was determined by NMR. The reaction mixture was washed twice with aqueous HCl (50 mL, 10 % v/v). The organic layer was then extracted thrice with CH<sub>2</sub>Cl<sub>2</sub> (50 mL). The combined organic layer was then washed once with deionized water (150 mL). The organic solvent was then removed using a rotovap to give a soft brown solid. The phosphonium bromide catalyst was precipitated and removed by gravity filtration after dissolving the product in acetone. Acetone was removed using a rotovap to give a brown crude solid. The crude polymer was precipitated twice when it was dissolved in a small amount of THF (10 mL) and precipitated in cold methanol. The precipitate was gravity filtered and dried to give a tan powder (29.9 g, 72% yield). <sup>1</sup>H NMR (300 MHz, CD<sub>3</sub>COCD<sub>3</sub>) (Figure 23) δ 2.9 (s, 1 H), 4.5 (s, 2 H), 5.3 (s, 1 H), 5.5 (s, 1 H), 6.1 (s, 1 H), 6.9 (s, 2 H).

## RESULTS AND DISCUSSION OF SOL-GELS AND MONOMERS

The synthesis and characterization of a series of sol-gel composites containing dispersed or grafted organic monomers will be discussed. Additionally, the synthesis and characterization of various functionalized monomers will be included for their potential use in hybrid organic sol-gels. Dispersion of organic monomers was chosen to facilitate rapid synthesis of multiple hybrid sol-gels. The sol-gels were prepared in small volume (< 2 mL) to decrease processing time using a combinatorial or parallel synthesis approach (Figure 6). The small samples allowed for convenient characterization of Raman scattering since they fit easily onto the microscope stage. Grafting of the organic monomers via a urethane linkage was chosen to see if better control of monomer incorporation could be achieved while at the same time obtaining the added benefit of the urethane functional group which is known to be strongly Raman scattering. Scattering frequencies and relative signal strengths for several functional groups are listed in Table 3.

Four primary molecular architectures were investigated to evaluate the capability of preparing the functionalized derivatives efficiently and to evaluate the Raman scattering for each of the derivatives based on different molecular architectures. Derivatives of a bis phenyl ring system were prepared from sulfonylbisphenol and isopropylidenediphenol (Bisphenol-S and Bisphenol-A), each resulting in difunctional derivatives. A third architecture was evaluated incorporating a single ring system based on triazine, resulting in trifunctional derivatives. Two additional series of derivatives were produced utilizing poly(4-hydroxystyrene) and brominated

poly(4-hydroxystyrene). Consequently, this resulted in five different series of monomers. The thio based derivatives were chosen due to the strong Raman scattering bands around 2600, 1150, 1100, and 500-700  $\text{cm}^{-1}$  due to the S-H, S=O, C-S, and S-S stretching modes respectively.

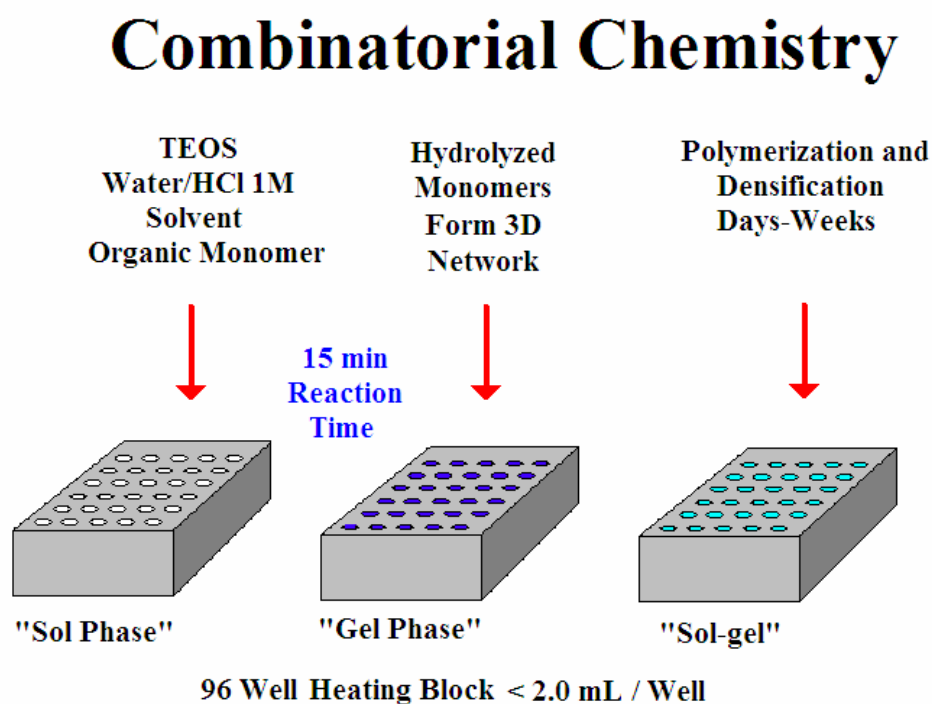


**Figure 6.** Synthetic approach for multiple sol-gel samples.



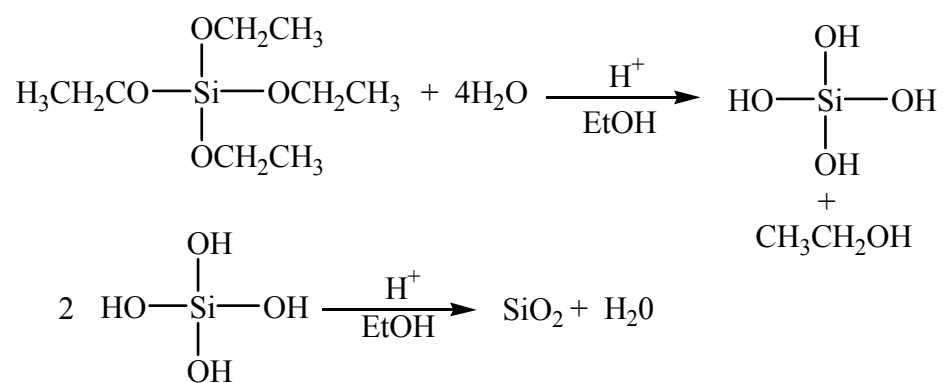
**Table 3.** Raman Scattering Frequencies for Common Functional Groups.

Functional Group	Intensity	Vibrational Frequency ( $\text{cm}^{-1}$ )
Alkane (CH)	m-s	2970-2840
Alkene (CH)	m	3096-3012
(CC)	v	1681-1621
Alkyne (CH)	s	3345-3295
(CC)	s	2265-2020
Aromatic (CH)	v	3030
(CC)	v	1640-1580
Thiol (SH)	s	2597-2551
(CS)	s	700-650
Thio carbonyl (C=S)	s	1200-1050
Sulfones (S=O)	s	1160-1140
	s	1350-1300
Azo (N=N)	v	1629-1575
Urethane carbonyl (C=O)	s	1739-1689
Aromatic Nitro (CNO <sub>2</sub> )	s	1570-1499
Aliphatic Nitro (CNO <sub>2</sub> )	s	1379-1370
Siloxane (Si-O-Si)	m-s	450-500

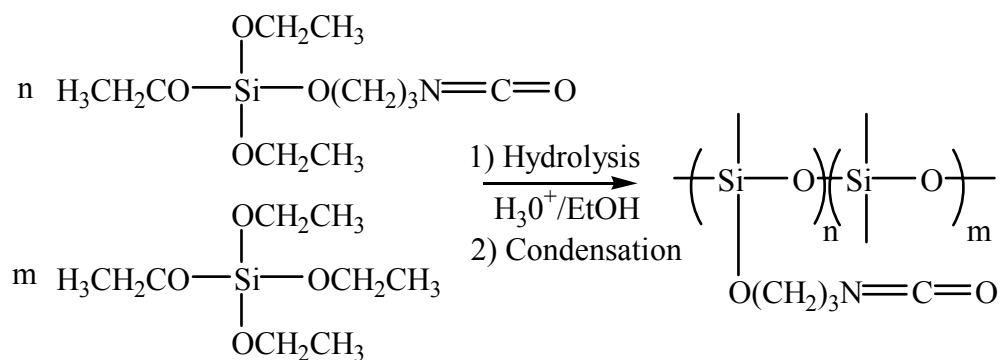
m = Medium, s = Strong, v = Very Strong

Characterization of sol-gel samples was accomplished using IR spectroscopy neat and in diffuse reflectance mode. Characterization of all monomer derivatives was accomplished using NMR and, for appropriate compounds, melting point. Raman scattering of all sol-gels and monomers was performed. Preliminary Raman gain data and laser damage threshold was obtained for a select sol-gel sample, and will be discussed briefly at the beginning of the discussion for Raman scattering.

Sol-gel **28** was synthesized (Scheme 1) to serve as a model compound for the dispersed monomer sol-gel series. Two other model compounds were prepared for the grafted monomer sol-gel series (Scheme 2). In all acid catalyzed sol-gel reactions, both the hydrolysis and condensation reactions occur simultaneously rather than two separate reactions. The model sol-gels (**28-30**) resulted in clear transparent rod like samples. Each sample shrunk by more than 70% from its original volume once it had fully polymerized into a hard dense sol-gel. The model compounds possessed good optical quality free of cracks and inclusions and were long cylindrical rods (3 mm x 1.5 mm). Samples **29** and **30** were only characterized for their Raman scattering efficiency due to their geometric configuration. These sol-gels did not have flat parallel surfaces which are required for Raman gain measurements. A complete discussion of Raman scattering of select samples and Raman gain obtained from sol-gel **28** will be discussed later.

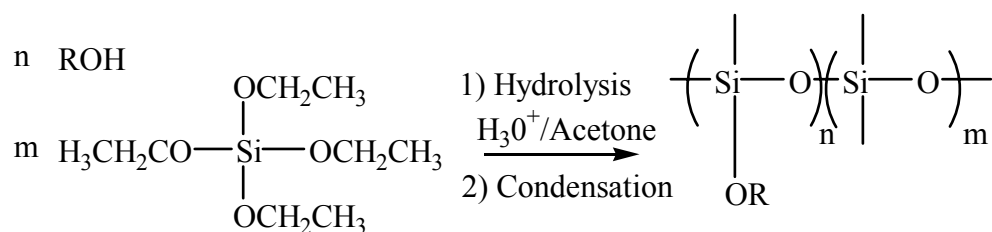


**Scheme 1.** Synthesis of model sol-gel **28**.



**Scheme 2.** Synthesis of model sol-gel **29, 30**.

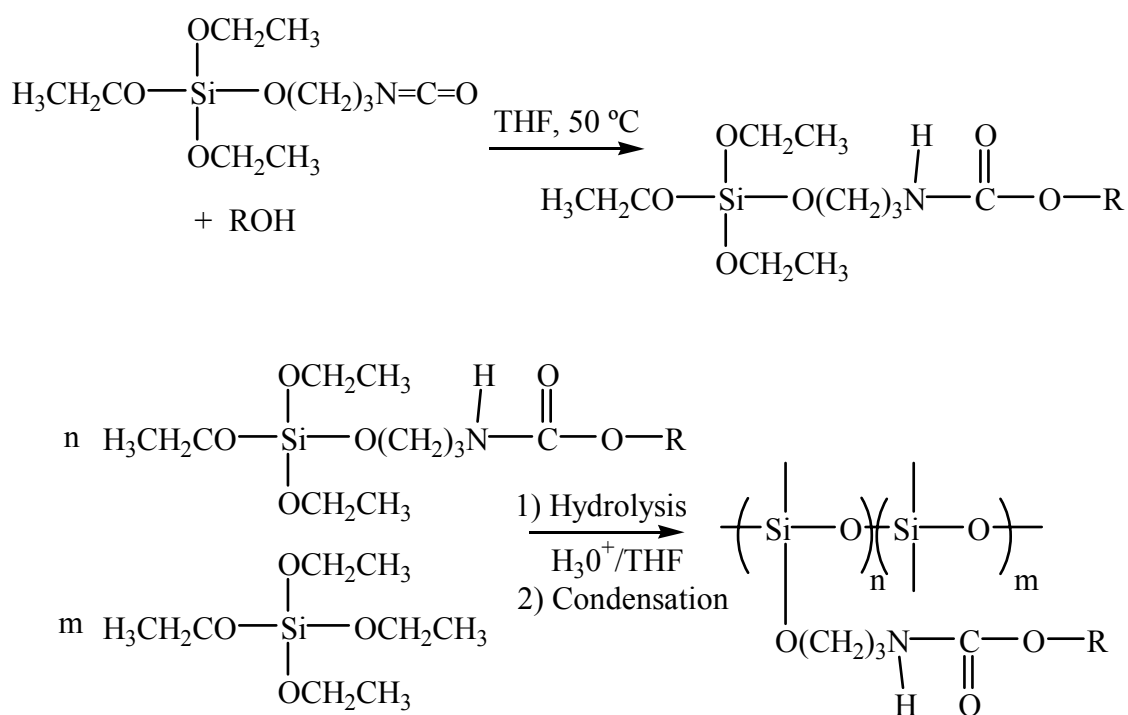
Doped sol-gels obtained by dispersing the monomer into the sol-gel matrix (Scheme 3) resulted in dense hard samples. A small centrifuge tube (1.7 mL) was used for each of the doped sol-gels. Small cone shaped samples (< 0.25 mL) were formed after they were fully polymerized. Each sol-gel was very hard and optically clear. The monomers used in sol-gels **1** and **4** (2-methyl-3-butyn-2-ol, 2,2',4,4',4''-pentamethoxy-triphenylmethanol) precipitated out of solution during the sol phase of the synthesis and did not form a sol-gel. It appeared that these samples were very reactive with TEOS and quickly formed colloidal particles resulting in the formation of the precipitate.



**Scheme 3.** Synthesis of dispersed monomer sol-gels **1-9**.

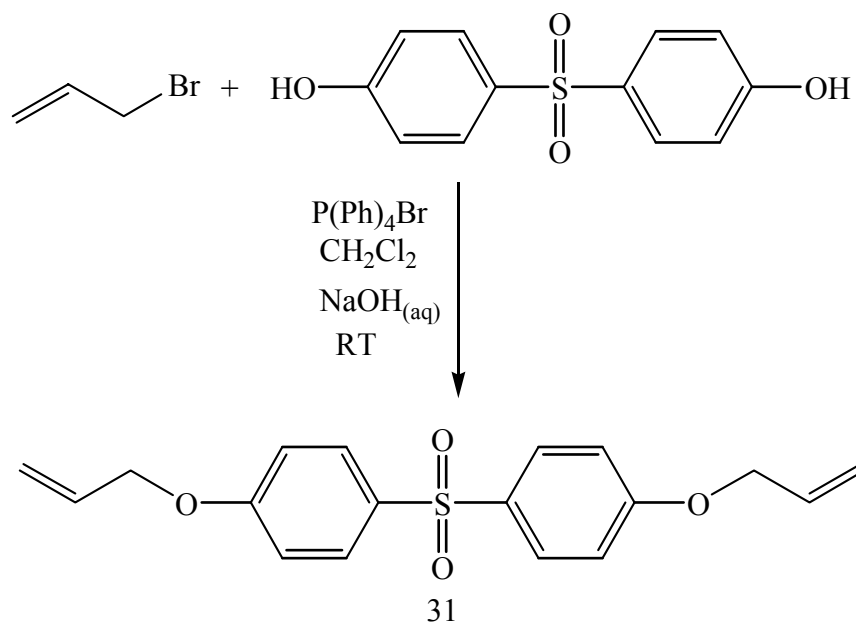
Grafting of the monomer into the sol-gel using 3-(trimethoxysilyl)propyl isocyanate eliminated the problem of precipitation of the monomer by physically attaching the monomer through a urethane type of linkage (Scheme 4). Precipitation is avoided because the silyl compound becomes chemically inactive once it reacts with the organic monomer under dry conditions. TEOS has four ethoxy groups that can undergo hydrolysis and condensation with the organic monomer as well as with other molecules of TEOS. As a result, TEOS can form low

molecular weight aggregates with the organic monomer which precipitate out of solution. This was avoided by simply reacting the monomer with the isocyanate group in dry THF at elevated temperatures to form the urethane linkage. The reaction was monitored by the disappearance of the characteristic OH stretching frequency ( $3500\text{ cm}^{-1}$ ) of the alcohol using IR spectroscopy (Appendix B).



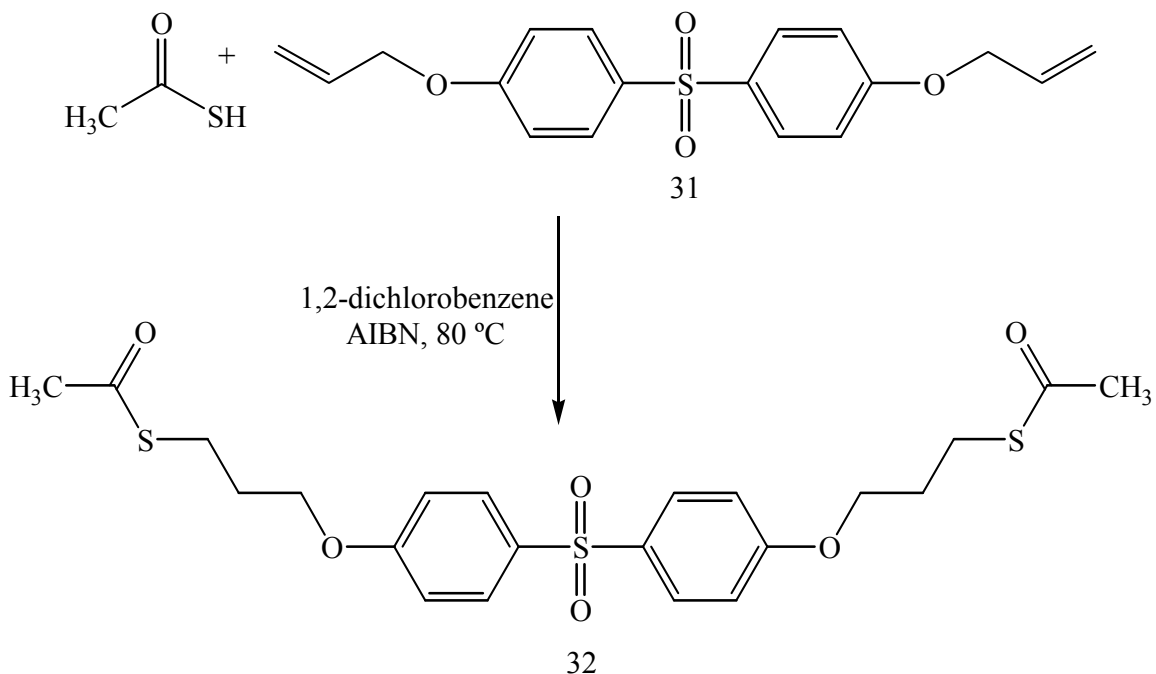
**Scheme 4.** Synthesis of grafted monomer sol-gels **10-27**.

1,1'-Sulfonylbis[4-(2-propenyloxy)benzene] (**31**) (Scheme 5) was prepared at room temperature, in 86% yield, by alkylation of 4,4'-sulfonyldiphenol with allyl bromide in a mixture of  $\text{CH}_2\text{Cl}_2$  and aqueous  $\text{NaOH}$ . Alkylation was accomplished using the phase transfer catalyst  $\text{P}(\text{Ph})_4\text{Br}$ .<sup>18</sup> The melting point (139-141 °C) was consistent with the literature value (141-142 °C)<sup>19</sup> after recrystallization from absolute  $\text{EtOH}$ . Figure 8 shows the  $^1\text{H}$  NMR of **31** where the allylic  $\text{CH}_2$  protons (4.6 ppm) were clearly shifted downfield compared to (3.9 ppm) the starting allyl bromide (Figure 7). Additionally, the OH proton from sulfonyldiphenol (9.3 ppm) (Figure 8) was no longer present in alkylated product of compound **31**.



**Scheme 5.** Synthesis of compound **31**.

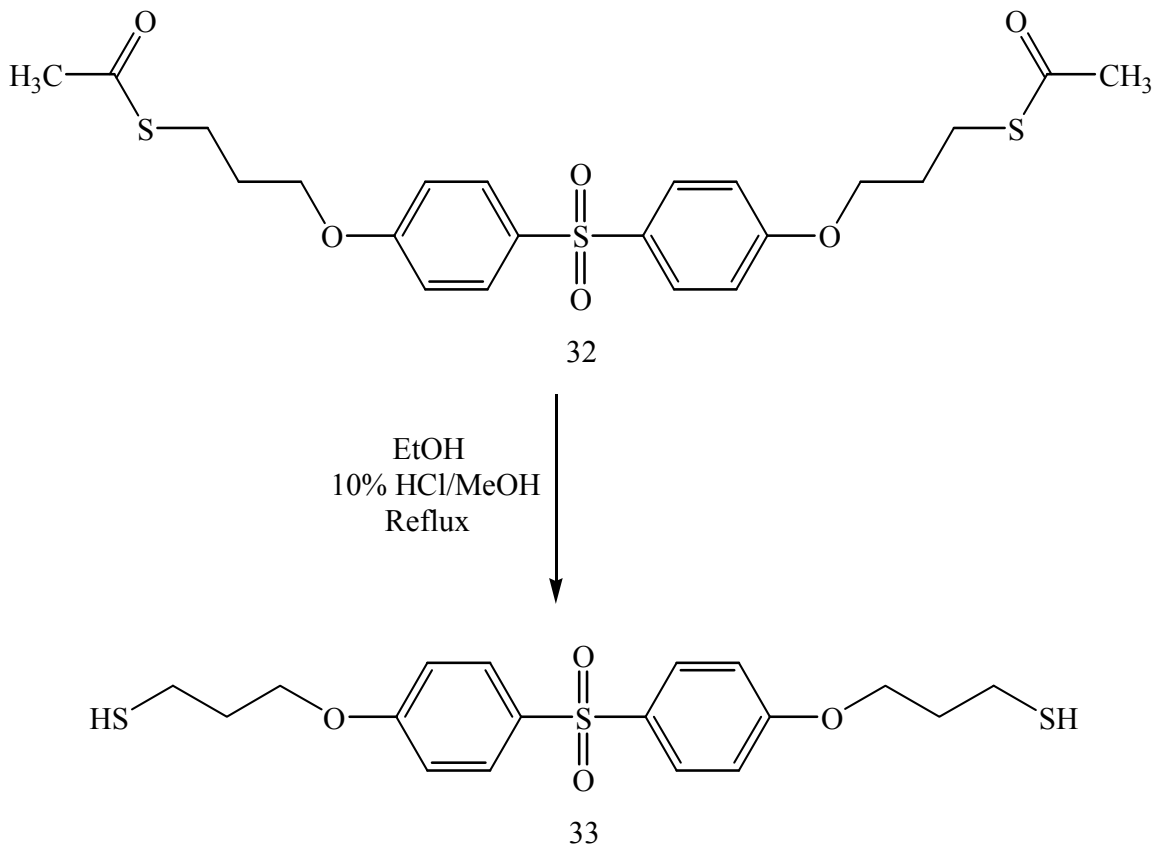
1,1'-Sulfonylbis[4-(3-acetylsulfanyl-propoxy)benzene] (**32**) was prepared by formation of the thioester from compound **31** (Scheme 6) through a radical initiated process.<sup>18</sup> Thermal decomposition of the radical initiator 2,2'-azobisisobutyronitrile (AIBN) was accomplished at 80 °C in dichlorobenzene. Unreacted solvent and thiolacetic acid were removed by short-pass distillation resulting in a dark red oil that later crystallized to give a 57% yield. Figure 10 shows the <sup>1</sup>H NMR of **32**, where the allylic protons CH<sub>2</sub> protons (4.6 ppm) have been shifted upfield (4.0 ppm). Additionally, the vinylic protons CH<sub>2</sub>, CH were no longer present (5.2, 5.4, 6.1 ppm). The methyl protons of the acetyl group were identified at 2.3 ppm.



**Scheme 6.** Synthesis of compound **32**.

Synthesis of 1,1'-sulfonylbis[4-(3-thiol-propoxy)benzene] (**33**) was achieved by acid catalyzed deprotection of the thioester (**32**) using a 10% HCl/MeOH solution in EtOH (Scheme 7).<sup>20</sup> The deprotected thiol was purified by column chromatography resulting in a white semi transparent oil to give a 76% yield. Figure 11 shows the  $^1\text{H}$  NMR of **33** where the methyl protons were no longer present (2.3 ppm). The aliphatic protons were only slightly shifted upfield by about 0.2 ppm or less due to the elimination of the carbonyl group. The triplet at 2.8 ppm was attributed to the thiol proton.

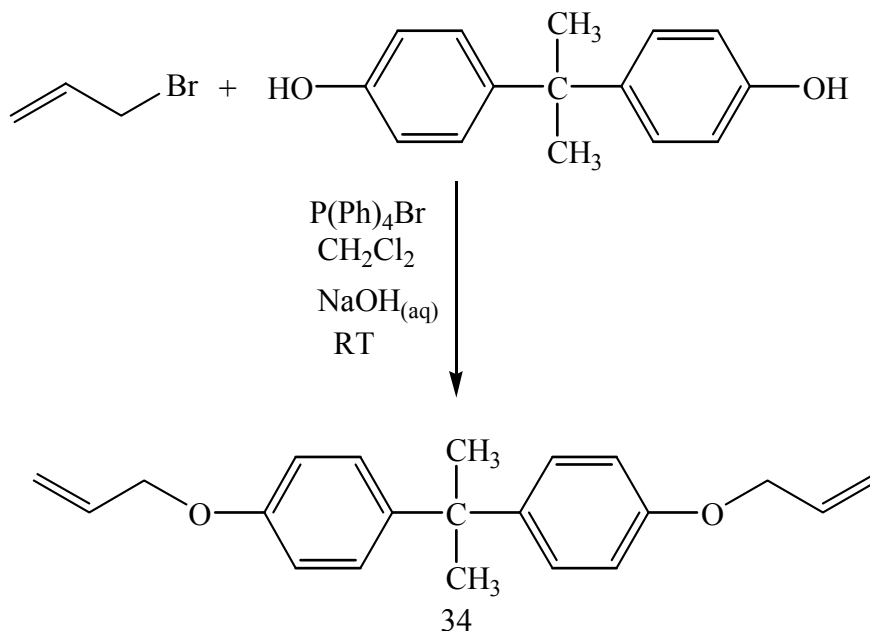




**Scheme 7.** Synthesis of compound **33**.

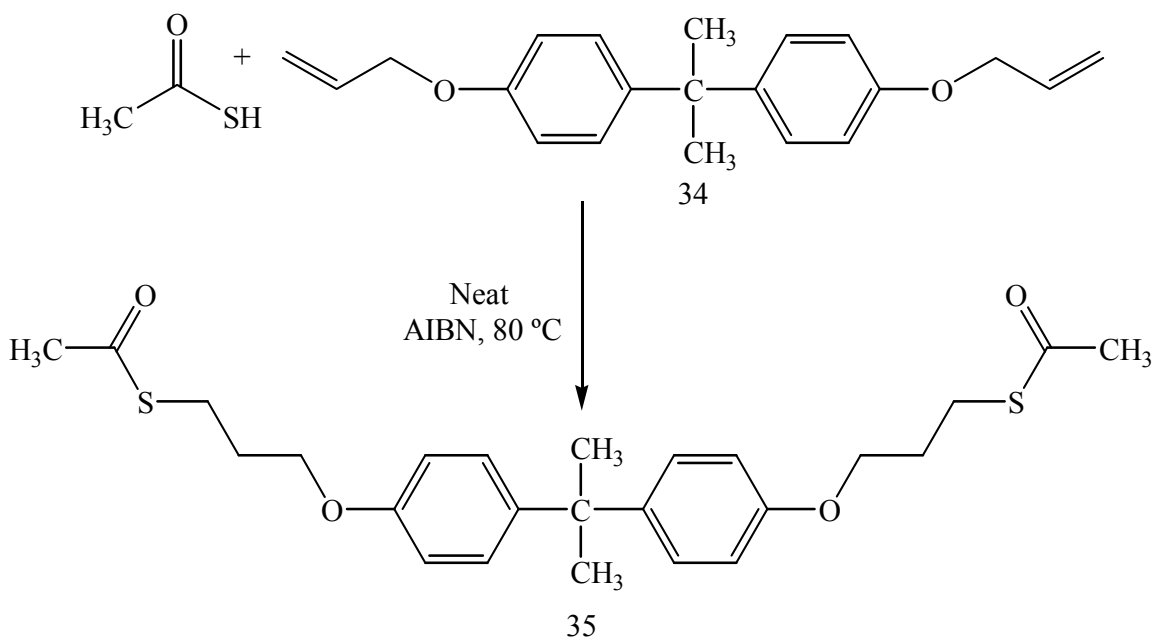
Synthesis of 1,1'-isopropylbis[4-(2-propenyloxy)benzene] (**34**) (Scheme 8) was accomplished by alkylation of 4,4'-isopropylidiphenol with allyl bromide using the phase transfer catalyst method previously described for compound **31**. After removal of the catalyst, a clear cloudy oil was obtained. The product was purified twice using a short plug of basic alumina resulting in a clear colorless oil, 97% yield. Figure 13 shows the  $^1\text{H}$  NMR of **34**. The OH protons

from the isopropylidiphenol (8.1 ppm) (Figure 12) were no longer present in alkylated product of compound **34**. The allylic CH<sub>2</sub> protons (4.5 ppm) were clearly shifted downfield compared to (3.9 ppm) the starting allyl bromide (Figure 7).



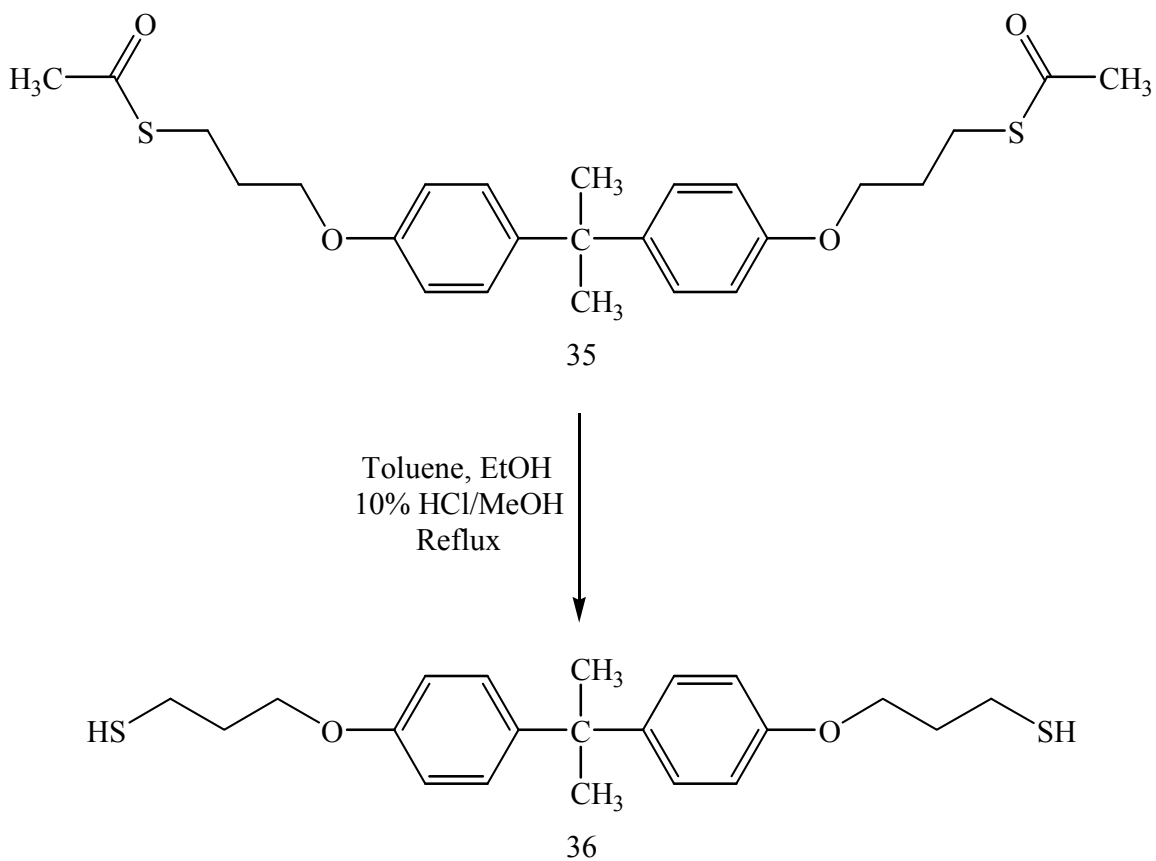
**Scheme 8.** Synthesis of compound **34**.

1,1'-Isopropylbis[4-(3-acetylsulfanyl-propoxy)benzene] (**35**) was obtained in 99% yield after purification by short pass distillation to give a dark red-orange oil. The reaction was performed neat, requiring only the removal of excess thiolacetic acid (Scheme 9). Figure 14 shows the <sup>1</sup>H NMR of **35**. The vinylic protons were no longer present (5.1, 5.4 ppm), and the alkyl and allylic protons were dramatically shifted upfield (3.0, 2.0 ppm). There was a new singlet (2.3 ppm), accounting for the presence of the methyl protons from the acetyl group.



**Scheme 9.** Synthesis of compound **35**.

1,1'-Isopropylbis[4-(3-thiol-propoxy)benzene] (**36**) was obtained after deprotection of the thioester (**35**) in 95% yield (Scheme 10). The thiol was purified by short pass distillation and characterized by  $^1\text{H}$  NMR (Figure 15). The methyl protons of the acetyl group were no longer present (2.3 ppm), and the alkyl  $\text{CH}_2$  protons were slightly shifted upfield (3.0 ppm to 2.7 ppm). The thiol proton was identified as a triplet at 1.4 ppm.

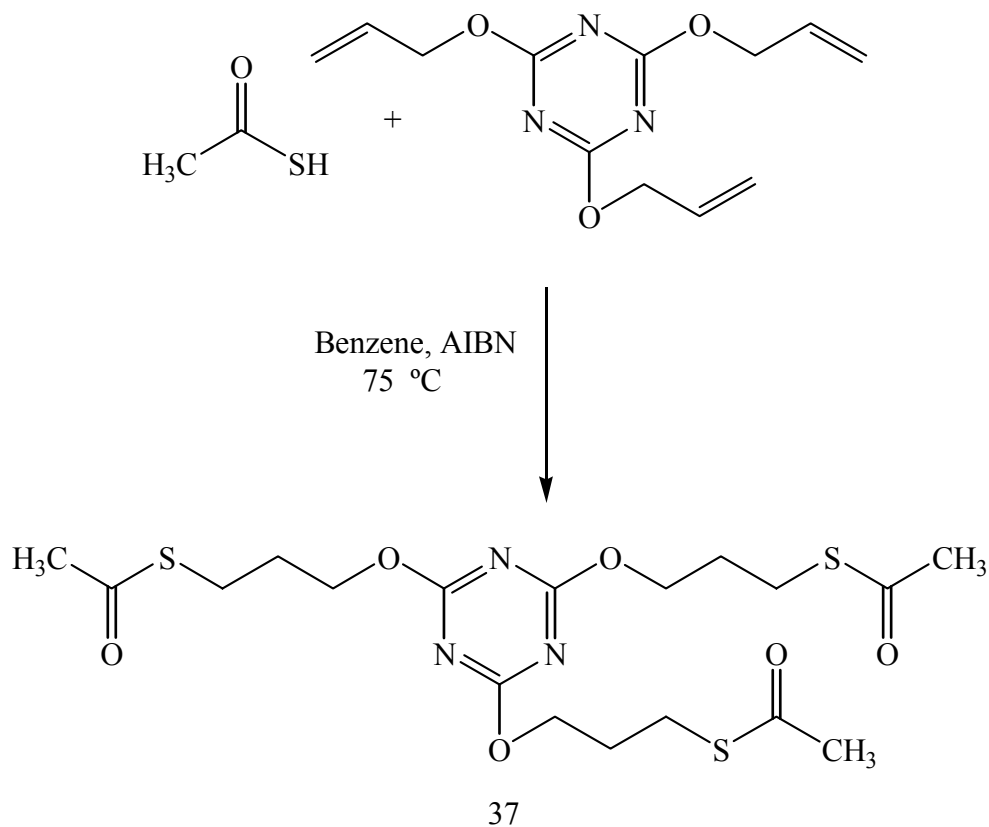


**Scheme 10.** Synthesis of compound **36**.

The synthesis of 2,4,6-(3-acetylsulfanyl-propoxy)-1,3,5-triazine (**37**) was first attempted, employing the same method used to produce the thioester of the sulfonyl and propyl diphenyl derivatives, but was unsuccessful. Rather than forming the thioester using the radical initiator AIBN, a highly cross-linked polymer resulted from the trifunctional alkene. The final product, after isolation, was a highly viscous tan material that was insoluble in most organic solvents,

with the exception of being only slightly soluble in DMSO. It was concluded that the polymer had been formed rather than the thioester and no further characterization was attempted.

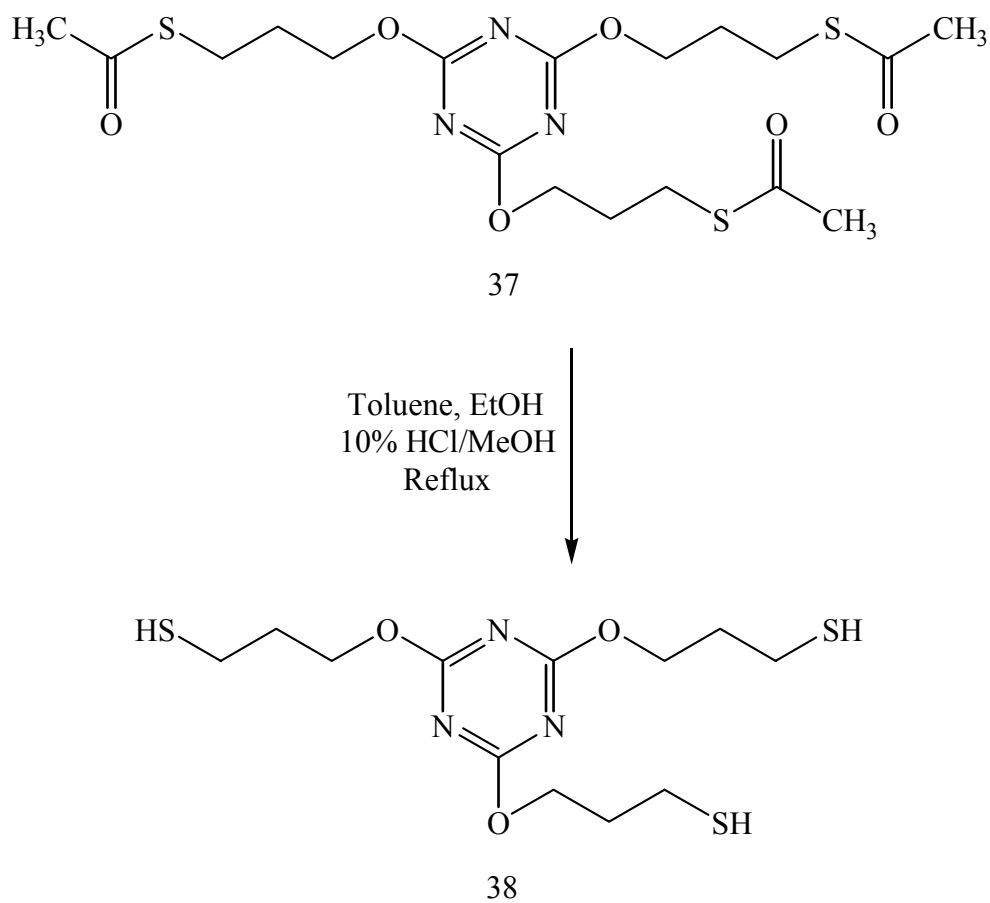
The original procedure was modified to circumvent the problem of polymerization during the formation of the thioester (Scheme 11). Two separate solutions were prepared. One solution contained the triazine compound and thiolacetic acid dissolved in benzene. Another solution was prepared contained the radical initiator AIBN dissolved in benzene. The triazine solution was brought up to the decomposition temperature of the initiator. Then the AIBN in benzene was added drop-wise to the triazine solution slowly over about a 30 min time period. Upon completion of the reaction, the solvent was removed and the product (**37**) was obtained in 91% yield. <sup>1</sup>H NMR (Figure 18) was obtained on the triazine thioester. The vinylic protons are no longer present (5.3, 5.4 ppm) (Figure 17) and the protons  $\alpha$ ,  $\beta$  and  $\gamma$  to the oxygen atom have been shifted upfield (4.4, 2.1, 3.0 ppm). The methyl proton from the acetyl group was identified at 2.3 ppm (Figure 38).



**Scheme 11.** Synthesis of compound **37**.

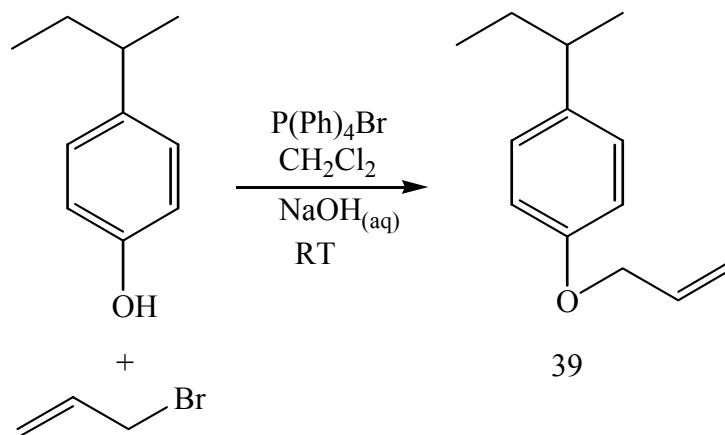
Deprotection of the thioester (**37**) afforded 2,4,6-(3-thiol-propoxy)-1,3,5-triazine (**38**) in 60% yield after purification by short pass distillation (Scheme 12). During the deprotection of the thioester a large amount of a white precipitate was formed. The thiol product was dissolved in  $\text{CH}_2\text{Cl}_2$  and the white precipitate was removed by gravity filtration. After isolation the white precipitate was characterized by mp and NMR. It was suspected that the white precipitate was due to the formation of cyanuric acid, as a result of complete hydrolysis of the ether rather than

the thioester. The melting point ( $> 360\text{ }^{\circ}\text{C}$ , lit.  $> 360\text{ }^{\circ}\text{C}$ )<sup>20</sup> was consistent with the reported value.  $^1\text{H}$  NMR (Figure 16) of the precipitate was in agreement with the proposed structure due to presence of a single peak (10.7 ppm) which was attributed to the OH proton.  $^1\text{H}$  NMR (Figure 19) of the purified thiol (**38**) no longer had the acetyl protons (2.3 ppm) from the original thioester. The alkyl protons (3.7, 1.9, 2.8 ppm) were also shifted upfield due to the elimination of the acetyl group.



**Scheme 12.** Synthesis of compound **38**.

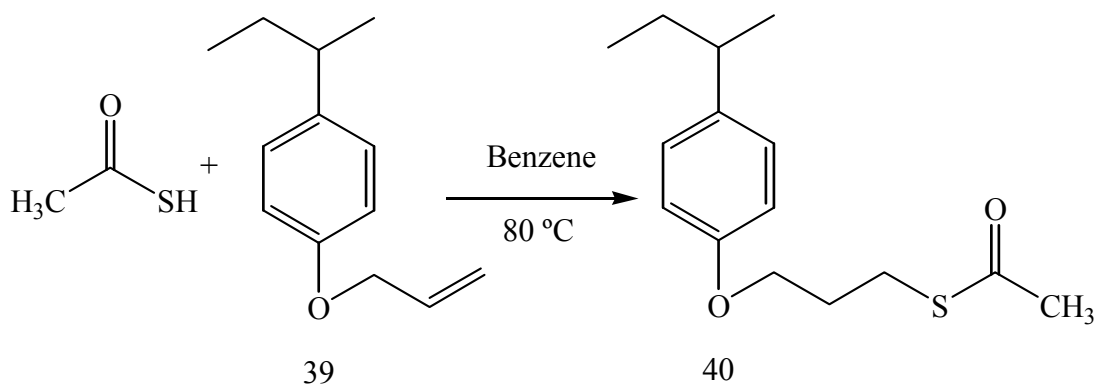
Poly(4-vinylphenol) (**39**) was obtained in 87% yield by alkylation of poly(4-hydroxyphenol) with allyl bromide (Scheme 13). The polymer was purified by precipitation in MeOH to give a tan powder. Characterization by  $^1\text{H}$  NMR (Figure 21) supported the successful synthesis of the alkylated polymer. The OH phenol proton from the starting material was no longer present in the alkylated product. The vinyl protons were identified as a broad doublet and a singlet (5.2, 5.4, and 6.1 ppm). The allylic protons were shifted downfield and were identified by a broad singlet (4.5 ppm).



**Scheme 13.** Synthesis of polymer **39**.



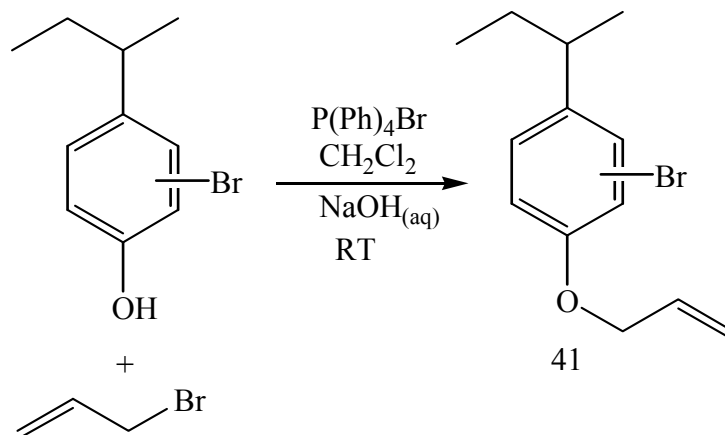
Synthesis of poly[4-(3-acetylsulfanyl-propoxy)-phenol] (**40**) was attempted from compound **39** in benzene but was unsuccessful (Scheme 14). Formation of the thioester was attempted using the previously reported procedure. The reaction was stopped after 72 hours and worked up. After purification, it was determined by  $^1\text{H}$  NMR that there was no formation of the desired thioester product. Apparently, the original NMR of the crude reaction was misinterpreted and the reaction was terminated prematurely.



**Scheme 14.** Attempted synthesis of polymer **40**.

Brominated poly(4-hydroxyphenol) was alkylated to give brominated poly(4-vinylphenol) (**41**) (Scheme 15) in 72% yield, after purification by precipitation in MeOH, resulting in a tan powder. Product formation was confirmed by  $^1\text{H}$  NMR (Figure 22), by the elimination of the phenol proton (8.2 ppm) and formation of the allylic protons (4.5 ppm). The

allylic protons are again shifted downfield as expected from the original allyl bromide (3.9 ppm) starting material. The vinyl protons were also shifted downfield and identified by a doublet and singlet (5.3, 5.5, and 6.1 ppm).



**Scheme 15.** Synthesis of polymer **41**.

## RESULTS AND DISCUSSION OF RAMAN SCATTERING FOR SELECT SOL-GELS AND MONOMERS

Raman scattering spectra were obtained for all sol-gels and monomers presented. Spectra were obtained on a JY Horiba LabRam Analytical Raman Microscope equipped with a HeNe laser (20 mW, 632.8 nm) and a holographic grating (600 g/mm). Some of the sol-gels and monomers presented were quite fluorescent at 632.8 nm. As a result, Raman scattering data was difficult to obtain for some compounds and will only be briefly discussed. For the remaining compounds, general trends and key features will be discussed regarding their respective Raman scattering spectra and applications to Raman gain.

Preliminary Raman gain data and laser damage threshold was obtained for a select sol-gel sample and will be discussed briefly. These measurements were performed in collaboration with Professor George Stegeman of CREOL and Robert Stegeman (physics graduate student). In short, Raman gain was obtained from sol-gel **28** using an excitation wavelength of 1.06  $\mu\text{m}$  (pump laser). Gain was obtained at 1122.5 nm and 1124.0 nm (Figure 28). The signal quickly fell off, away from the peak, when measured at 1119.0 nm and 1129.0 nm. The gain measured was 70% that of fused silica when measured in this same region ( $440\text{ cm}^{-1}$  from the pump laser). The reported error in the gain measurement was approximately 15%. Measurement for laser damage threshold was evaluated at 47 ps pulses producing intensities of about  $55\text{ GW/cm}^2$ .

There was no reported damage to the sample. These results demonstrate that gain can be achieved in a sol-gel using the vibrational frequency mode attributed to the Si-O-Si symmetric stretching ( $450\text{ cm}^{-1}$ ) (Figure 54).

Raman gain was measured and demonstrated in only one sol-gel. Most of the sol-gel samples prepared lacked the optical quality and flat parallel surfaces required for gain measurements but were acceptable for Raman scattering measurements. Since there were such a large number of samples, we attempted to cut and polish the ones that had good optical quality but possessed poor geometry. Some samples possessed good optical quality but had such high intensity fluorescence the Raman spectra could not be obtained. Additionally, some samples had to be rejected because they were too small for polishing or gain measurements. This limited the number of possible samples to only a few. However, these samples could not withstand the mechanical grinding and polishing required. The samples either crumbled beyond use or had multiple cracks that propagated through the sample as it was polished.

All of the monomers used in the doping of the sol-gels resulted in fluorescence making it difficult or impossible to obtain reliable Raman scattering spectra. Nonetheless, some of the sol-gels did produce good reliable data due to strong Raman scattering. Higher monomer concentrations were achieved when the monomers were grafted to the sol-gel matrix. These compounds produced spectra with slightly higher scattering intensities. Therefore, the fluorescence was much easier to subtract from the data. Sol-gel **5** (1,5-pentanediol) (Figure 31) was very fluorescent when it was dispersed into the sol-gel, but when this monomer was grafted to the sol-gel matrix it resulted in good Raman scattering data (Figure 44, 45). Sol-gels **3**, **6**, and

**8** containing disperse red-19, 2-(N-ethyl-anilino)ethanol, hydroxypropyl acrylate, respectively were very fluorescent when dispersed or grafted into the sol-gel and did not result in any usable data (Figure 30, 32, 34).

When possible, the fluorescence was subtracted in order to obtain the Raman spectrum. Compounds **31-37** did not exhibit the same amount of fluorescence as did the dispersed and grafted monomers (Figure 57-61). However, the polymers (**39, 41**) prepared for dispersion into the sol-gel did exhibit fluorescence (Figure 62, 63). Compounds derived from the two bisphenol main architectures as well as the triazine derivatives did not exhibit the same problems of fluorescence.

The most significant features of the Raman scattering spectra of the reference sol-gels **28-30** are attributed to the Si-O-Si symmetric stretching mode ( $450\text{ cm}^{-1}$ ) and the asymmetric stretching mode ( $1000\text{ cm}^{-1}$ ) (Figure 54-56). There was also a very broad peak ( $2500\text{--}4000\text{ cm}^{-1}$ ) attributed to residual water, since none of the sol-gels were sintered. The two sol-gels with the isocyanate group (**29, 30**) had a broad sharp peak ( $2800\text{--}3000\text{ cm}^{-1}$ ) attributed to the C-H stretching mode of the propyl group.

There are a few features evident with the sol-gels. First, the presence of the alkyl and alkene C-H stretching modes produces a broad and intense peak ( $2800\text{--}3100\text{ cm}^{-1}$ ) that was very distinctive particularly when these groups occur within the same compound. Second, the region from  $1700\text{ cm}^{-1}$  down into the fingerprint region was largely unimpressive for most all of the sol-gels. Many of the organic hybrid sol-gels have various low intensity peaks in this region that are half the intensity or less than that of the alkyl region ( $2800\text{--}3100\text{ cm}^{-1}$ ). Finally, it appears sulfur containing compounds can greatly improve the region from  $1700\text{ cm}^{-1}$  down into the finger print

region. Although, these peaks are not as broad as that of the alkyl stretching mode they are quite intense. For example, the Raman spectrum for sol-gel **9** (mercaptophenol) (Figure 35) had three sharp peaks in this region with intensities equal to or greater than that of the alkyl region. This was also very evident with the Raman characterization for the thio based monomers that were synthesized and will be discussed later.

Dispersal of the monomer (2-methyl-3-butyn-2-ol) into the matrix of sol-gel **1** was of interest due to methyl and alkyne functional groups (Figure 29). The methyl groups were clearly identified as a relatively broad sharp peak ( $3000\text{ cm}^{-1}$ ) whereas the alkyne group was not present in the expected region ( $3325, 2250\text{ cm}^{-1}$ ). The alkyne C-H and C-C triple bond are known to have intense peaks in these regions, respectively. Since the alkyne group could not be identified it was speculated that the concentration of the monomer was too low to be clearly observed, and the alkyl peak was due to unhydrolyzed ethoxy groups of TEOS.

Incorporation of disperse red-19 (sol-gel **3**) into the matrix resulted in a great deal of fluorescence which was subtracted from the spectral data (Figure 30). The C-C stretching mode of the aromatic ring is very intense and was observed in the expected region ( $1600\text{ cm}^{-1}$ ), but the C-H stretching mode was not observed ( $3000\text{ cm}^{-1}$ ). It appears the later signal was missing as a result of the fluorescence subtraction leading to unreliable interpretation of the data. Due to intense fluorescence, DR-19 was not considered for further study.

A key feature of sol-gel **7** (pentaerythritol triallyl ether) (Figure 33) was the broad peak in the area of  $2900\text{ cm}^{-1}$ . This broad peak is a result of the C-H stretch from both the alkyl ( $2840\text{-}2970\text{ cm}^{-1}$ ) and alkene ( $3010\text{-}3095\text{ cm}^{-1}$ ) stretching modes and was observed in many of the compounds studied. The alkene C=C stretching mode is typically very strong and was observed

as a very narrow intense peak ( $1650\text{ cm}^{-1}$ ). The C-O stretching mode of the ether group is typically weak to medium intensity, and was observed as a broad low intensity peak ( $900\text{ cm}^{-1}$ ).

Sol-gel **9** (mercaptophenol) incorporated the C-S stretching mode (Figure 35). Organic compounds containing sulfur are known to be strong Raman scattering. Here an intense peak attributed to the aryl C-S stretching mode was identified ( $1100\text{ cm}^{-1}$ ). The peak was nearly twice the intensity of the next highest intensity peak in the spectrum. Additionally, a slightly less intense peak was also identified ( $500\text{ cm}^{-1}$ ) as a result of the alkyl C-S stretching mode. Another important feature of this spectrum is the absence of a broad intense peak ( $2840\text{-}3000\text{ cm}^{-1}$ ) due to the alkyl C-H stretching mode. This clearly demonstrates the importance the alkyl C-H stretch is to broadening the peak in this region. The aromatic C-H stretch ( $3050\text{ cm}^{-1}$ ) was observed as a sharp peak in this region.

Due to difficulties already reported in the synthesis of sol-gels **2, 4** (octadecane thiol, pentamethoxy-triphenylmethanol), there was no Raman scattering data to report. Sol-gels **5, 6,** and **8** (1,5-pentanediol, 2-(n-ethylanylino)ethanol, and hydroxypropyl acrylate) resulted in very high fluorescence and did not produce any usable data as well (Figure 31, 32, 34).

Grafting of the monomers into the sol-gel matrix via a urethane linkage allowed for better chemical control when incorporating the monomers into the sol-gel matrix. There are spectra for two additional compounds (octadecane thiol, pentamethoxy-triphenylmethanol) that were not previously mentioned in the discussion of dispersed sol-gel monomers. The spectra for the grafted sol-gels using pentamethoxy triphenylmethanol were very fluorescent (Figure 42, 43) and will not be discussed, but details of sol-gels grafted with octadecane thiol can be found in the following discussion. When comparing the spectra of the dispersed monomers to those of the

grafted monomers, one finds no noticeable difference between the two methods. Therefore, grafting of the monomer provides a useful alternative for introducing the monomer into the sol-gel matrix.

The grafted sol-gels **13**, and **19** (octadecane thiol, 1,5-pentanediol) are similar in structure. The C-H stretching mode of the long alkyl chain was observed ( $2850\text{-}3050\text{ cm}^{-1}$ ) for each compound, although, the peak was much more intense for the diol than that of the thiol (Figure 39, 45). The alkyl C-S stretching mode was also not as intense as expected ( $500\text{ cm}^{-1}$ ) for sol-gel **13**. It appears that the C-S stretching mode is much more intense for aryl-S than alkyl-S stretching modes. The lower peak intensities for sol-gel **13** compared to that of sol-gel **19** may be due to a difference in monomer concentration within the matrix of the two sol-gels.

Raman scattering for the pure monomers resulted in much better spectra. Excluding the polymers, the monomers were free of all fluorescence at the excitation wavelength, leading to clean spectra with good peak intensities. The two polymer derivatives of poly(hydroxystyrene) were very fluorescent, but spectra were obtained after the fluorescence was removed. Raman scattering was obtained for all sulfonyl derivatives (**31**, **32**, and **33**). However, only spectra from the thioesters (**35**, **37**) of the isopropyl and triazine derivatives were obtained. The ene and thiol derivatives for these compounds were liquids and were not characterized for their Raman scattering spectra.

All derivatives of sulfonylbisphenol resulted in spectra with large peak intensities relative to the sol-gel samples. The sulfonyl S=O stretching mode was identified as a sharp narrow peak ( $1150\text{ cm}^{-1}$ ) and was particularly strong in all of the derivatives presented (**31-33**) (Figure 57-59). In fact, the sulfonyl mode was about 2-8 times larger than the alkyl C-H stretching mode ( $2850\text{-}$



3050  $\text{cm}^{-1}$ ). The C-S stretching mode (650  $\text{cm}^{-1}$ ) of the thioester was rather intense for compound **32** and was comparable in intensity to the C-H mode (2850-3050  $\text{cm}^{-1}$ ). The aromatic C=C stretching mode was also very intense (1600  $\text{cm}^{-1}$ ) for each of the derivatives providing an additional sharp intense peak. The peak height and width can be increased for the C-H mode by introducing an acetyl group such as that from the thioester (**32**). The C-H stretching mode of the methyl group results in broad peaks with higher intensities for this region. Once the thioester was deprotected the relative intensity was decreased (**33**). However, the newly formed thiol resulted in a new peak (2550  $\text{cm}^{-1}$ ) due to the S-H stretching mode. This is significant because there are not very many functional groups found with stretching modes in this region (1800-2800  $\text{cm}^{-1}$ ).

The spectrum for the thioester of isopropylbisphenol (**35**) (Figure 60) demonstrated the significance of the methyl C-H stretching mode. Compound **35** has four methyl groups. The C-H stretching mode for the alkyl, methyl, and aromatic region (2850-3050  $\text{cm}^{-1}$ ) had clearly been broadened. The peak intensity for this region has also been dramatically increased and is about three times larger than the rest of the spectrum. Even the C=C stretching mode (1600  $\text{cm}^{-1}$ ) appears to be much smaller than the C-H mode.

The triazine thioester (**37**) (Figure 61) has no hydrogen atoms attached to aromatic carbons, resulting in a narrowing of the peak (3050  $\text{cm}^{-1}$ ). In addition, we no longer have a sharp peak due to the aromatic C=C mode (1600  $\text{cm}^{-1}$ ). However, the C=N stretching mode was identified (1700  $\text{cm}^{-1}$ ) but was not nearly as intense as the C=C mode. The C-S stretching mode of the thioester was also identified (650  $\text{cm}^{-1}$ ). This peak is slightly broader and more intense for compound **37** than previously reported for the other monomers.

The two spectra of the poly(hydroxystyrene) derivatives (**39**, **41**) resulted in a large amount of fluorescence but deserves a brief discussion (Figure 62, 63). After the fluorescence was subtracted the two spectra did not appear to be significantly different from one another. What appeared to be significant was that the peaks corresponding to the C=C and C-H stretching modes ( $1600\text{ cm}^{-1}$ ,  $2850\text{-}3050\text{ cm}^{-1}$ ) appeared to be broader than some of the other monomers containing vinyl substituted phenyl compounds. This would suggest that the peak widths can be increased, an aspect that would be helpful in obtaining broadband Raman gain.

## CONCLUSIONS AND FUTURE WORK

An investigation in developing new materials capable of broadband amplification of optical data transmission has been initiated. Raman gain was demonstrated using an undoped sol-gel producing a signal gain 70% that of fused silica. A series of new monomer intermediates were synthesized for introduction into a sol-gel matrix based on specific derivatives of sulfonylbisphenol, isopropylbisphenol, triazine, and poly(hydroxystyrene). Nearly all sol-gels and monomers were characterized for molecular structure and Raman scattering spectra using mp where appropriate, FT-IR,  $^1\text{H}$  NMR, and Raman scattering.

The ability to synthesize multiple doped sol-gels simultaneously in a parallel synthesis strategy proved to be very efficient. Preparation of small samples reduced reaction time and facilitated Raman characterization. Very reactive monomers (**2**, **4**) that were difficult to introduce into the sol-gel matrix were grafted using 3-(trimethoxysilyl)propylisocyanate. Precipitation of the monomer was avoided and there was no noticeable change in the Raman spectra of the grafted sol-gel.

An interesting feature of the synthesized monomers was the ability to produce strong Raman scattering peaks. In particular, the sulfonyl group (**31-33**) proved to be interesting due to a very strong peak at about  $1150\text{ cm}^{-1}$ . Alkyl and aromatic compounds were also quite interesting because these compounds resulted in very strong and broad scattering peaks ( $2859\text{-}3050\text{ cm}^{-1}$ ). The peak width and intensity in this region appears to be increased by the presence of

compounds (**32, 35, 37**) containing methyl groups. Such strong scattering lines in selective areas may have applications such as obtaining Raman gain for specific wavelengths. Another possibility may be to formulate sol-gels containing blends of various monomers in order to obtain broader and or additional Raman scattering peaks in one spectra.

Synthesis of grafted polymers using some of the monomers presented here may be of interest as well. Raman scattering peaks for the poly(hydroxystyrene) derivatives were broadened compared to those of the monomers. Grafted polymers may be one method to obtain broader peaks in Raman spectra making it easier to obtain broadband Raman gain. Fluorescence is certainly a major concern with the polymers and will have to be reduced or eliminated if they are to be used in the doping of sol-gels. This requires further investigation.

Grafting of the monomers to the sol-gel back bone may be another method to obtain broadening of the Raman scattering peaks, such as that found in the styrene based polymers. Further investigation needs to be done on the urethane modified sol-gels. One possibility may be to formulate sol-gels with high percentages of one or more different grafted monomers into the sol-gel in order to obtain additional broader peaks in the Raman scattering spectrum.

In conclusion, it has been demonstrated that Raman gain can be obtained in organic/inorganic hybrid sol-gel material. A method has been demonstrated for rapid synthesis of the sol-gels in small volume, reducing processing time and the time required for characterization. Finally, four major molecular architectures were proposed and investigated for the synthesis of functionalized monomers in relatively high yield. The synthesis of these monomers resulted very promising Raman spectra in terms of their applications for broadband Raman gain.

APPENDIX A  
 $^1\text{H}$  NMR SPECTRA

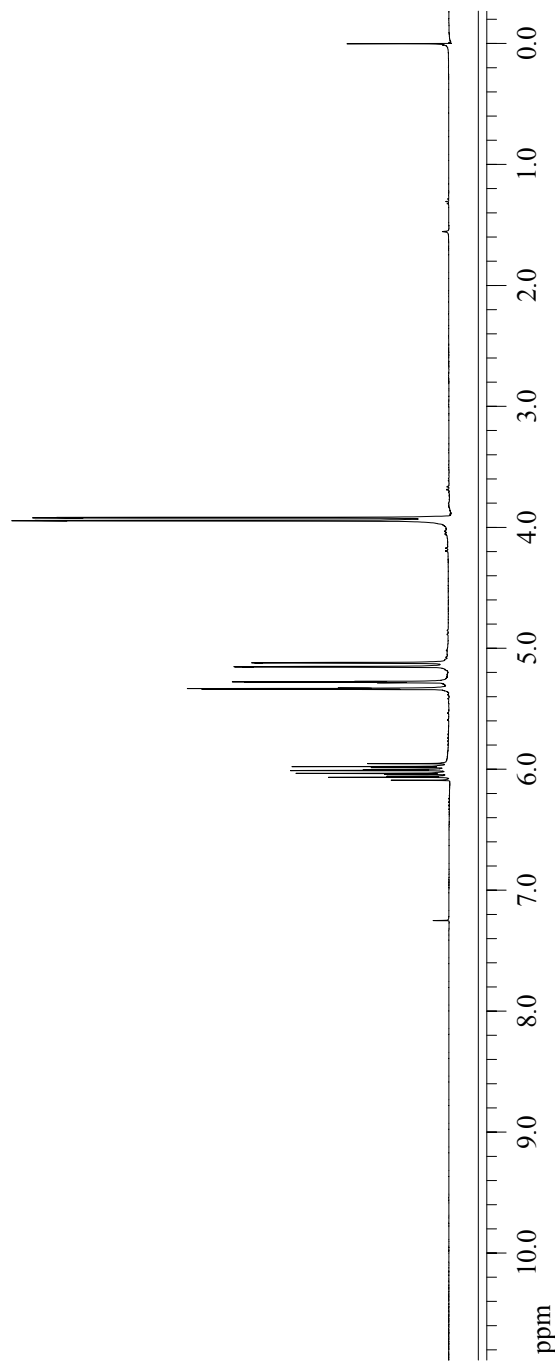


**Figure 7.** 300 MHz  $^1\text{H}$  NMR of allyl bromide in  $\text{CDCl}_3$ .

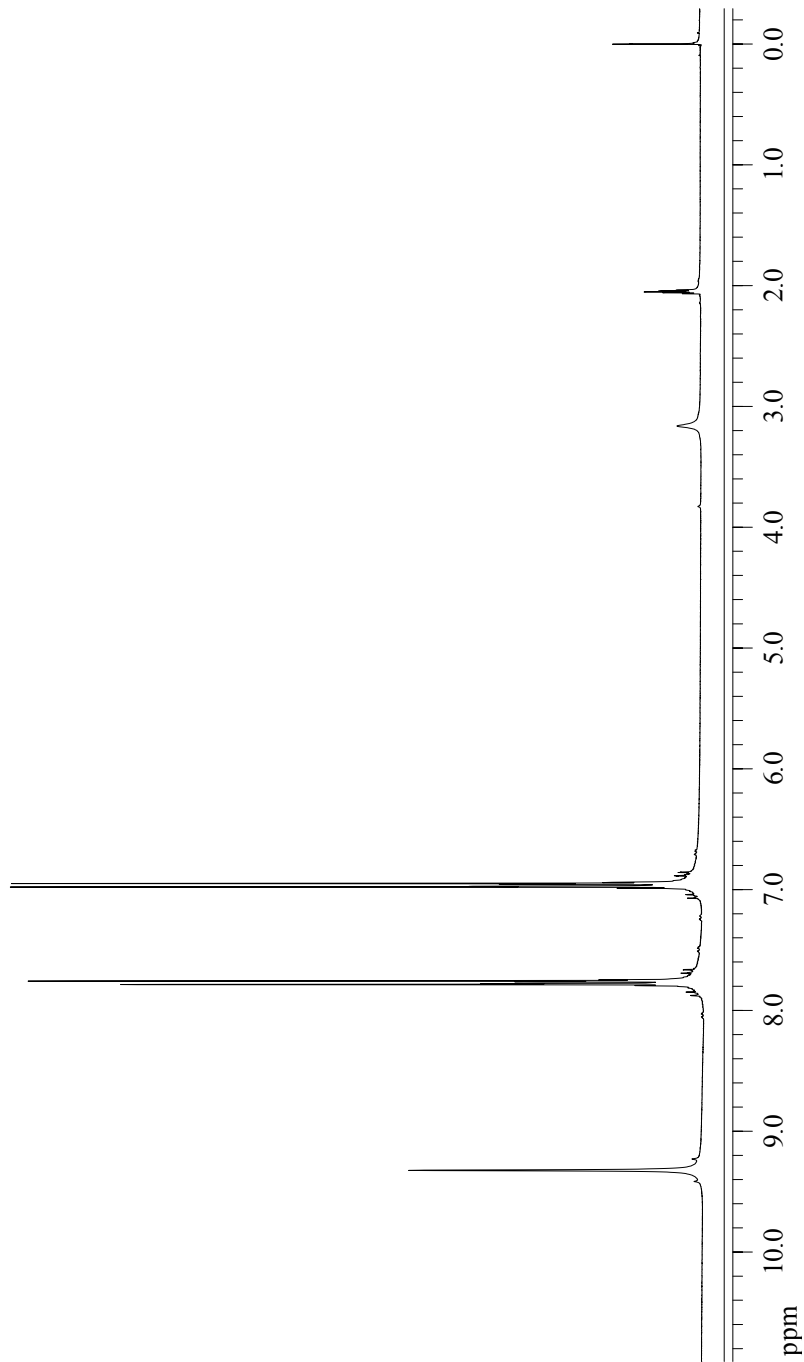


**Figure 8.** 300 MHz <sup>1</sup>H NMR of sulfonylbisphenol in CD<sub>3</sub>COCD<sub>3</sub>.

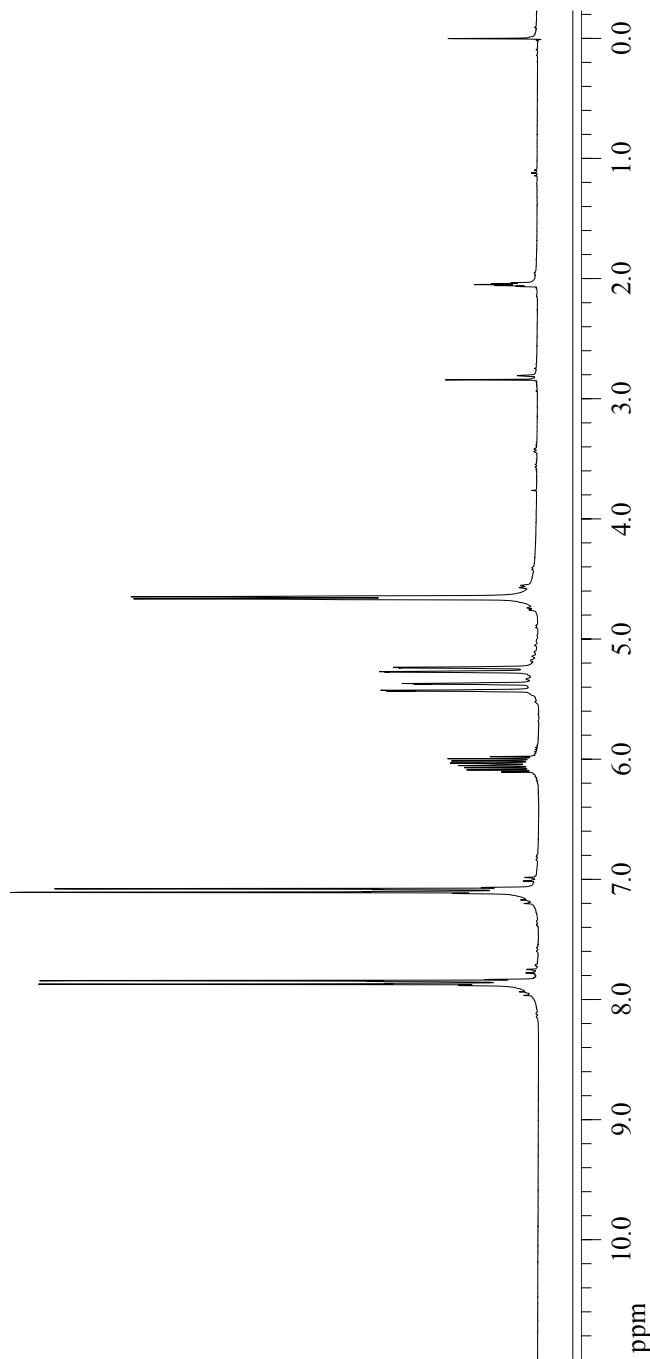


**Figure 9.** 300 MHz  $^1\text{H}$  NMR of **31** in  $\text{CD}_3\text{COCD}_3$ .



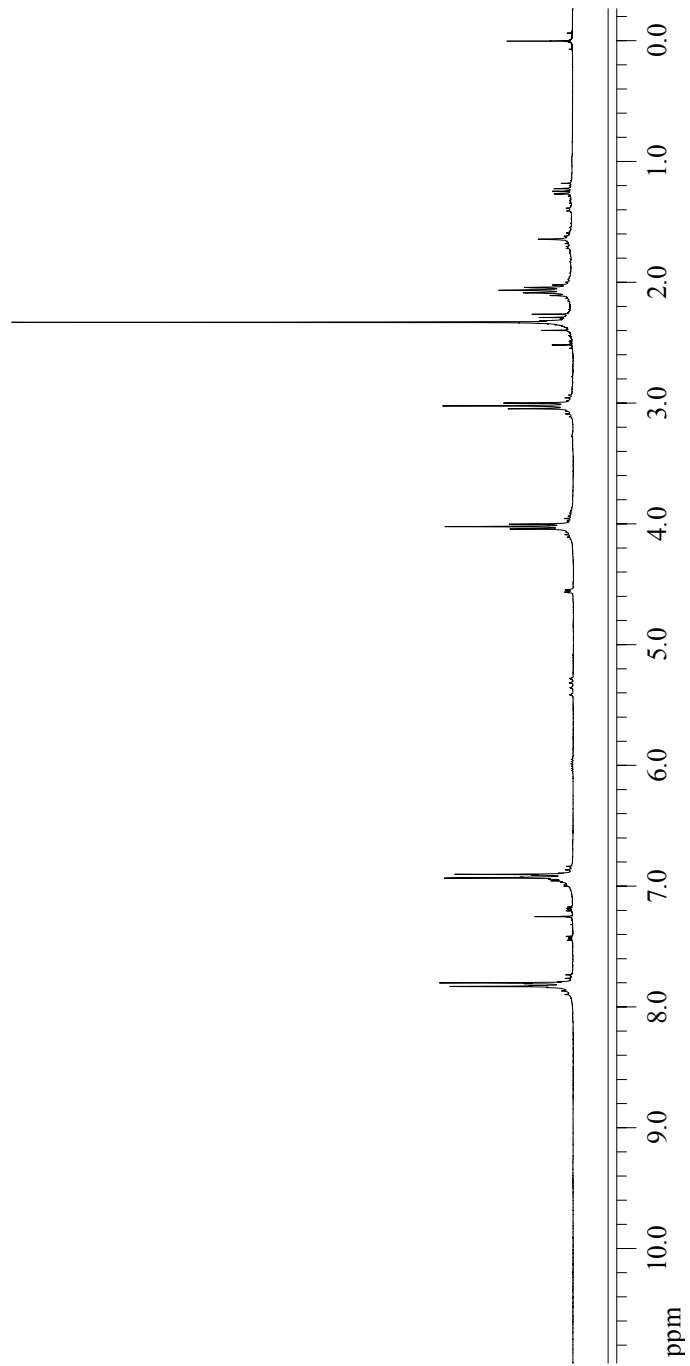


**Figure 10.** 300 MHz  $^1\text{H}$  NMR of **32** in  $\text{CDCl}_3$ .

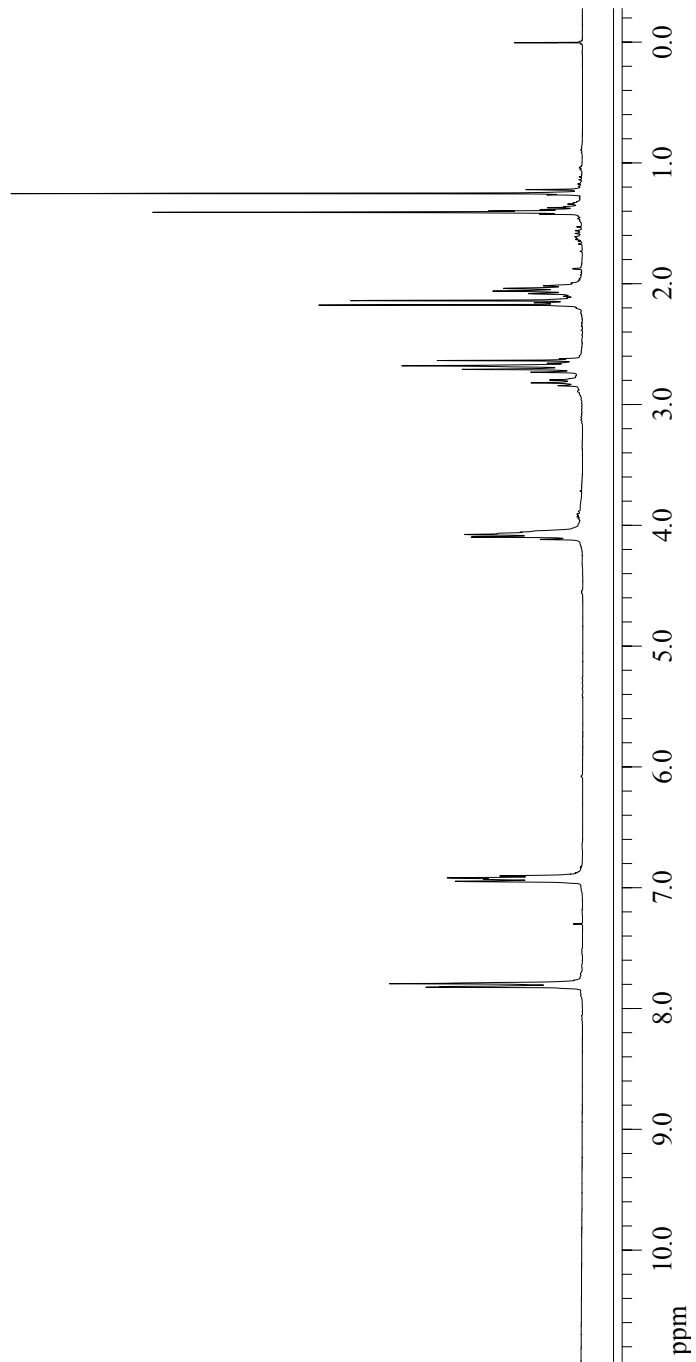


**Figure 11.** 300 MHz  $^1\text{H}$  NMR of **33** in  $\text{CDCl}_3$ .

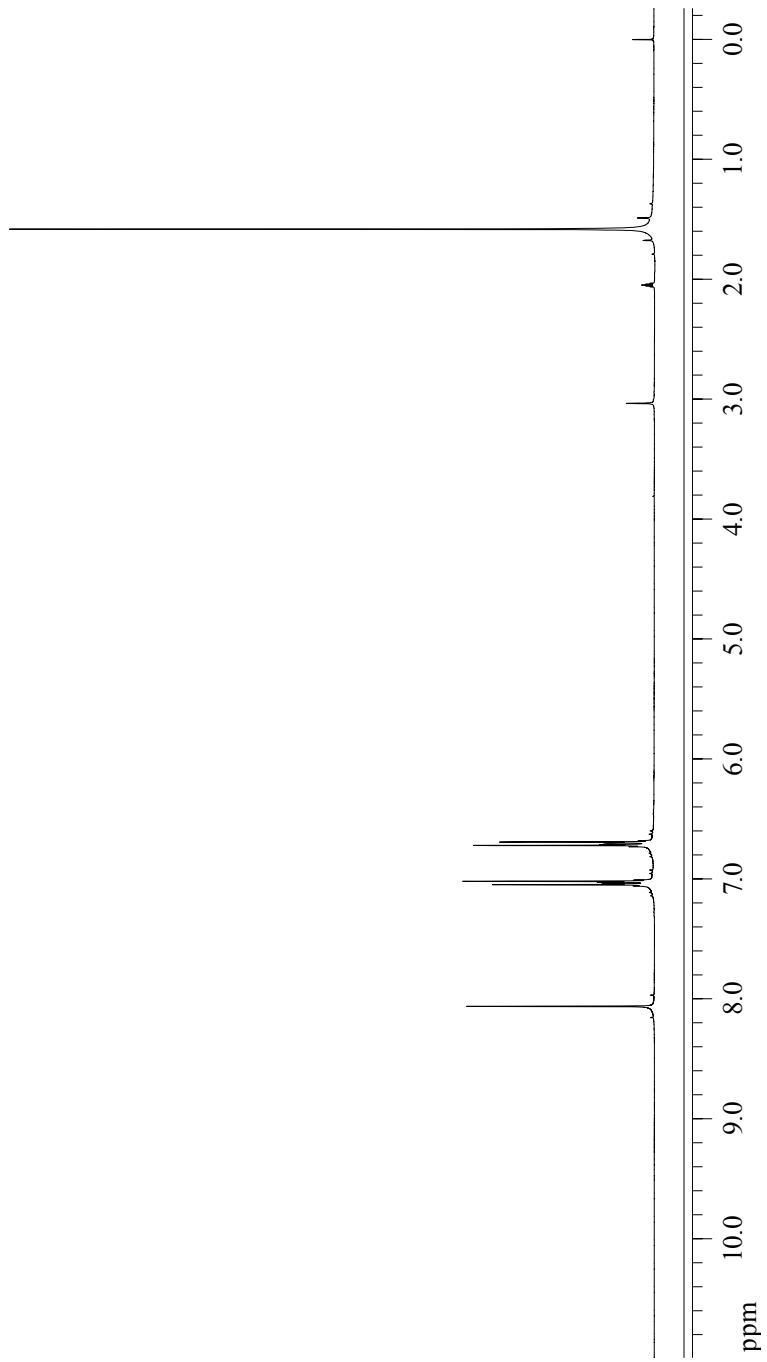


**Figure 12.** 300 MHz <sup>1</sup>H NMR of isopropylidenediphenol in CD<sub>3</sub>COCD<sub>3</sub>.

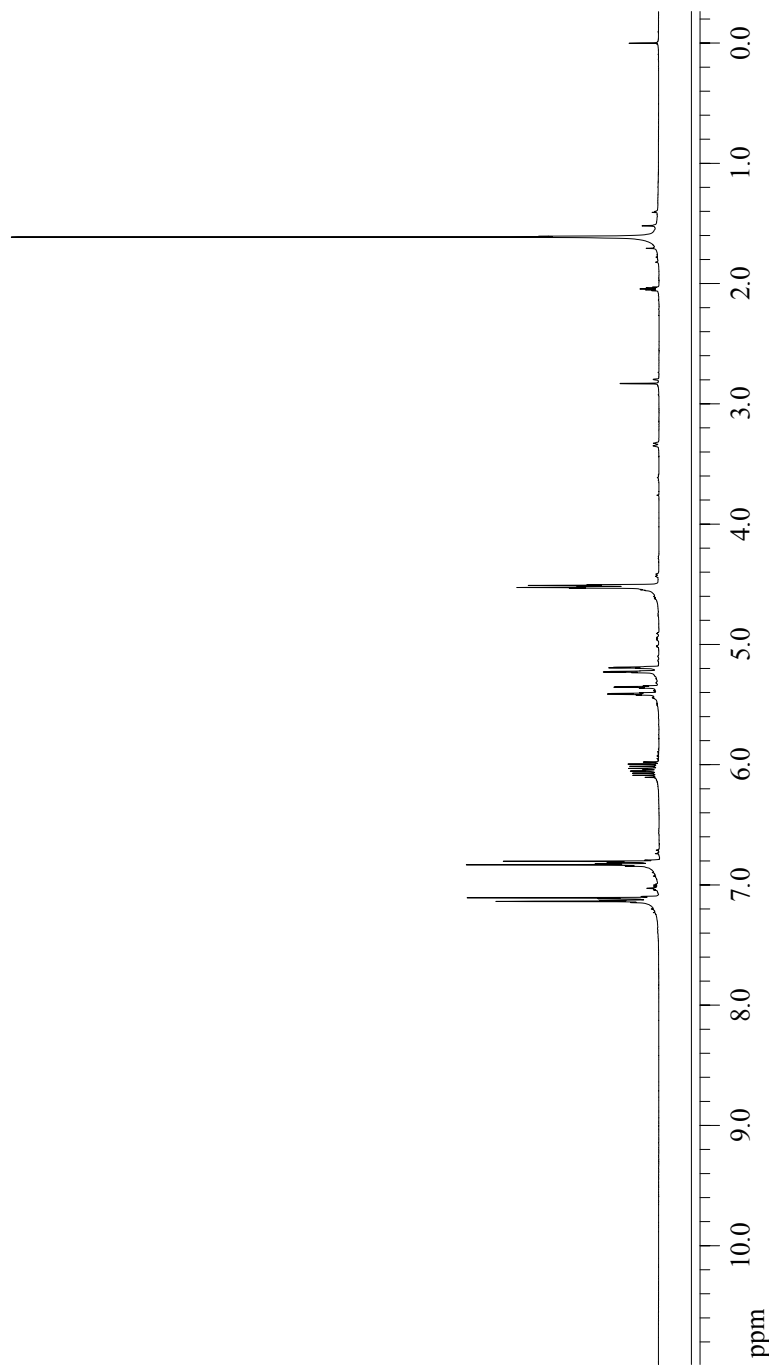


**Figure 13.** 300 MHz  $^1\text{H}$  NMR of **34** in  $\text{CD}_3\text{COCD}_3$ .

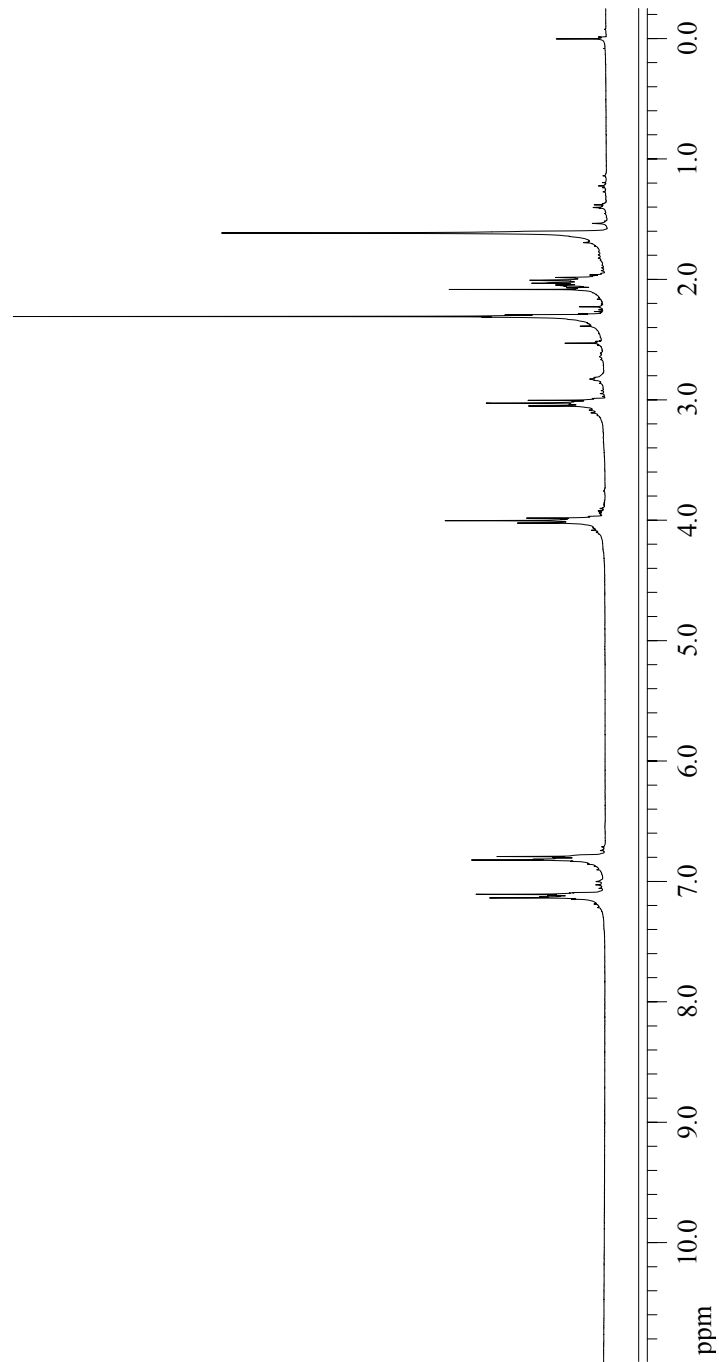


**Figure 14.** 300 MHz  $^1\text{H}$  NMR of **35** in  $\text{CD}_3\text{COCD}_3$ .

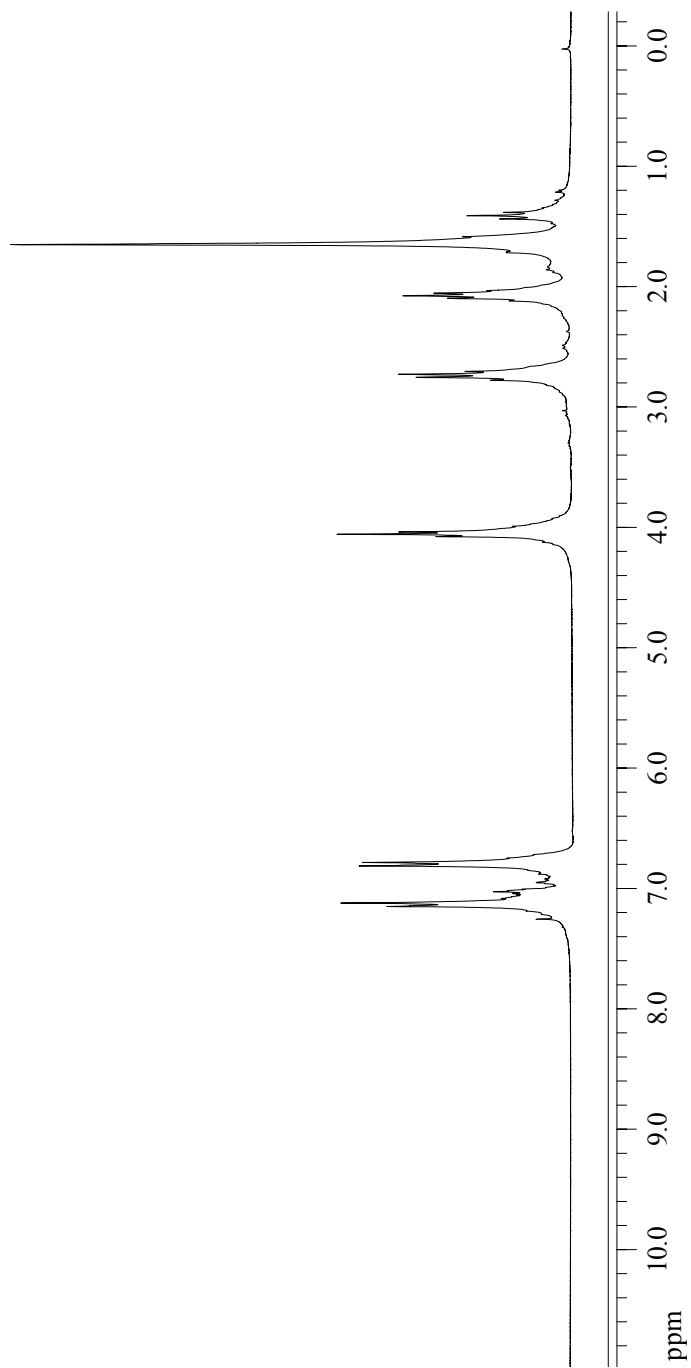


**Figure 15.** 300 MHz  $^1\text{H}$  NMR of **36** in  $\text{CDCl}_3$ .

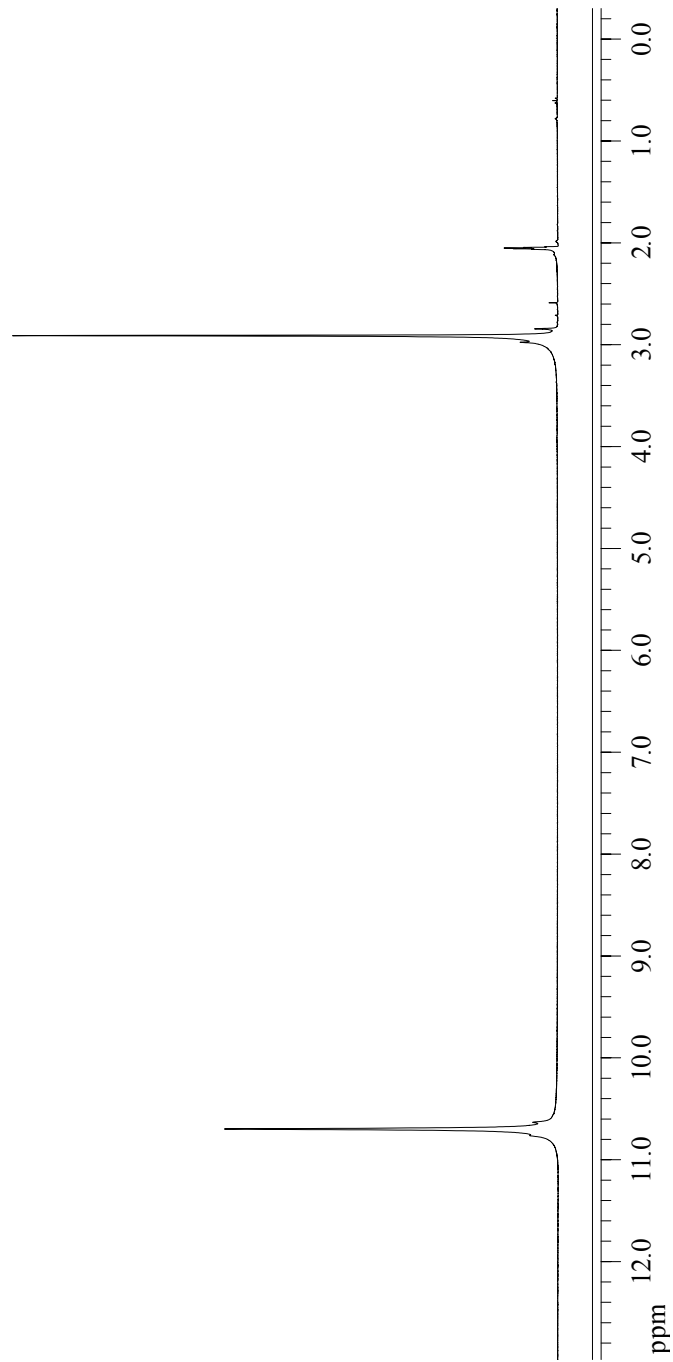


**Figure 16.** 300 MHz <sup>1</sup>H NMR of cyanuric acid in CD<sub>3</sub>COCD<sub>3</sub>.

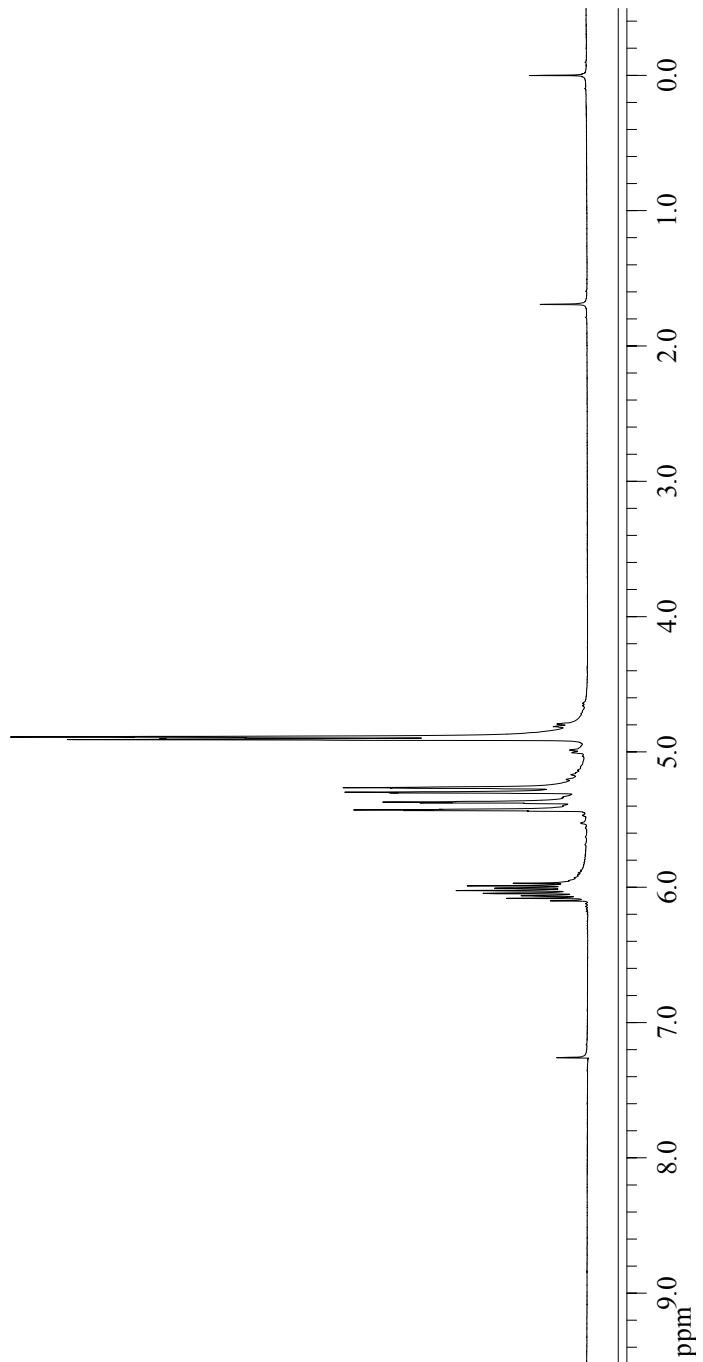


**Figure 17.** 300 MHz <sup>1</sup>H NMR of triallyloxy-1,3,5-triazine in CDCl<sub>3</sub>.



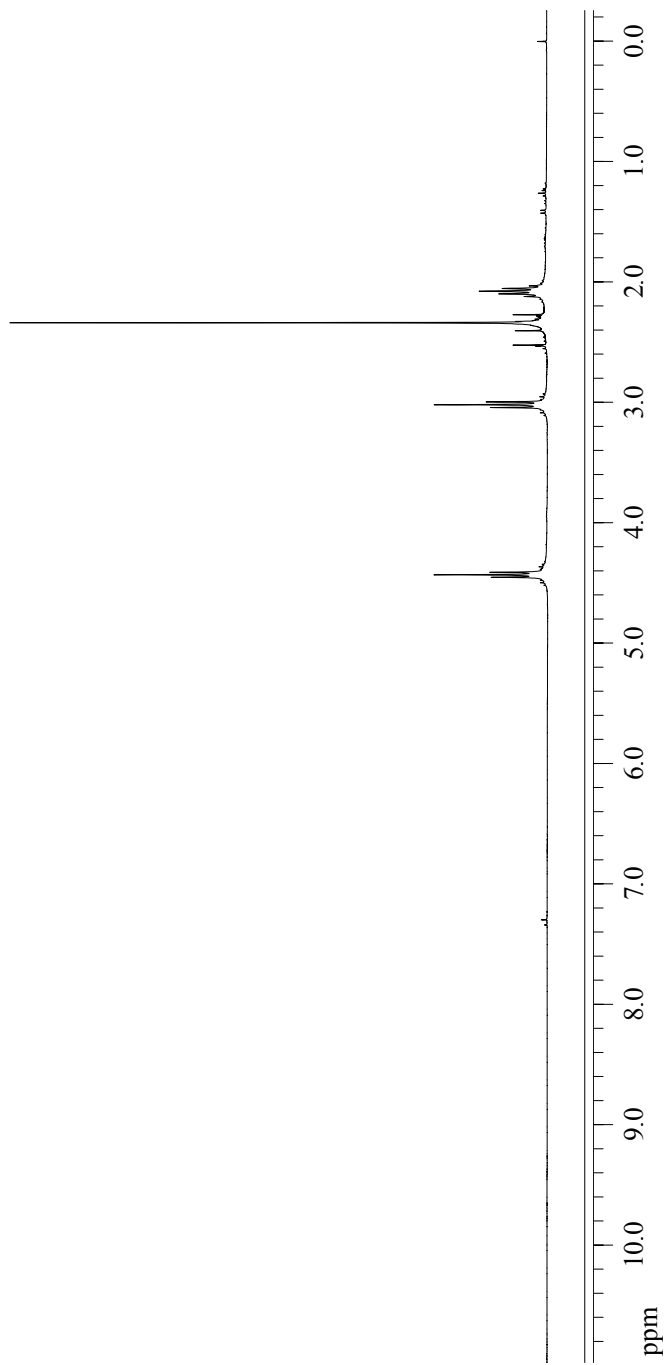


**Figure 18.** 300 MHz  $^1\text{H}$  NMR of **37** in  $\text{CDCl}_3$ .

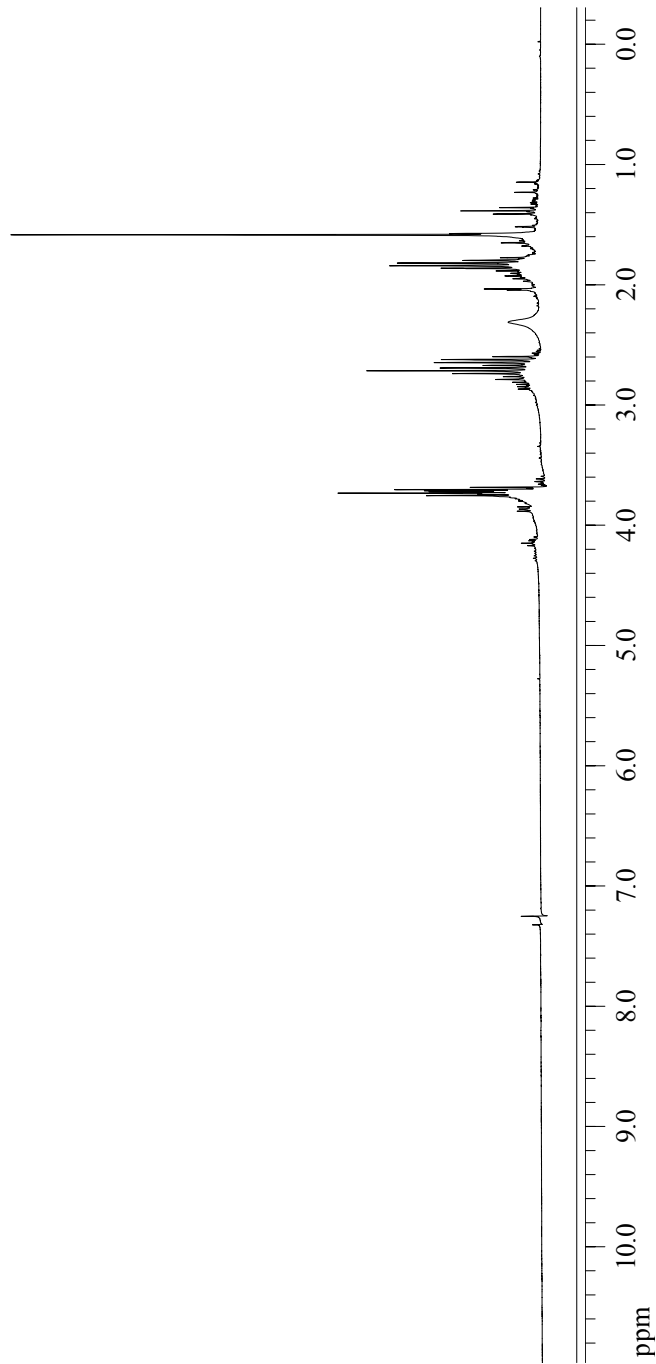


**Figure 19.** 300 MHz  $^1\text{H}$  NMR of **38** in  $\text{CDCl}_3$ .

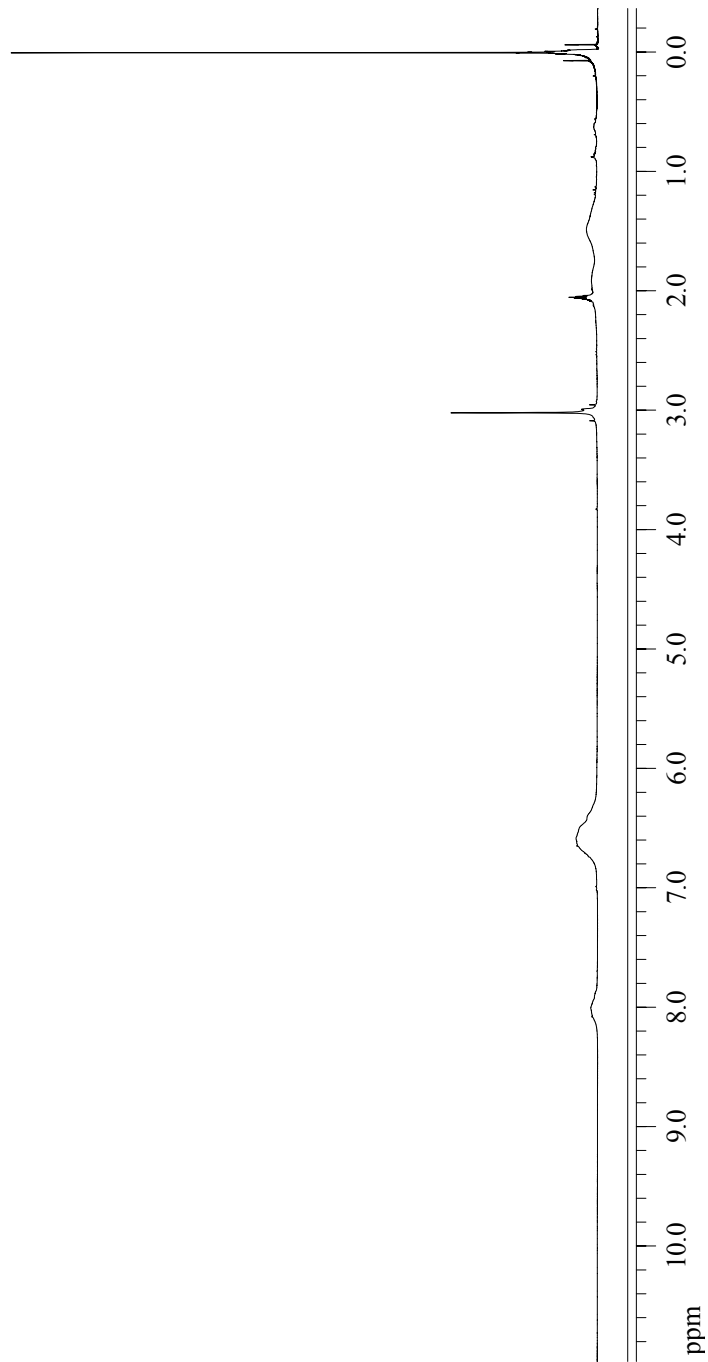


**Figure 20.** 300 MHz <sup>1</sup>H NMR of poly(4-hydroxystyrene) in CD<sub>3</sub>COCD<sub>3</sub>.

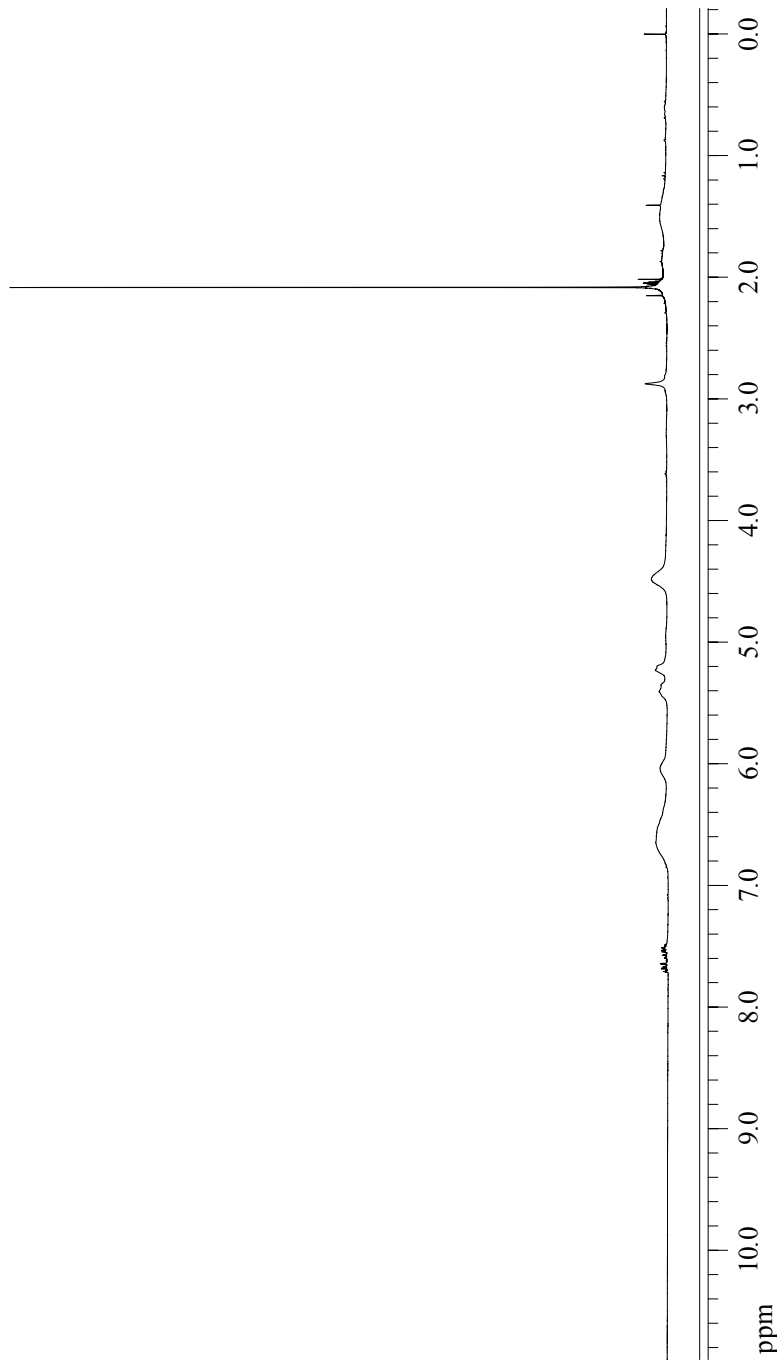


**Figure 21.** 300 MHz  $^1\text{H}$  NMR of **39** in  $\text{CD}_3\text{COCD}_3$ .

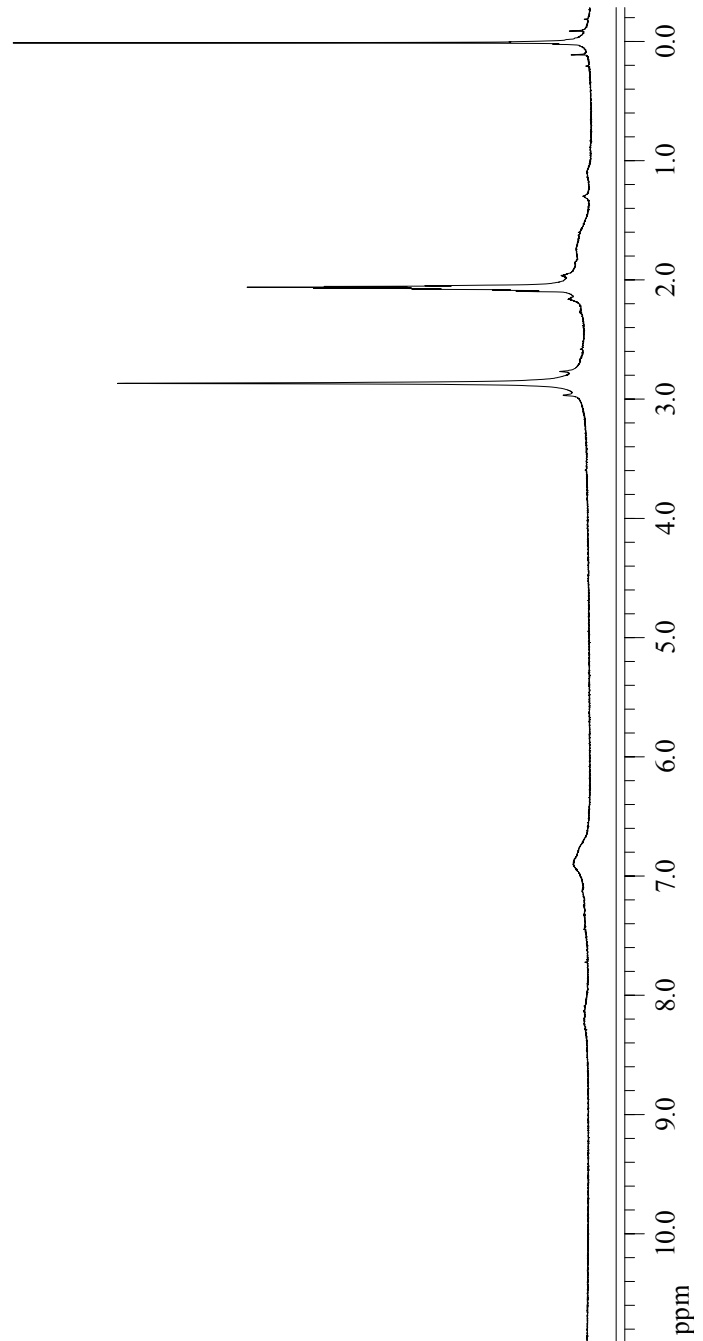


**Figure 22.** 300 MHz <sup>1</sup>H NMR of brominated poly(4-hydroxystyrene) in CD<sub>3</sub>COCD<sub>3</sub>.

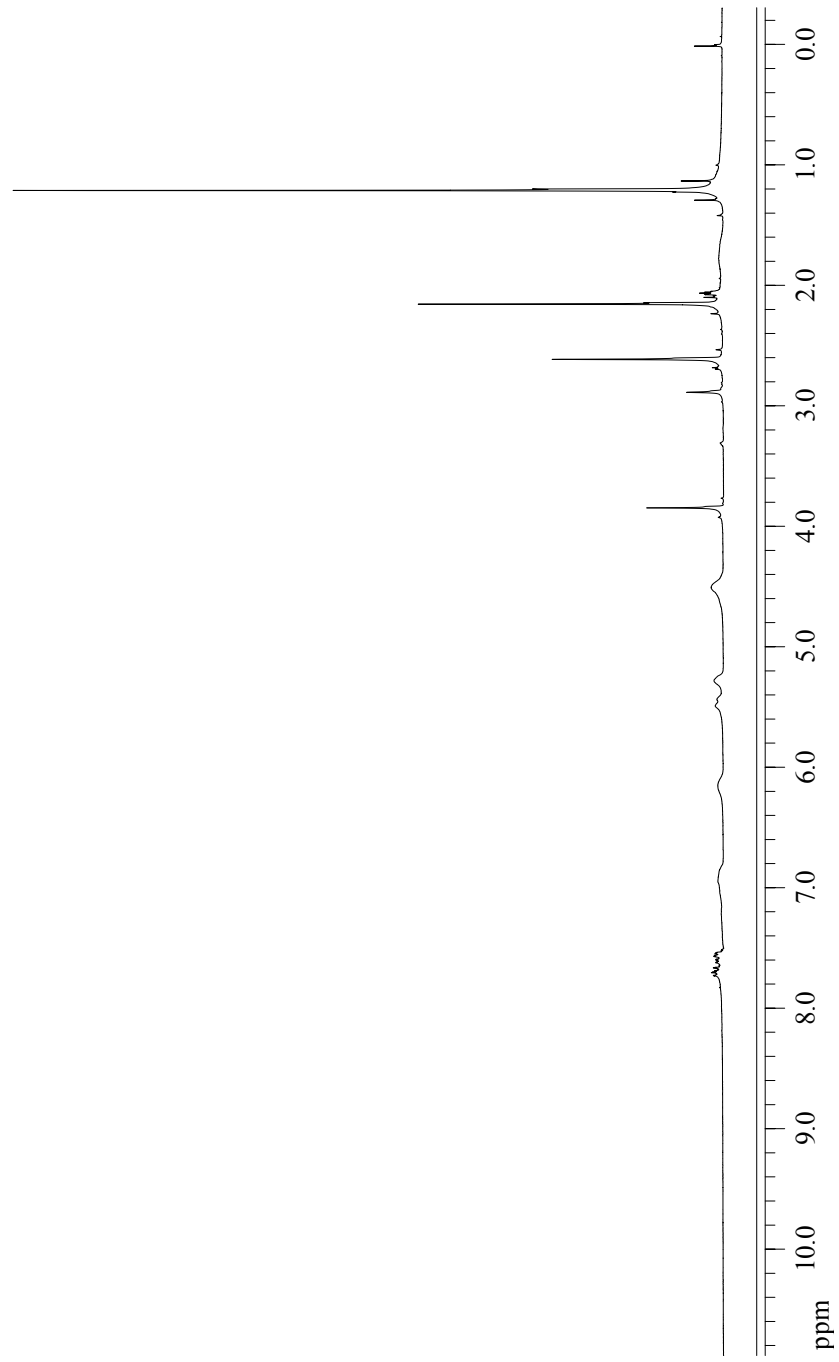


**Figure 23.** 300 MHz  $^1\text{H}$  NMR of **41** in  $\text{CD}_3\text{COCD}_3$ .

APPENDIX B  
SELECT IR SPECTRA

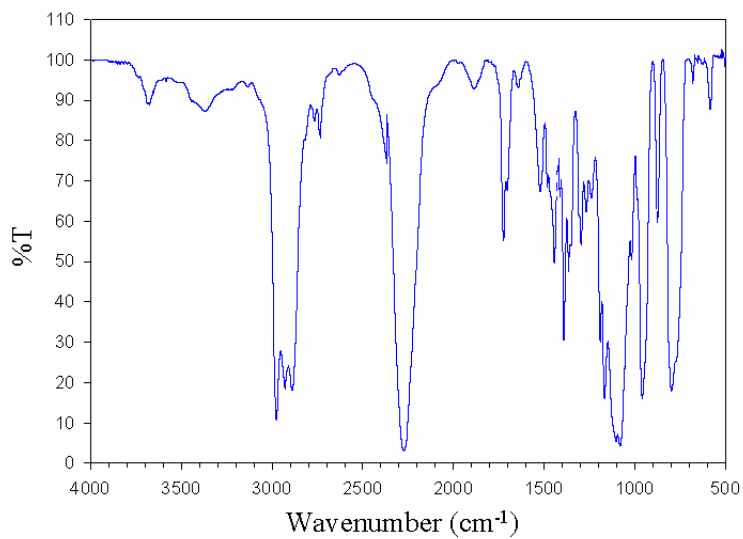


**Figure 24.** IR Spectrum 3-(Trimethoxysilyl)propyl Isocyanate.

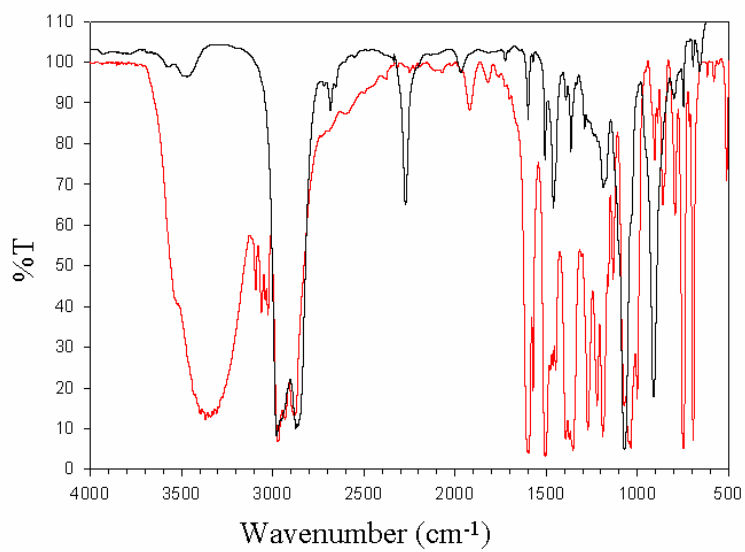


**Figure 25.** IR spectrum of 2(ethylanimino)ethanol reaction mixture.

Red plot represents pure 2(ethylanimino)ethanol.

Black plot represents reaction mixture at 48 hours.



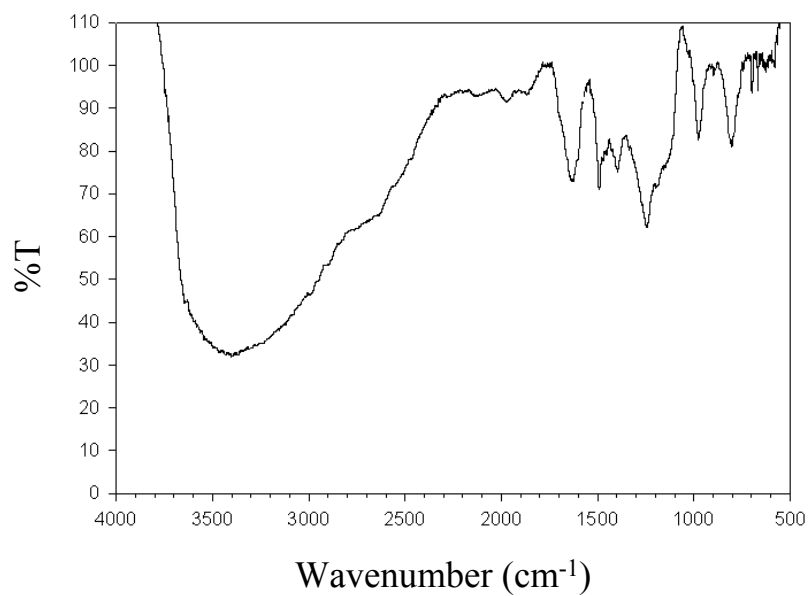


**Figure 26.** IR spectrum of sol-gel **6** in diffuse reflectance mode.

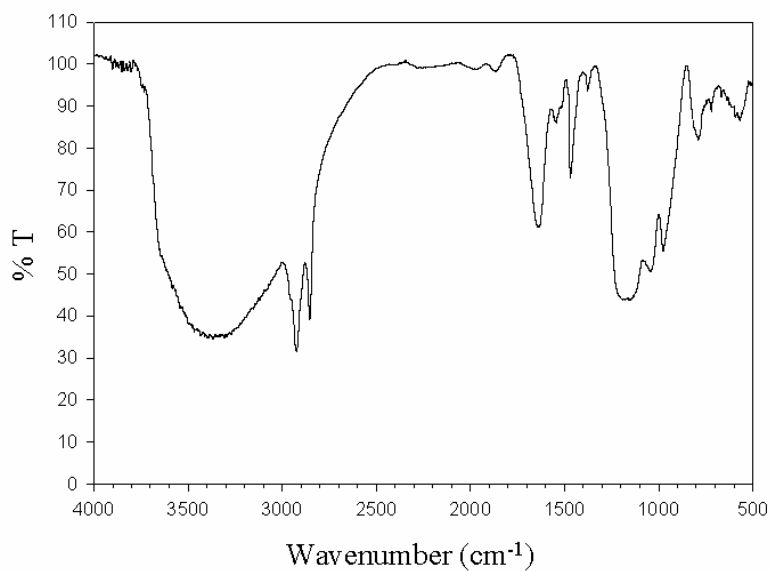


**Figure 27.** IR spectrum of sol-gel **13** in diffuse reflectance mode.

APPENDIX C  
RAMAN GAIN

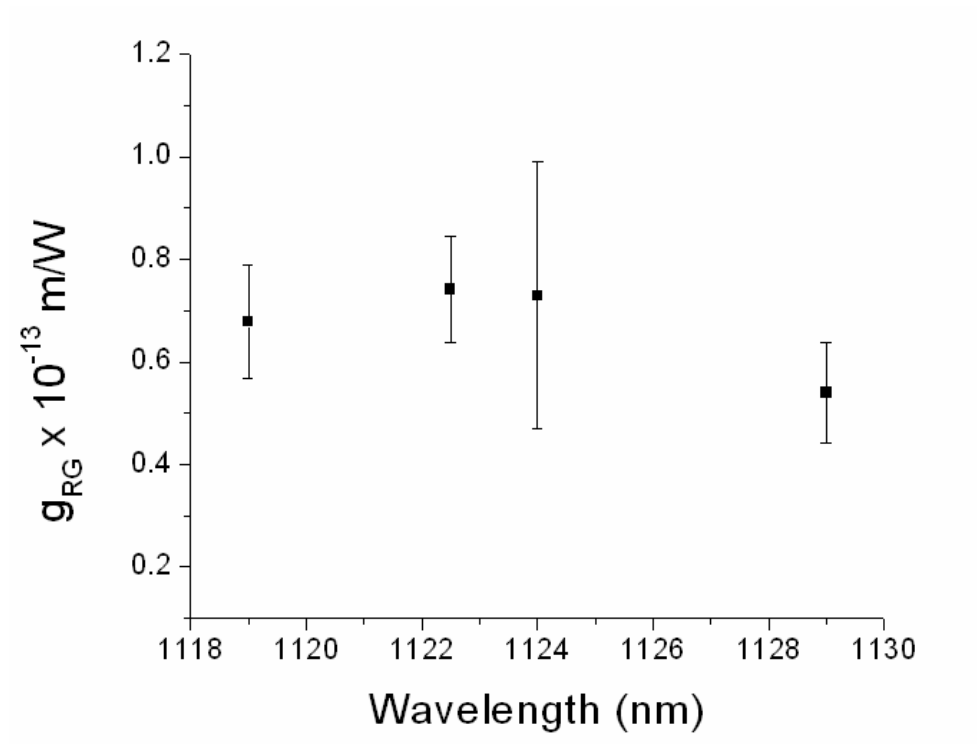


**Figure 28.** Raman Gain Model Sol-gel 28

APPENDIX D  
RAMAN SPECTRA

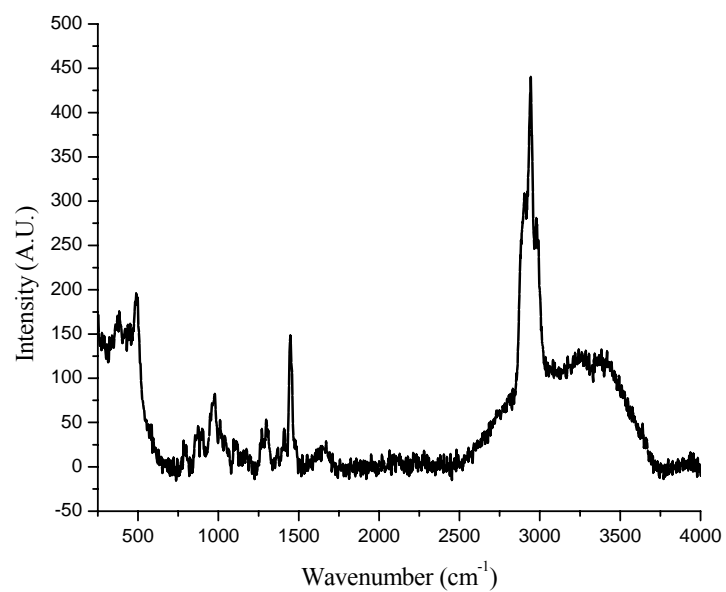


**Figure 29.** Raman Spectrum Sol-gel 1

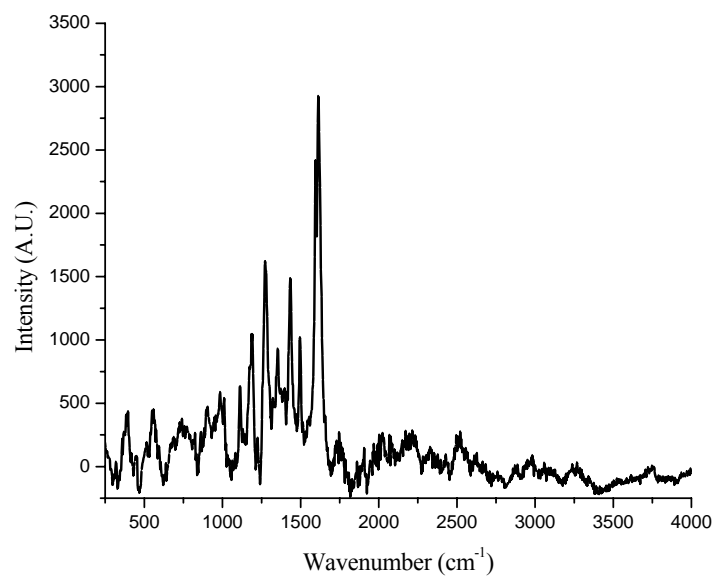


**Figure 30.** Raman Spectrum Sol-gel 3

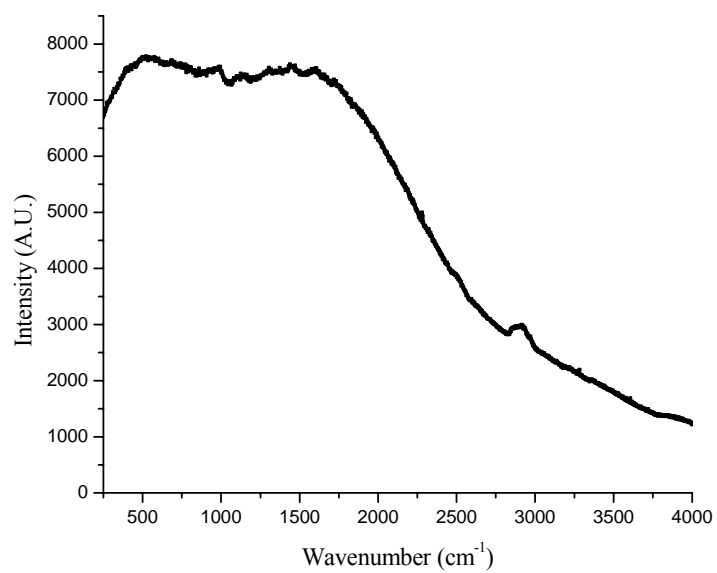


**Figure 31.** Raman Spectrum Sol-gel 5

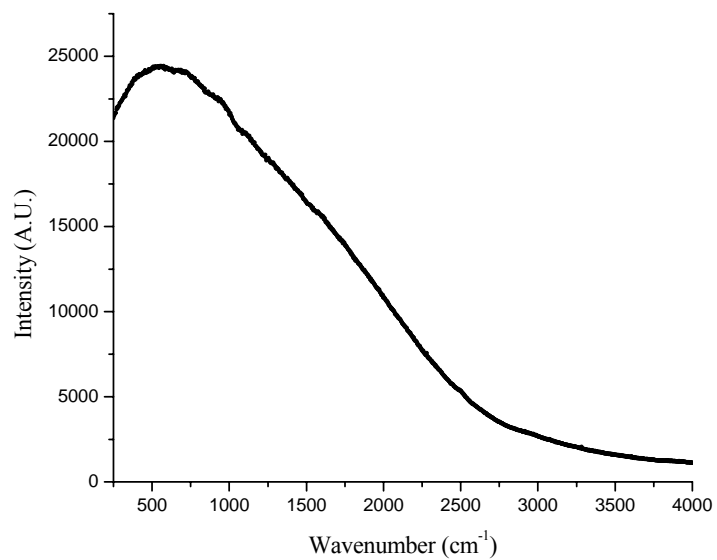


**Figure 32.** Raman Spectrum Sol-gel 6

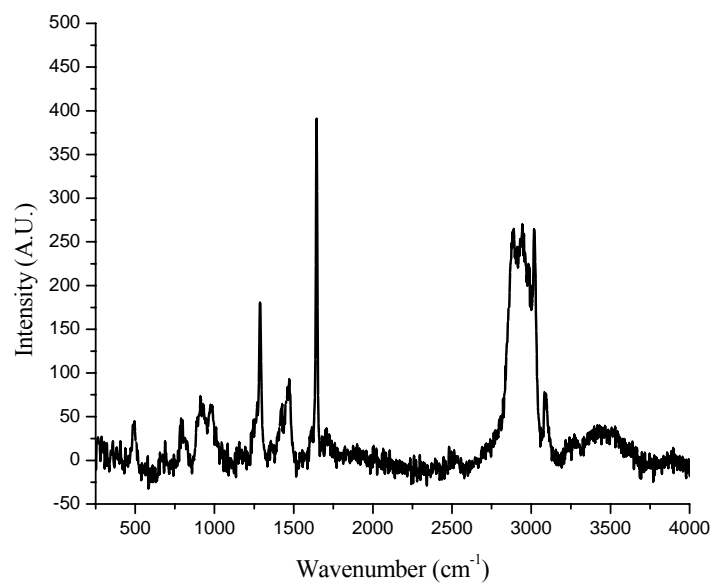


**Figure 33.** Raman Spectrum Sol-gel 7

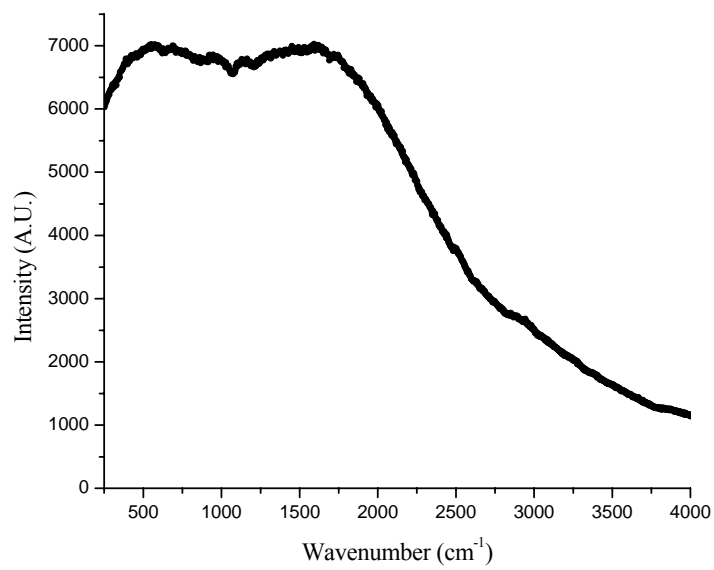


**Figure 34.** Raman Spectrum Sol-gel 8

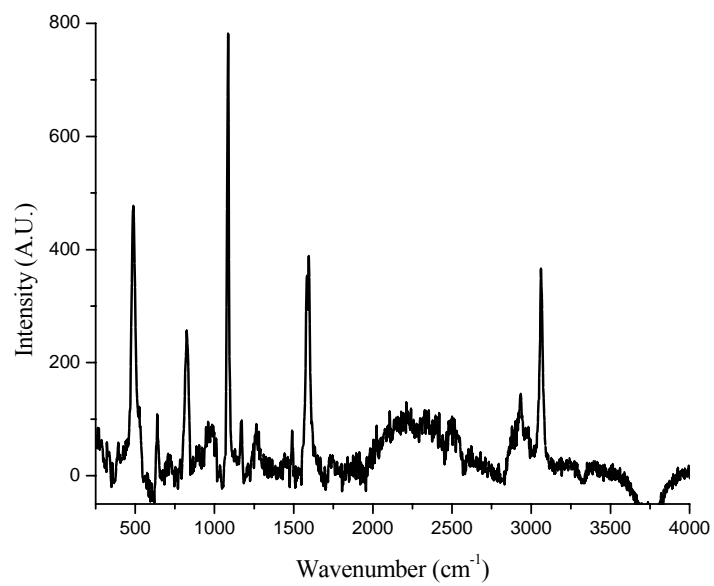


**Figure 35.** Raman Spectrum Sol-gel **9**

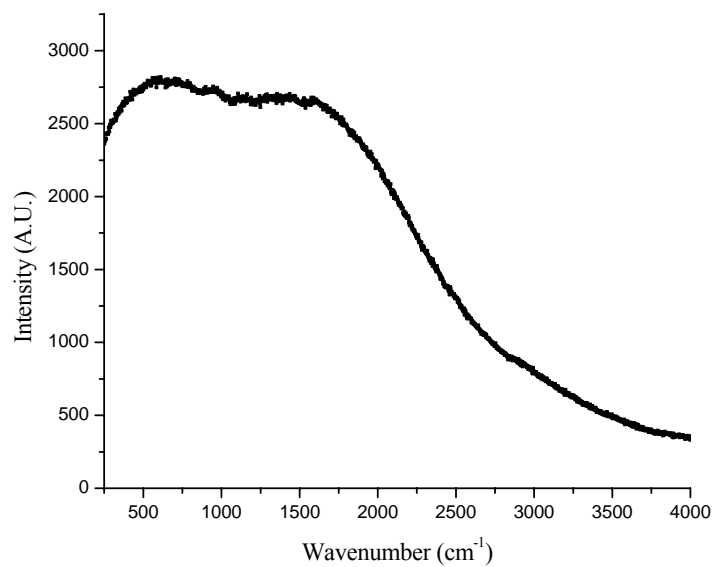


**Figure 36.** Raman Spectrum Sol-gel **10**



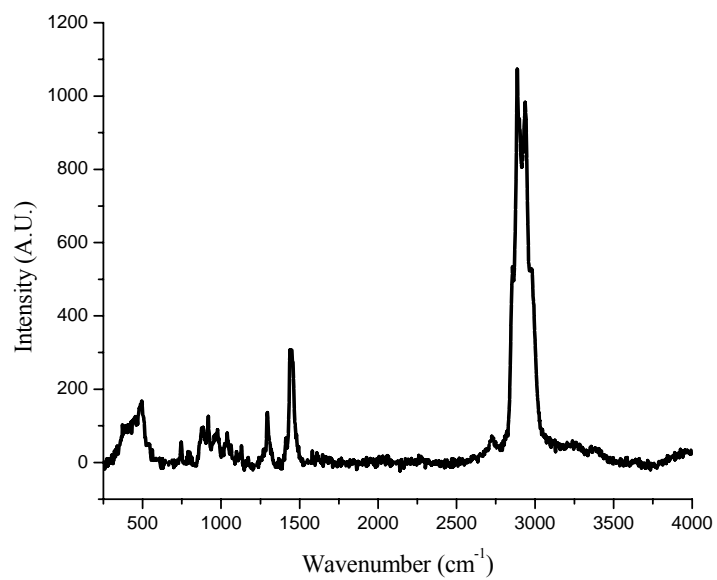


**Figure 37.** Raman Spectrum Sol-gel 11

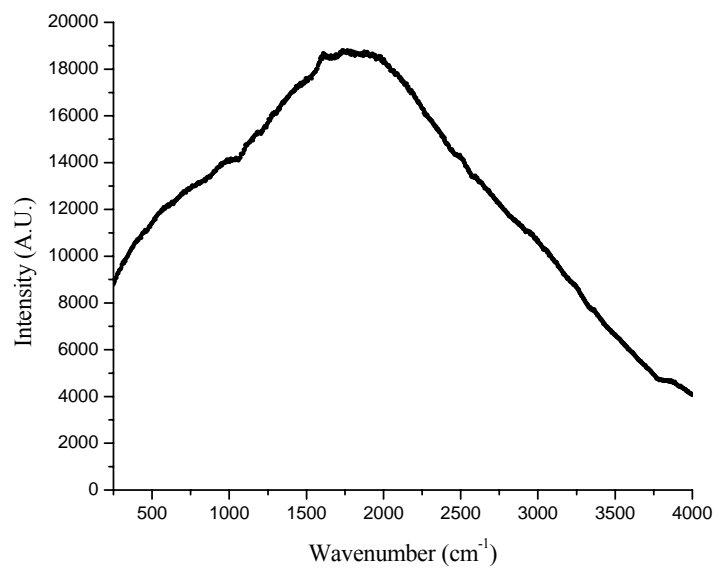


**Figure 38.** Raman Spectrum Sol-gel 12

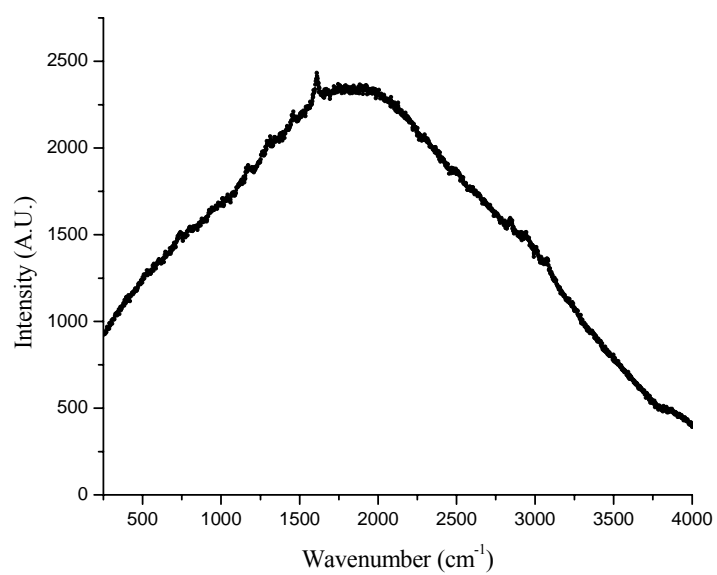


**Figure 39.** Raman Spectrum Sol-gel 13

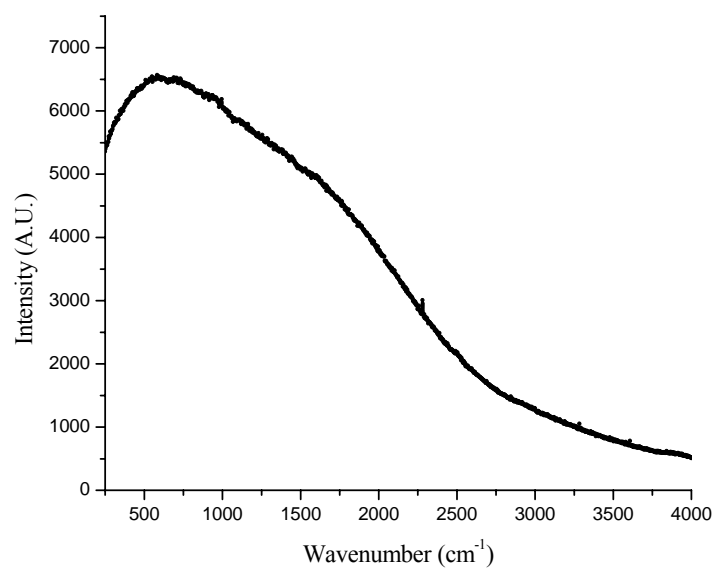


**Figure 40.** Raman Spectrum Sol-gel 14

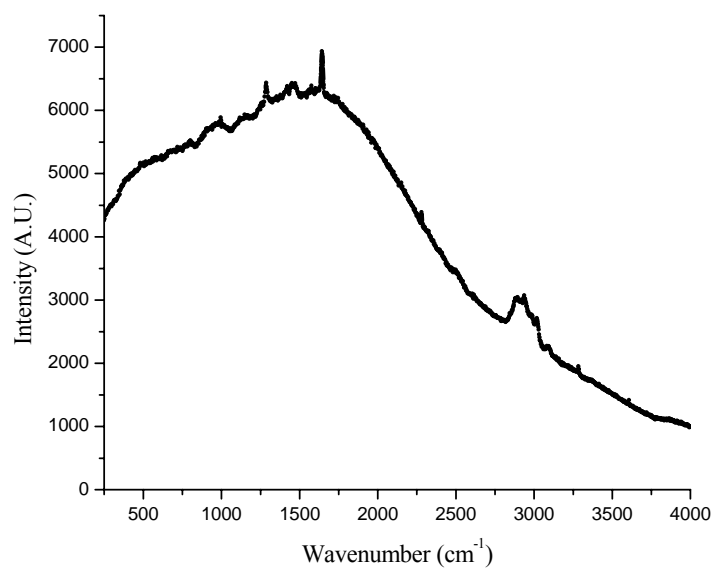


**Figure 41.** Raman Spectrum Sol-gel 15

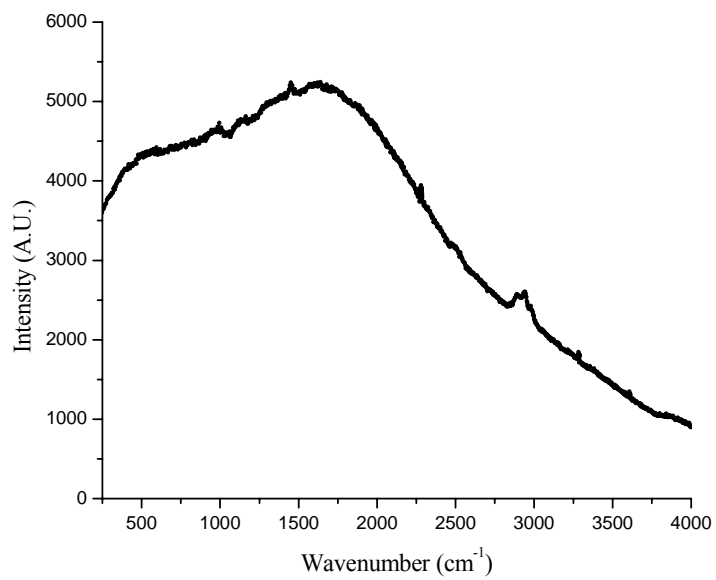


**Figure 42.** Raman Spectrum Sol-gel 16

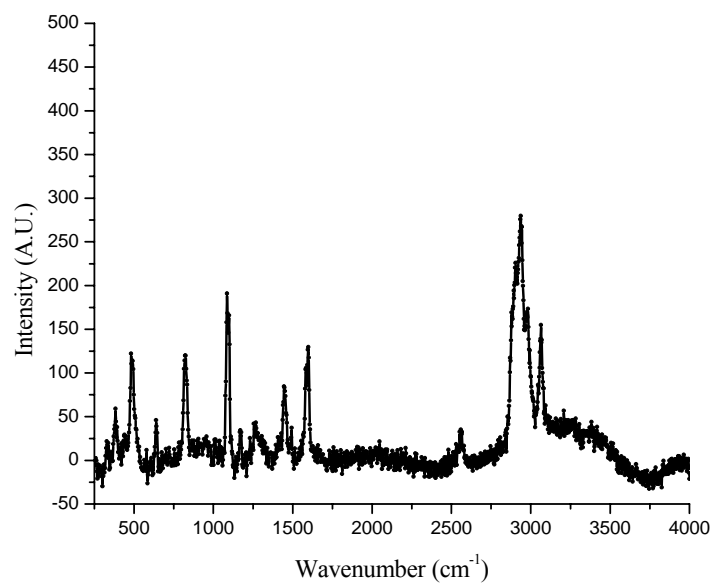


**Figure 43.** Raman Spectrum Sol-gel 17

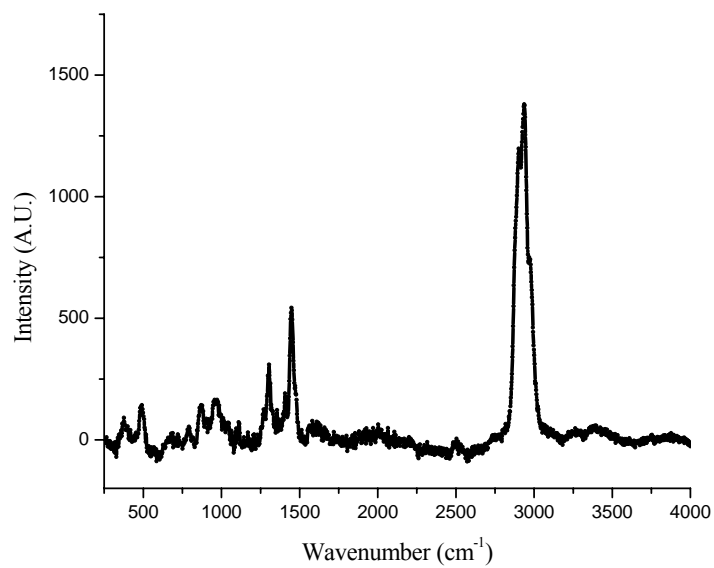


**Figure 44.** Raman Spectrum Sol-gel 18

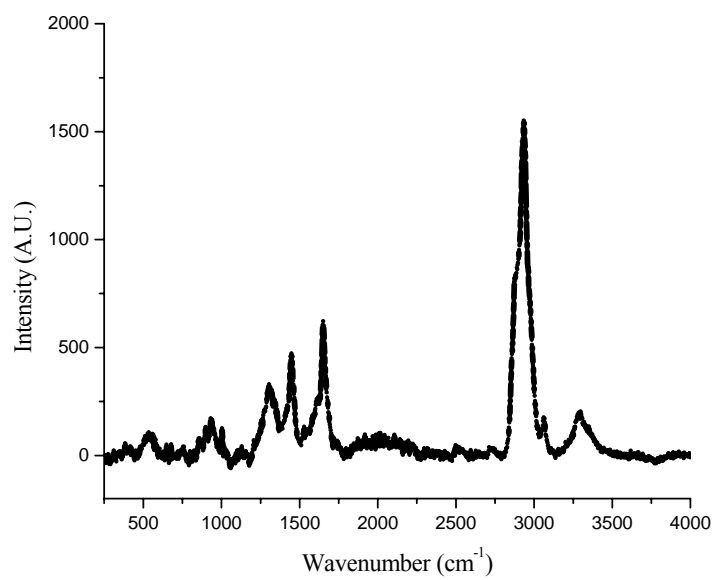


**Figure 45.** Raman Spectrum Sol-gel 19

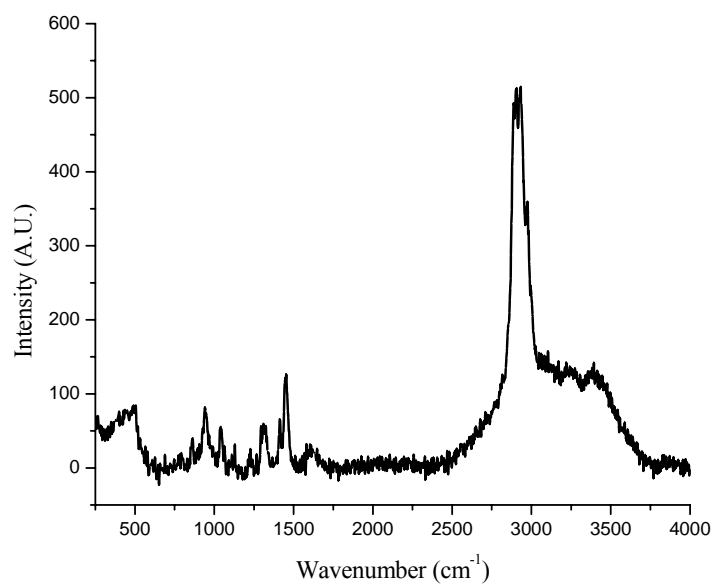


**Figure 46.** Raman Spectrum Sol-gel 20

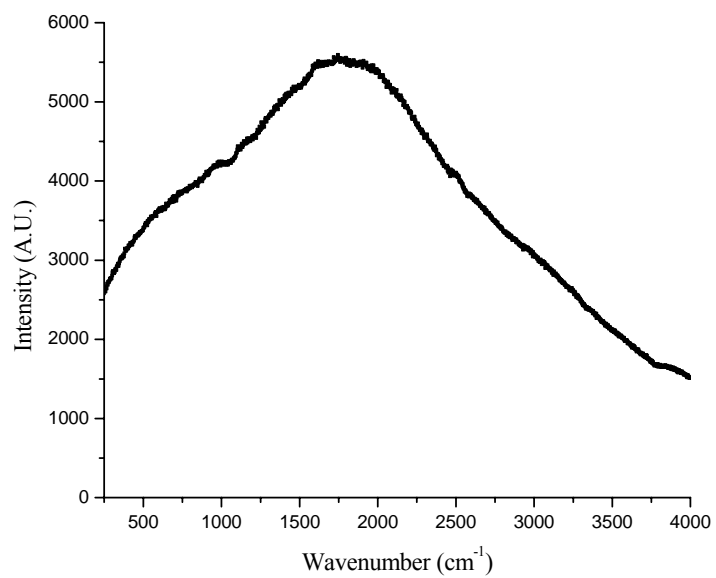


**Figure 47.** Raman Spectrum Sol-gel 21

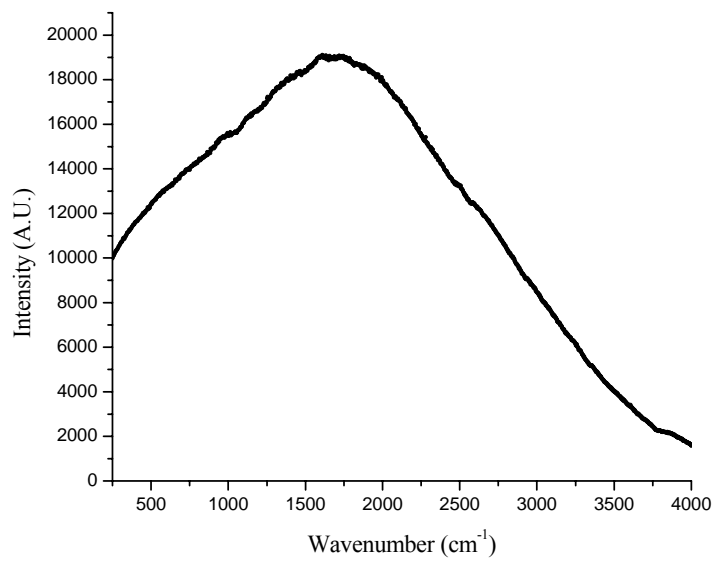


**Figure 48.** Raman Spectrum Sol-gel 22

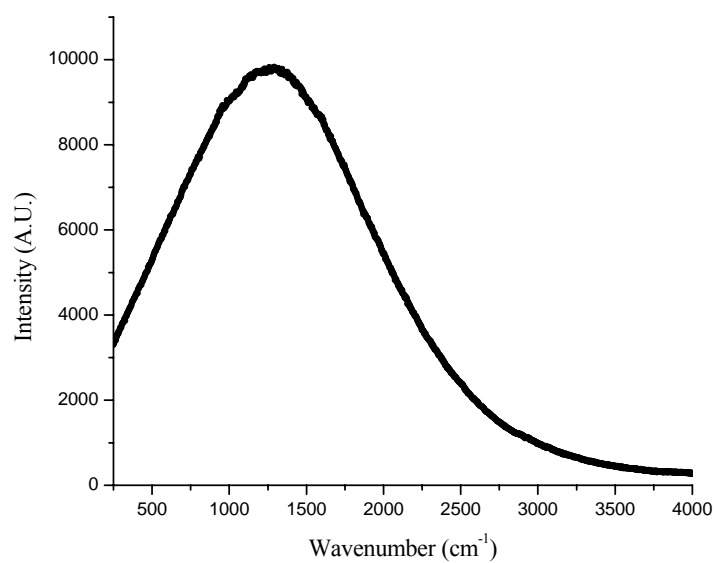


**Figure 49.** Raman Spectrum Sol-gel 23

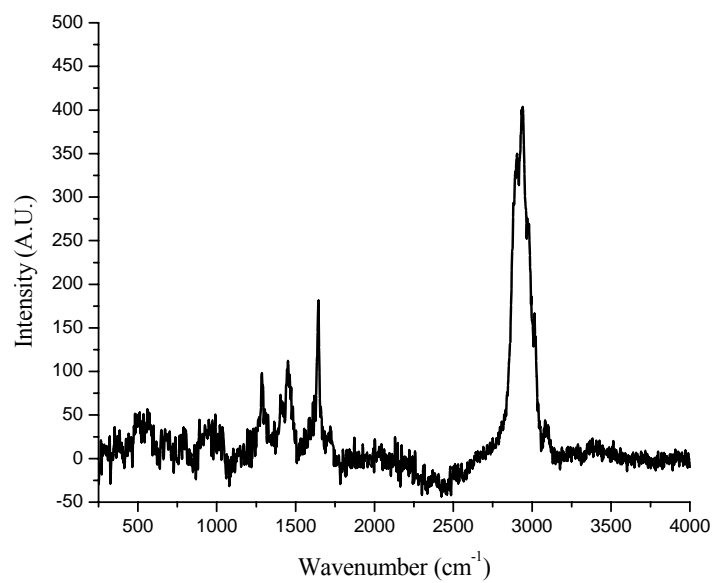


**Figure 50.** Raman Spectrum Sol-gel 24

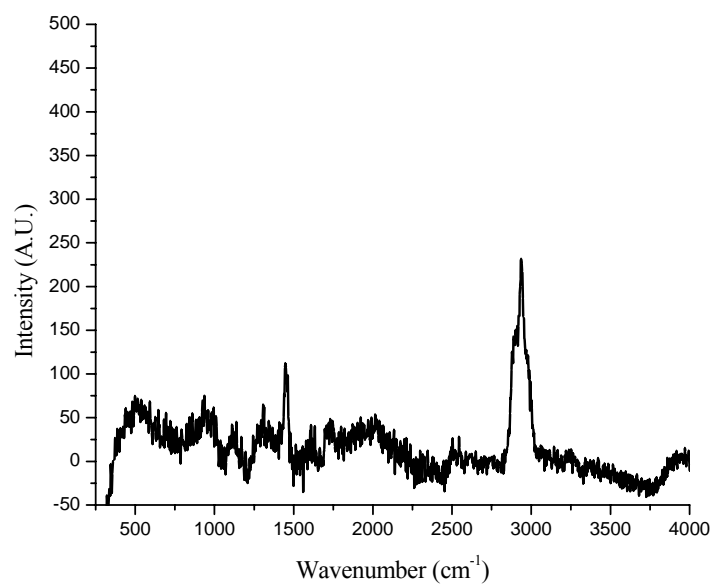


**Figure 51.** Raman Spectrum Sol-gel 25

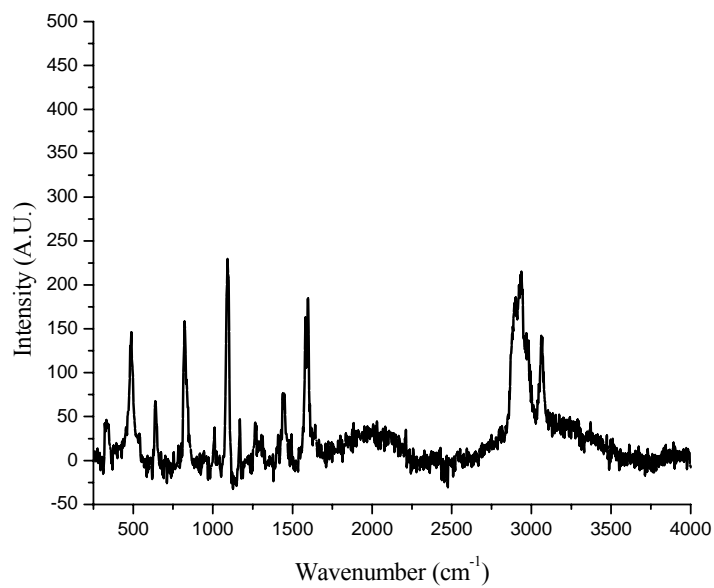


**Figure 52.** Raman Spectrum Sol-gel 26



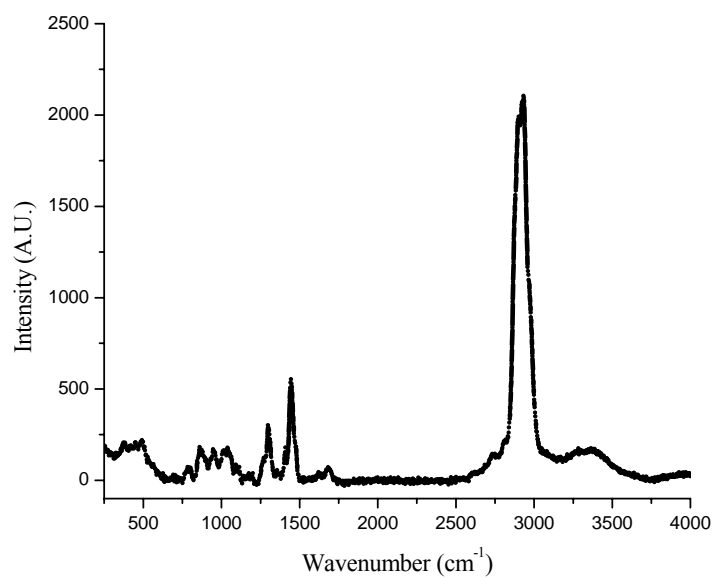


**Figure 53.** Raman Spectrum Sol-gel 27

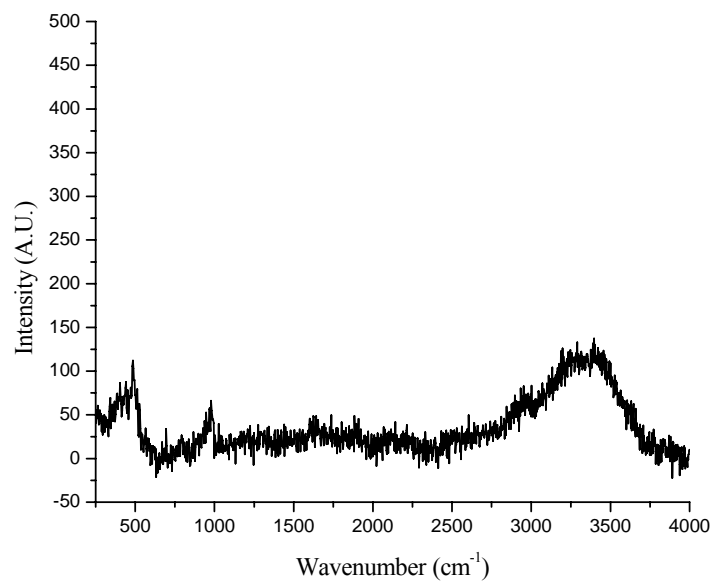


**Figure 54.** Raman Spectrum Model Sol-gel 28

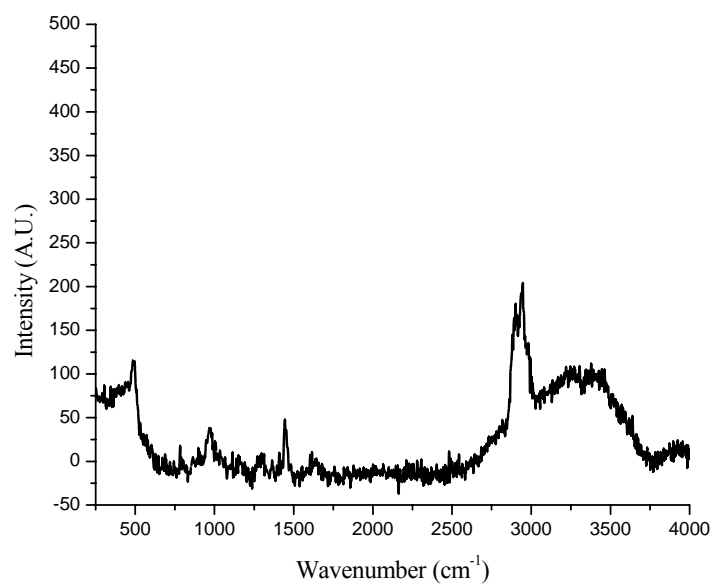


**Figure 55.** Raman Spectrum Model Sol-gel 29

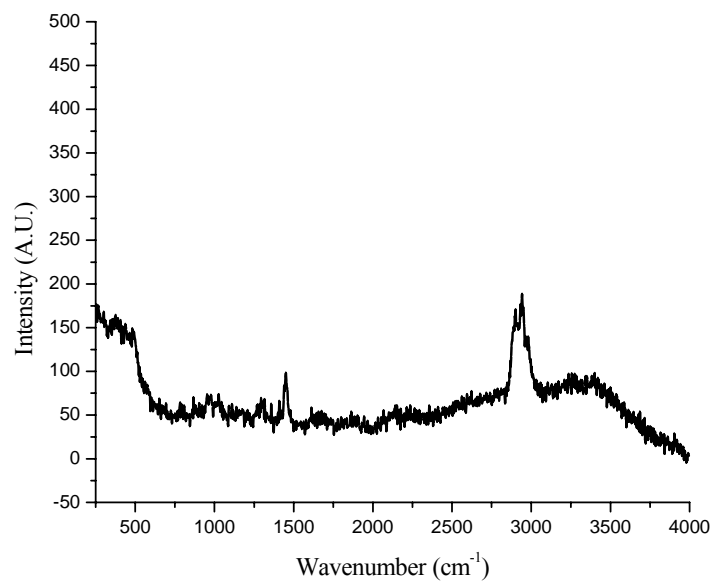


**Figure 56.** Raman Spectrum Model Sol-gel 30

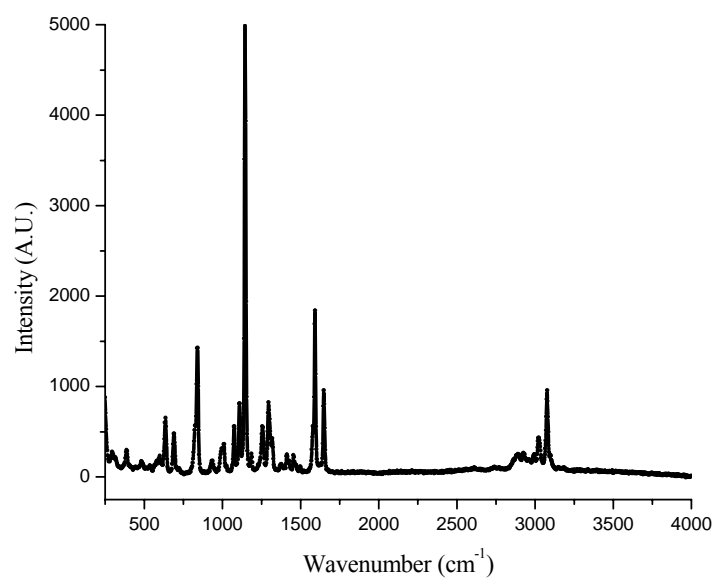


**Figure 57.** Raman Spectrum Compound 31

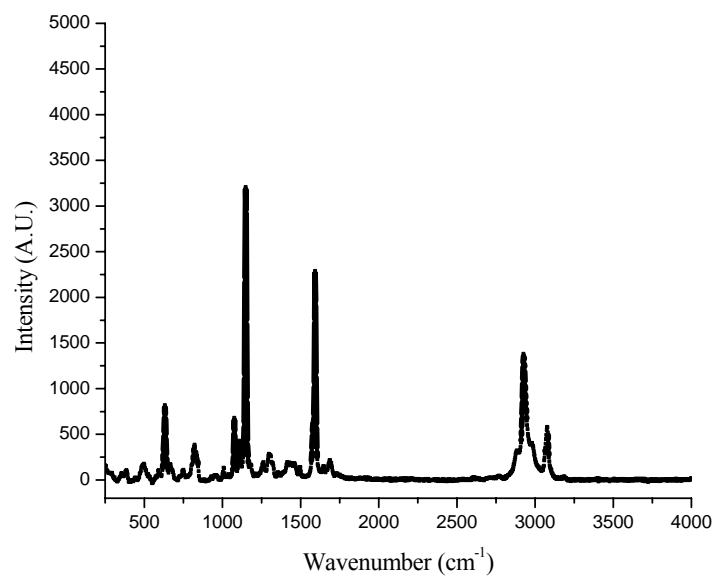


**Figure 58.** Raman Spectrum Compound 32

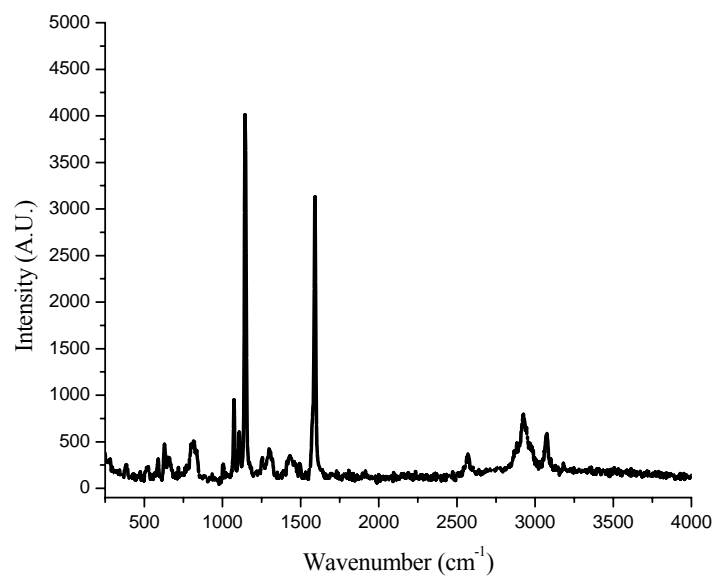


**Figure 59.** Raman Spectrum Compound 33

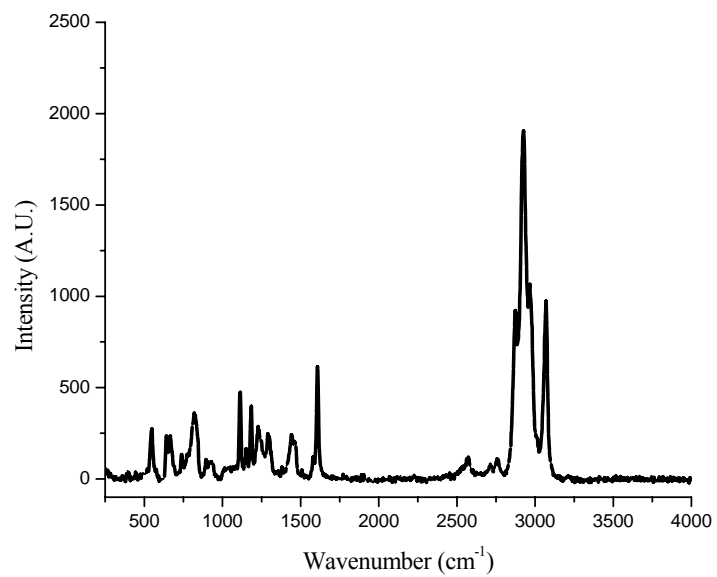


**Figure 60.** Raman Spectrum Compound 35

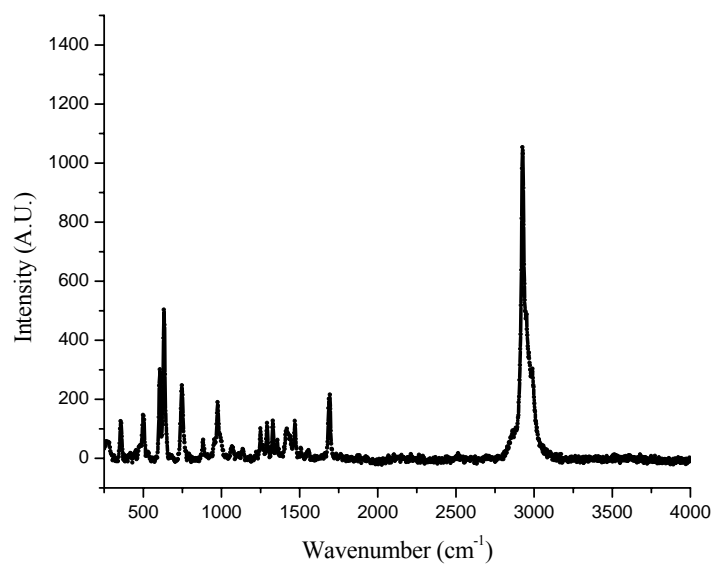


**Figure 61.** Raman Spectrum Compound 37

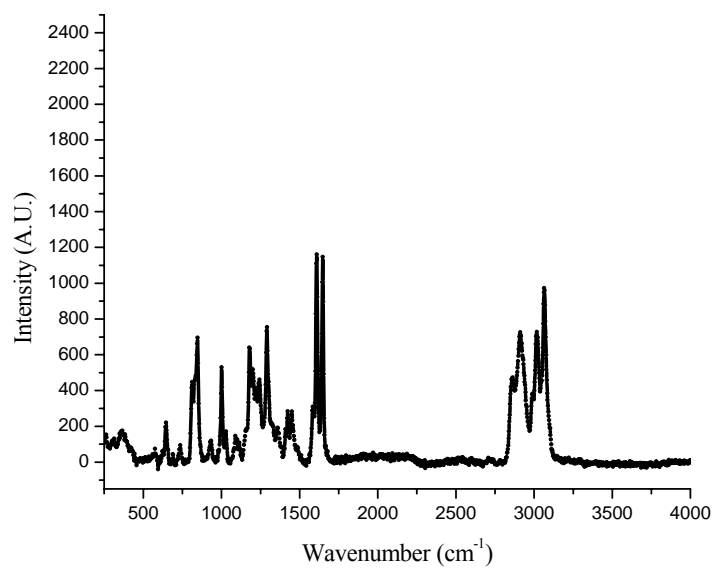


**Figure 62.** Raman Spectrum Compound 39

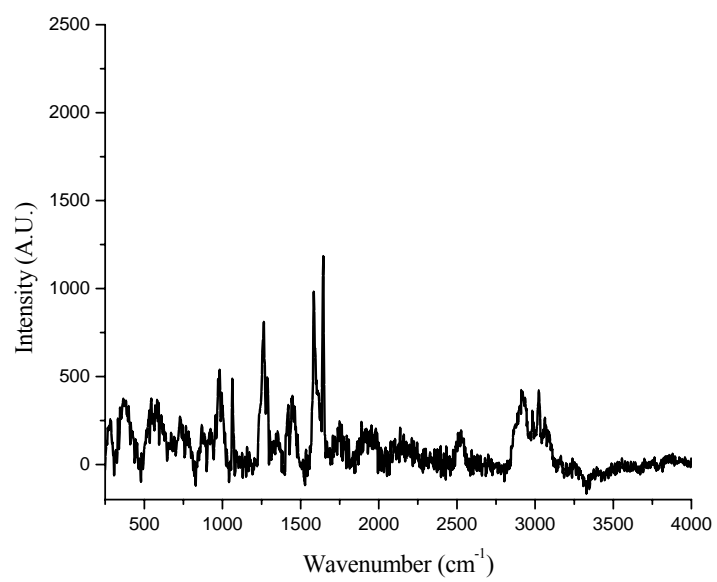


**Figure 63.** Raman Spectrum Compound **41**

## LIST OF REFERENCES

1. Chang, K. H.; Miller, T. J.; Kalish, D.; Pearsall, M. L. Eur. Patent EP 0 887 670 A2, 1998.
2. *Fiber Optic Data communication: Technological Trends and Advances*; DeCusatis, Casimer, Ed.; Academic: New York, 2002; p 89.
3. Toupin, L., *Designs for the Long Haul*; *Spie Int. Soc. Opt. Eng.* **2001**, 1(1), 24-26.
4. *Sol-Gel Optics: Processing and Applications*; Klein, Lisa C., Ed. Kluwer Academic: Boston, 1994; p 39.
5. Eldada, L., Shacklette, L.W. *Advances in Polymer Integrated Optics*; *IEEE J. Quantum Electron.* **2000**, 6(1), 54-68.
6. Emori, Y.; Kado, S.; Namiki, S. *Simple gain control method for broadband Raman amplifiers gain-flattened by multi-wavelength pumping*; *Proc. 27<sup>th</sup> Eur. Conf. On Opt. Comm.* **2001**, 158-159.
7. Namiki, S.; Emori, Y. *Ultrabroad-band Raman amplifiers pumped and gain-equalized by wavelength-division-multiplexed high-power laser diodes*; *IEEE J. Quantum Electron.* **2001**, 7(1), 3-16.
8. Morita, I.; Tanaka, K.; Edagawa, N. *Benefit of Raman amplification in ultra-long-distance 40 Gbit/s-based WDM transmission using dispersion-flattened fibre span*;

- Elec. Lett.* **2001**, 37(8), 507-509.
9. Koch, F.; Lewis, S. A. E.; Chernikov, S. V.; Taylor, J. R. *Broadband Raman gain characterisation in various optical fibres*; *Elec. Lett.* **2001**, 37(24), 1437-1439.
  10. Hansen, P.B.; Eskildsen, L.; Grubb, S.G.; Stentz, A.J.; Strasser, T.A.; Judkins, J.; DeMarco, J.J.; Pedrazzani, R.; DiGiovanni, D.J. *Capacity Upgrades of Transmission Systems by Raman Amplification*; *IEEE Phot. Tech. Lett.* **1997**, 9(2), 262-264.
  11. Hoss, Robert J. *Fiber Optic Communications: Design Handbook*; Prentice Hall: New Jersey, 1990; pp 105-128.
  12. Okazaki, H.; Kitagawa, T.; Shibata, S.; Kimura, T. *Mechanical Strength Improvement of Sol-Gel Derived Dry Gels for Optical Fiber Preforms*; *J. Non-Crystalline Solids* **1990**, 116(1), 272-283.
  13. Chaput, F.; Riehl, D.; Lévy, Y.; Boilot, J. *Azo Oxide Gels for Optical Storage*; *Chem. Mater.* **1993**, 5, 589-591.
  14. Kim, H.; Kang, S.; Choi, S.; Min, Y.; Yoon, C. *Highly Efficient Organic/Inorganic Hybrid Nonlinear Optic Materials via Sol-Gel Process: Synthesis, Optical Properties, and Photobleaching for Channel Waveguides*; *Chem. Mater.* **1999**, 11, 779-788.



15. Chaput, F.; Riehl, D.; Boilot, J.; Cargnelli, K.; Canva, M.; Lévy, Y.; Brun, A. *New Nonlinear Sol-Gel Films Exhibiting Photorefractivity*; *Chem. Mater.* **1996**, 8, 312-314.
16. Lucent Technologies Bell Labs Innovations  
<http://www.lucent.com/press/0299/990223.bla.html>.
17. Nobel e-Museum <http://www.nobel.se/>.
18. Lehmann, H., *et al.* US Patent 4,694,096 1987.
19. Prajapati, S. P.; Pardnani, J. H.; Sethna, S. *Studies on 4,4'-Dihydroxydiphenyl Sulfone and 4,4'-dihydroxydiphenyl Ether*; *J. Ind. Chem. Soc.* 1977, 54 (10), 971-984.
20. Aldrich Handbook of Fine Chemicals and Laboratory Equipment, 2003-2004.
21. Abbey, K. J. US Patent 6,313,257 B1 1999.
22. Bass, M., Van Stryland, E. W. *Fiber Optics Handbook : Fiber, Devices, and Systems for Optical Communications*: McGraw Hill, NY, 2002; pp 8-42.